SMALL MOLECULE PROFILING AND IMAGING OF THE ZEBRA FINCH SONG SYSTEM

BY

KENSEY R AMAYA

DISSERTATION

Submitted in partial fulfillment of the requirements
for the degree of Doctor of Philosophy in Cell and Developmental Biology
in the Graduate College of the
University of Illinois at Urbana-Champaign, 2010

Urbana, Illinois

Doctoral Committee:

Associate Professor Jo Ann Cameron, Chair
Professor David F. Clayton, Director of Research
Professor Jonathan V. Sweedler
Associate Professor Stephanie Ceman
Associate Professor Michel Bellini

ABSTRACT

The ability of songbirds to communicate though learned vocalization and the discovery of discreet interconnected "song nuclei" involved in vocal learning has made them a valuable model to study the neuronal mechanisms behind learning and memory. This dissertation focuses on studying small molecules (i.e. lipids and metabolites) in the zebra finch song system, a songbird. I will use analytical tools and methods to detect and image the spatial distribution of small molecules (e.g. lipids) across the song system. In addition I will investigate changes in small molecules in the auditory lobule, a brain region involved in interpreting and processing auditory inputs, in response to song stimulation.

Applying advances in Time of Flight - Secondary Ion Mass Spectrometry (ToF-SIMS) small molecules (e.g. fatty acids) are detected and high spatial resolution images (2.3 μm) are generated, forming 11.5 megapixel chemical images using a sagittal brain section collected from an adult male zebra finch. ToF-SIMS analysis reveals a heterogeneous distribution of small molecules across the brain section corresponding to different anatomical structures, including two song nuclei that are important in song-motor control.

Expanding upon the ToF-SIMS results I increase the number of identifiable small molecules; and expand the number of brain regions to include all of the major song nuclei in the zebra finch brain. Using ToF-SIMS and applying multivate statistical methods (e.g. principle component analysis) I show chemical differences between functionally distinct and tissue specific brain areas; as well as at different developmental stages in the male songbird brain.

Metabolites are a diverse group of small molecules that act as end products and intermediates in biochemical pathways such as signaling molecules (i.e. dopamine), amino acids (i.e. glutamate) and in energy metabolism (i.e. glucose). Metabolomic studies focusing on the auditory lobule, a brain region involved in the acquisition, processing, and interpreting of auditory inputs, exhibited unique metabolomic profiles between birds exposed to novel song exposure, habituation song, and silence. Biochemical pathways involved in sugar metabolism (e.g. glycolysis), RNA synthesis,

and GHB metabolism exhibit overall changes upon novel song stimulation compared to silent control birds. Integrating genomic data and metabolomic data suggests other biochemical pathways are responding to song stimulation.

This dissertation reveals the heterogeneous distribution of small molecules across the major song nuclei in the zebra finch brain and at different developmental stages and the metabolomic response to song. These experiments serve as a stating point to study the role lipids play in the development of the song system and learning and memory. It also serves as a starting point to conduct more rigorous metabolomic studies and integrating metabolomic, genomic, and proteomic information to better study song response in the zebra finch brain.

ACKNOWLEDGMENTS

I would first like to thank my mentor Dr. David Clayton for his constant encouragement, advice, and support. I am especially grateful that he encouraged and gave me the freedom to explore my own ideas. His mentoring style encouraged my scientific development and rekindled my interest and love of science. Thanks to Dr. Sara London who has provided much advice and suggestions over the years.

Thanks to my committee members Dr. Stephanie Ceman, Dr. Jo Ann Cameron, Dr. Michel Bellini, and especially Dr. Jonathan Sweedler for their support, encouragement, and advice. I would like to thank Dr. Maurice Southworth and Dr. Fran Perler for giving the opportunity to do research at an early age. Dr. Brian Akerley for encouraging my scientific interests during my undergraduate years in his lab at the University of Michigan, and Dr. Isaac Cann for bringing me into his lab and being both a mentor and friend.

I would also like to thank all of my friends who have been supportive and have always been there for me over the years, they have truly made the past six years more enjoyable. Finally I would like to thank my parents who have always been supportive and for their constant encouragement to continue through my PhD and pursue my aspirations.

TABLE OF CONTENTS

CHAPTER 1
INTRODUCTION

SONGBIRDS AND SMALL MOLECULES

Songbirds (Passeriformes: Oscines) represent approximately half of all avian species and are one of the few animals, including humans, with the ability to communicate through learned vocalizations (Doupe & Kuhl 1999, Jarvis 2004). The discovery of discrete, interconnected "song nuclei" involved in vocal learning in songbirds has made them a valuable model for the study of the neuronal mechanisms behind learning and memory, and brain development. The zebra finch (*Taeniopygia guttata*), a songbird, is a valuable animal model in which small molecule binding and interacting molecules (e.g. lipid and lipophilic molecules) have been discovered to be associated with the song nuclei. Changes in these small molecules (e.g. lipophilic molecules) during development and their importance in song development have made them of significant interest. However, traditional methods lack the capacity to visualize them in tissues thus limiting their study. Developments in Secondary Ion Mass Spectrometry (SIMS), however, now permit its application towards biological tissues, making the study and imaging of small molecules such as lipids possible (Sjovall *et al.* 2004, Ewing 2006, Guerquin-Kern *et al.* 2005).

The zebra finch has recently been used as a model system to study transcriptomic and proteomic changes upon song exposure (Dong *et al.* 2009, Pinaud *et al.* 2008), to study molecular changes during learning and memory formation. These studies are limited in that they do not investigate potential biochemical changes metabolites (i.e. sugars, amino acids, and nucleic acids). Therefore, applying metabolomic studies to measure small molecule changes has the potential to enhance our understanding of the biochemical and cellular changes that occur upon song exposure in the zebra finch brain. Combining metabolomic information and harnessing information generated though genomic and proteomic studies from the zebra finch one can study global cellular changes at different levels using a systems biology approach. For these reasons the zebra finch is a unique model system to uncover small molecule heterogeneities across the

brain and study biochemical and molecular changes during learning and memory formation.

The zebra finch song system

Complex avian behaviors were traditionally viewed as instinctive with birds being incapable of adaptive or higher order cognition; this view significantly limited communication between mammalian and avian researchers. However recent changes in the nomenclature of the avian brain more accurately reflects similarities between avian and mammalian brain structures allowing for direct comparisons (Reiner *et al.* 2004). Current nomenclature now reflects that a major part of the avian telencephalon as pallial, with many of the major song nuclei involved in song perception, learning, and production now located within this region (Reiner *et al.* 2004).

The neuronal network of the song system was originally revealed in the canary and described as three large interconnected nuclei (HVC), robust nucleus of the arcopallium (RA), and Area X) (Nottebohm *et al.* 1976). Since then our understanding of the song system has expanded revealing other areas of the brain critical to song learning and memory including: the dorsolateral thalamic nucleus (DLM), lateral magnocellular nucleus of the nidopallium (LMAN), and the auditory lobule (AL) composed of the caudal medial nidopallium (NCM), caudal medial mesopallium (CMM), and field L. These song nuclei are major processing centers in the zebra finch brain forming an interconnected network that can be broken down into three functional systems: 1) auditory forebrain, responsible for processing auditory inputs, 2) "anterior forebrain pathway" (AFP), responsible for song learning and storing auditory memories, and 3) song motor control (Fig. 1.1).

Auditory inputs play an important role in songbird biology by developing long-term memories of conspecific song, allowing for vocal imitation necessary for successful reproduction and communication. Electrophysiological and gene expression studies have shown that NCM and CMM undergo significant activity upon auditory stimulation, suggesting their role in formation of long-term memories (Huesmann & Clayton 2006, Dong et al. 2009, Mello & Clayton 1995, Mooney & Rao 1994). Although a major connection between AL and the other song nuclei has not been discovered it is suggested

Field L, part of AL, plays an important role as a conduit, connecting the auditory pathway to the song-motor pathway via the interfacial nucleus of the nidopallium (NIf) (Vates *et al.* 1996).

The anterior forebrain pathway is essential for song learning and recognition, consisting of a projection from HVC to AreaX and AreaX to DLM, located in the thalamus (Fig.1.1). Neuronal projections also form between DLM and LMAN, from LMAN to AreaX, and LMAN to RA (Doupe & Solis 1997, Margoliash 1997) (Fig. 1.1). Pathway development has been shown to occur as early as post hatch day 15 with axonal projections from LMAN innervating RA (Mooney & Rao 1994). Both learning and memory and pathway development are time dependent. Lesion studies targeting AreaX, LMAN, or DLM show little affect on previously crystallized song in adult males (Bottjer & Johnson 1997). However, in juveniles lesions targeting LMAN disrupts normal song development (Bottjer *et al.* 1984), while lesion studies targeting AreaX impairs song development and prevents song crystallization, in other words its song remains plastic (Sohrabji *et al.* 1990).

In male zebra finches a major axonal projection descends from nucleus HVC in the nidopallium to nucleus RA in the arcopallium, this pathway is necessary for production of learned song and is only completed in males, despite the presence of neuronal projections from HVC on the periphery of RA in both juvenile male and female birds. Around post-hatch day 30 RA becomes innervated in males, but not in females, at which point a major reorganization of synaptic contacts occurs (Herrmann & Arnold 1991). However in females this pathway is not completed instead RA exhibits a decrease in neuronal numbers and an increase in cell density and cell atrophy (Konishi & Akutagawa 1985). Soon after the innervation of RA by HVC projection neurons, juvenile males begin mimicking the adult male tutor song marking the beginning of the song-motor phase. The factors controlling development of the HVC-RA pathway are still unknown, however numerous studies have implicated locally synthesized steroids, specifically estrogen, as major factors in controlling its development (Holloway & Clayton 2001, Konishi & Akutagawa 1988, Grisham & Arnold 1995, Grisham *et al.* 1994).

Small molecules and the song system

Development of the zebra finch song system has largely centered on the study of anatomical changes (Konishi & Akutagawa 1985), effects of lesioning brain regions (Bottjer et al. 1984, Sohrabji et al. 1990), electrophysiology (Mooney & Rao 1994), and molecular and gene expression changes (London *et al.* 2009, George *et al.* 1995). One of the first genes to have been studied as playing an important role in initial memory formations in the songbird is synuclein. A study by George et al. found synuclein to be enriched at presynaptic terminals in some song nuclei of the zebra finch, with a notable decrease in expression in adults compared to juvenile birds (George *et al.* 1995). Interestingly homologous proteins have been found in other species including humans and it being associated with amyloid plaques found in Alzheimer's and Parkinson's disease patients (Ueda *et al.* 1993, Polymeropoulos *et al.* 1997). Studies have also identified androgen receptors and aldehyde dehydrogenase (ALDH), related to neuronal trajectory development, and melatonin receptor and myelin basic protein (MBP), associated with song system maturation, as having time and region dependent expression levels (Clayton 1997).

Small molecules are low molecular weight (<1,000 Daltons) organic compounds that include but are not limited to fatty acids, lipids, steroids, and vitamins. They are both intermediate and end product metabolites that act as cell structure components, as cell signaling molecules, and energy storage molecules.

In songbird neurobiology, lipid and lipophilic small molecules have been shown to play a direct and indirect role in zebra finch song system development. One such molecule is cholesterol, it is a steroid precursor and localized steroid production in male zebra finches is important for development of the song control pathway (Holloway & Clayton 2001). In addition to cholesterol, fatty acids (FA's) and lipids are suggested to play an important role in development, evidenced by developmental changes in expression of synuclein, a lipid associated protein (Davidson *et al.* 1998, Ellis *et al.* 2005). Other small molecules of interest in songbird neurobiology include retinoic acid whose synthetic enzymes are locally expressed around the song nuclei and exhibit expression differences in development (Denisenko-Nehrbass *et al.* 2000). Despite the importance of small molecules in songbird brain development they have not been studied

in great length, in part because we have lacked methods to detect and image their distribution in biological samples.

IMAGING LIPIDS IN BIOLOGICAL TISSUES USING ToF-SIMS

Historically, the study of brain lipid composition has relied on crude dissection, homogenization, and detection by thin-layer-chromatography or other chromatography methods. A major limitation of these methods is that information pertaining to the cellular distribution of lipids is not known. Advances with fluorescently labeled and tagged lipids have successfully been used to study cell membrane dynamics and myelination (Bilderback *et al.* 1997), however adding fluorophores to lipids adversely affects lipid-lipid and lipid-protein interactions (Maier *et al.* 2002). The emergence of new and enhanced analytical tools such as Matrix-Assisted Laser Desorption/Ionization (MALDI) and Secondary Ion Mass Spectrometry (SIMS) have now allowed us to detect and image small molecules in complex biological tissues, such as the brain.

Three commonly used mass spectrometric imaging techniques used on biological samples are MALDI, nano-Secondary Ion Mass Spectrometry (nano-SIMS), and Time of Flight – Secondary Ion Mass Spectrometry (ToF-SIMS). The strength of MALDI imaging is in the detection of molecules >2000 Da (i.e. peptides and proteins) across whole tissues, however typical MALDI imaging can not achieve cellular resolution (Jackson & Woods 2009). Nano-SIMS strength lies in its ability to image molecules at a subcellular resolution (lateral resolution of 50-150 nm), however it is limited to elemental analysis (Guerquin-Kern *et al.* 2005) due to the low abundance of most molecular species. ToF-SIMS bridges the gap between MALDI and nano-SIMS being able to achieve a sub-cellular resolution (approximately 1μm) for organic molecules (<1000 Da) and nanometer resolution for inorganic molecules (Ewing 2006). This technology has been shown to be well suited for the detecting and imaging of lipids and other lipophilic molecules in biological samples.

What is ToF-SIMS?

Time of Flight – Secondary Ion Mass Spectrometry is a surface analysis tool in which a primary ion beam is directed towards a sample surface, ionizing and desorbing

the surface molecules upon impact. The resulting secondary ions are then separated by their time of flight, which is dependent on their mass/charge ratio (*m/z*), followed by their detection (Fig. 1.2). The detected secondary ions, representing unique molecular species, can then be selected from the resulting spectrum generating an image depicting the relative concentration of the molecule on the sample surface.

In SIMS, analysis is carried out either in "static" or "dynamic" mode. In static SIMS the ion dosage, the number of incident ions, remains approximately an order of magnitude less then the number of atoms at the sample surface, with the static limit generally accepted as ~10^{13} ions / cm^2 (Vickerman *et al.* 2001). This method is used to gain molecular information about the sample surface, however ion counts are lower making this method suitable for abundant ions. This is in contrast to "dynamic" SIMS where the number of incident ions exceeds the number of surface atoms on the sample, yielding a high ion count but is typically used to acquire elemental information permitting trace element analysis (Guerquin-Kern et al. 2005).

Conventional secondary ion mass spectrometric (SIMS) methods have traditionally relied on low molecular weight primary ions (e.g. Ga^+, Ar^+) for ionizing analyte molecules. The use of these primary ions for biological SIMS is limited due to the extensive fragmentation of surface molecules, allowing for only the detection of low mass surface compounds. Advances with liquid metals such as Au and Bi have significantly increased the mass range of analyte detection to ~1,000 *m/z* making it a robust method for the detection and imaging of lipids. The use of polyatomic cluster ions (i.e. Au_2, Bi_2) can increase the mass range of detection further >1000 *m/z*, however the primary ion dosage is lower requiring longer collection times (Kollmer 2004).

Challenges and opportunities for SIMS

Advantages of using SIMS on biological samples is its ability to simultaneous detect molecules over a wide mass range (0 to ~1000 m/z), generating a spatial resolution of around 1μm, analysis of the sample surface layer (~5 nm), and the minimal need for tissue processing. These benefits make ToF-SIMS a unique and ideal biological tool for studying small molecules (e.g. lipids) in brain tissues.

Despite these benefits SIMS does suffer some limitations; chemical fragmentation of molecular ion species is a major issue in SIMS, as is molecular ionization efficiency, and the inability to quantitate. Other consideration that should be taken into account when designing and carrying out experiments on biological samples using SIMS include: rapidly freezing of tissue to prevent molecular redistribution, minimizing tissue processing, exclusion of fixatives and embedding material to avoid contaminating peaks in the SIMS spectrum, and avoidance of freeze-thawing and long-term storage, which can cause decreased analyte signals (Wu *et al.* 2007).

What are lipids and their biological role?

Traditionally lipids are thought of simply as natural saturated hydrocarbons with high solubility in organic solvents, however this view excludes partially water-soluble lipid derived compounds such as gangliosides and phosphoinositides, while also including structurally and functionally unrelated compounds. An alternate and arguably more adequate definition was proposed by W. Christie: "Lipids are fatty acids and their derivatives, and substances related biosynthetically or functionally to these compounds" (Christie 1989). By this definition biomolecules that are structurally and functionally similar and derived from the condensation of malonyl-coenzyme A subunit should be considered lipids (Piomelli 2005).

Most lipids are amphipathic molecules with a polar head group pointing outwards exposed to the extracellular environment, and hydrophobic tails forming a membrane core and bilayer. In the brain, lipids can account for approximately 10% of the wet weight and half of the dry weight (Sastry 1985). There is a wide diversity of lipid classes in brain and nervous tissue, with some occurring in appreciable quantities while others occur in minor but significant amount. Broadly, lipids can exist in non-esterified form with differing levels of unsatruation and chain length. They can also exist in esterified form with differing headgroups and composed of a wide variety of fatty acid side chain lengths and saturation levels. In addition some complex lipids can have their headgroup modified with carbohydrate groups, vastly increasing the complexity of lipid structures found in biological tissues.

Cholesterol is a unique lipid and a major structural component of cell membranes where it helps regulate membrane fluidity and cell permeability but does not form a bilayer on its own. Cholesterol helps regulate membrane fluidity by inserting itself within the membrane, with its polar (-OH) group aligned with the polar headgroup of the adjacent lipid. Within the membrane, the ridged hydrophobic ring structure interacts with the hydrocarbon tail of the lipids decreasing their mobility. In addition to influencing membrane fluidity cholesterol is an important precursor for the synthesis of steroids, fat-soluble vitamins (e.g. vitamin A), and adrenal hormones. Cholesterol along with fatty acid chain length, saturation, and lipid headgroup are determinant factors in controlling membrane fluidity, permeability, and influencing cell membrane protein interactions.

Non-esterified fatty acids

Fatty acids in the nervous tissue mainly occur as esterified components of complex lipids of glycerolipids and sphingolipids. Typically fatty acids have even number of carbon side chains, although some odd-numbered side chain fatty acids are known to exist. Fatty acids exist as either saturated, mono-unsaturated, or in polyunsaturated form and are important molecules in cell signaling and as precursors for the synthesis of other metabolites (i.e. ecosenoids) (Das 2006, Chen & Bazan 2005). In addition they are associated with important neurological diseases and disorders such as Parkinson's, Alzheimer's, Schizophrenia, and bi-polar disorder (Assayag *et al.* 2007, Fenton *et al.* 2000, Igarashi *et al.* 2009, Hartmann *et al.* 2007).

Non-essential fatty acids are major constituents of the cell lipid profile, they are synthesized de-novo from acetyl Co-A to palmitate, a 16 carbon saturated fatty acid (C16:0) by the multienzyme complex fatty acid synthase (FAS). Palmitic acid subsequently undergoes desaturation and elongation steps converting it into a series of long-chain saturated and mono-unsaturated FAs.

Functionally esterified non-essential fatty acids maintain proper cell integrity (e.g. phospholipids), act as energy storage units in adipose tissue (e.g. triglycerides), and maintain proper membrane fluidity. Non-esterified non-essential fatty acids are identified as important molecules in brain cell function for example, palmitate has been shown to regulate protein trafficking in the neurons (el-Husseini Ael & Bredt 2002), and both

palmitate and stearate can activate caspase-3 and -8 to control cell nerve growth (Ulloth *et al.* 2003).

Essential fatty acids (EFAs) are a distinct class of fatty acids in that they are not synthesized de-novo in mammal or avian species, instead they are required though dietary input. EFAs are of two families: omega-3 FAs derived from α-linolenic acid (C18:3) and omega-6 FAs derived from linoleic acid (C18:2). Both α-linolenic acid and linoleic acid serve as precursor fatty acids that can undergo a series of elongation and desaturation steps, utilizing the cells own machinery, to convert them into other long-chain fatty acids or cellular metabolites.

Two polyunsaturated EFAs that have been well studied in brain are the omega-3 FA docosahexaenoic acid (DHA; C22:6), and the omega-6 FA, arachidonic acid (AA; C20:4). In brain DHA is linked to improved learning and memory in rats, mice (He *et al.* 2009) and humans (Innis 2008). Cellular DHA has been shown to promote neurite growth in hippocampal neurons by increasing neurite length and branching (Calderon & Kim 2004, He et al. 2009), accelerating neuron growth, and inducing immediate-early gene responses during neurogenesis (Dagai *et al.* 2009). Conversely deficiencies in DHA negatively impact cognitive function and learning and memory in rats (Moriguchi *et al.* 2000), is associated with reduced neuron size (Ahmad *et al.* 2002) and delayed cell migration in developing rat brains (Yavin *et al.* 2009).

In contrast to DHA, arachidonic acid is associated with numerous neurodegenerative diseases and disorders, such as Alzheimer's and Parkinson's (Youdim *et al.* 2000, Adamczyk *et al.* 2007). Arachidonic acid can also be metabolized into proinflammatory immunological response agents (e.g. prostaglandin and lukotrienes), act as a vasoconstrictor, and induce platelet aggregation (Sublette *et al.* 2004). Despite the deleterious roles, arachidonic acid is an important second messenger signaling molecule in the nervous system. For example arachidonic acid is proposed to act as a neuromodulator in glutamatergic synapses, modulating acetylcholine release, and in modulating gene expression (Boksa *et al.* 1988, Berger *et al.* 2002). It also modulates ion channels, induces long-term potentiation, and regulates enzyme activity (Yehuda *et al.* 1998, Clements *et al.* 1991). The functional diversity of fatty acids makes these small molecules of significant interest in the study of brain function and disease.

Complex Lipids

Complex lipids can be broadly divided into two classes, the glycerol-containing lipids, those derived from glycerol-3-phosphate, termed 'glycerolipids', and the sphingosine-containing lipids, or 'sphingolipids'. Glycerolipids consist of three subclasses: 1) neutral glycerides, consiting of mono-, di- and triacyl glycerols; 2) glycolipids which are carbohydrate-attached lipids; and 3) glycerophospholipids, or phospholipids, consisting of phosphatidic acid, choline-, ethanolamine-, serine-, inositol-, phosphatidyl-, and bisphosphatidyl-. The diverse number of head groups as well as substituents on the glycerol hydroxyl gives rise to many molecular species of lipids with distinct chemical properties, making them of great interest in the study of neurological function and neuropathalogy.

Membrane lipids serve several important functional roles. First, they can act as signaling molecules (i.e. arachidonic acid) regulating cell activity, but unlike neurotransmitters and neuropeptides they are not stored in vesicles, instead they are produced on demand through enzymatic cleavage of fatty acids from membrane phospholipids by phospholipases (Sublette *et al.* 2004). The free fatty acid can then be metabolized into second messenger signaling molecules (e.g. ecosinoids). Second, membrane lipids can form microdomains or 'lipid rafts' influencing neurotransmission, cell signaling, membrane fluidity, and protein trafficking. These microdomains are typically enriched in cholesterol and sphingolipids and are approximately 50-200nm in size (Suzuki 2002, Simons & Toomre 2000). Third, the lipid headgroup can influence membrane voltage gated transporter proteins and electrochemical gradients (Schmidt *et al.* 2006). Lipids are a diverse group of small molecules associated with a wide array of cellular functions including cell structure, signaling, and disease. However, many of the methods available to study them have remained limited to crude dissection and homogenization techniques, thus limiting their study.

Lipids and songbirds

A limited number of lipid studies have focused on songbirds, most focusing on lipid changes in a variety of tissues related to physiological responses to migration and

environmental changes (Conway *et al.* 1994, Pierce *et al.* 2005, Smith *et al.* 2007). Only a few studies have focused on lipids and the zebra finch brain with most focusing on the interaction of lipids and synuclein, a protein associated with β-amyloid plaques in patients with Parkinson's and Alzheimer's disease (Clayton & George 1999, Perrin *et al.* 2000). However, a recent study did investigate the relative change in lipid and fatty acid content in different zebra finch tissues, including the brain, under different diets. In it the authors concluded that brain lipid and fatty acid profiles show little variation with dietary changes (McCue *et al.* 2009). Due to the importance of the zebra finch as a model organism in neurobiology there is significant benefit to applying analytical tools such as ToF-SIMS to study lipids in the zebra finch brain.

Studies with biological samples using ToF-SIMS

ToF-SIMS analysis has been applied across a variety of biological and biosynthetic surfaces revealing unique distributions of lipids and other small molecules. Imaging lipid heterogeneities across chemically complex samples has helped address their potential role and biological importance.

One of the first cellular applications with ToF-SIMS was to study the heterogeneity of lipid membrane distribution during *Tetrahymena* mating (Ostrowski *et al.* 2004). It was shown that at the membrane fusion region between the two cells there is a relative decrease in phosphocholine but an elevated concentration of a phosphatidylethanolamine analogue, which is thought to allow greater membrane curvature required during matting. Cellular studies using ToF-SIMS imaging have also revealed increased levels of vitamin E at the soma-neurite junction in isolated neurons from *Aplysia californica* (Monroe *et al.* 2005). Thus, supporting the idea that vitamin E plays a functional role in the transport and/or cellular signaling in neurons (Rimbach *et al.* 2002). In addition, ToF-SIMS has been used to localize membrane lipids in blood cells (Sjovall *et al.* 2003) and thyroid tumor cells (Nygren *et al.* 2007), and used to differentiate breast cancer cells (Kulp *et al.* 2006).

A number of ToF-SIMS studies have been carried out on whole tissues, detecting and imaging lipids to reveal their subcellular distribution. One of the first studies involved imaging lipid distributions across a whole coronal mouse brain section (Sjovall

et al. 2004). Here the spatial distribution of various lipids including sulfatides, phophatidylinositols and cholesterol were imaged showing large variations in lipid composition across different regions of the mouse brain. More recently a whole mouse embryo was imaged and chemical differences were identified between different tissues (Wu et al. 2007). Lipid heterogeneities have also been identified on rat kidney tissue (Nygren *et al.* 2004) and in rat cerebellum showing distribution differences between the molecular layer, the Purkinje cells, and granular layer (Pernber *et al.* 2007, Nygren *et al.* 2005). Although ToF-SIMS cannot address questions related to the functional role of lipids, it does allow us to correlate functional biochemical evidence with imaging data.

The ability of ToF-SIMS to image at a submicron level, surface molecules, has made it a unique tool to study lipid-lipid and lipid-protein interaction or "lipid rafts" (McQuaw *et al.* 2006). Langmuir-Blodgett (LB) films subjected to ToF-SIMS have shown that sphingomyelin preferentially localizes with cholesterol on surface monolayers (McQuaw *et al.* 2007), and that cholesterol preferentially interacts with saturated lipids in the formation of lipid-cholesterol rafts (Zheng *et al.* 2007, Zheng *et al.* 2008). These experiments demonstrate that ToF-SIMS is a powerful tool in visualizing the subcellular resolution of lipids and other small molecules across complex biological tissues. It also serves to chemically profile and differentiate samples, and investigate small molecule interactions.

ToF-SIMS data analysis

SIMS imaging analysis often involves simply observing the spatial distribution of a particular molecule across the collected area as well as overlaying images that represent different molecules to observe differences in distribution. Other methods that are used involve analyzing relative signal across an image (i.e. linescan analysis) and comparing spectra from different spots on an image (i.e. region of interest analysis). A major limitation of these methods are that it is time consuming especially with complex SIMS spectra, spatial distribution differences are difficult to observe with low signal intensity molecules, and comparisons between different samples is challenging. To address these issues multivariate statistical methods have been adopted for SIMS data analysis.

Principle component analysis (PCA) and partial least squares discriminant analysis (PLS-DA) are two multivariate statistical analysis (MVA) methods used to reduce large complex chemical data sets into a few manageable variables that can efficiently extract information representing chemical differences and similarities between samples (Lindon et al. 2007). They are used to describe observations (e.g. mass spectra) with regard to one or more latent variables termed principle components (PCs). From the original variables a set of PCs are generated, each accounting for a decreasing proportion of the variance in the data. Each observation is subsequently assigned a score along each PC and is graphically represented on a scores plot, therefore similar observations will cluster together. To determine which variables of the original data are responsible for the separation on the scores plot, the corresponding loadings plot can be analyzed. A loadings plot represents the weights given to each variable within a given PC and its influence on the relation between variables to each other. PCA and PLS-DA are similar methods and are typically used together in data analysis, with PCA often being used as an initial data processing step. A major difference between PCA and PLS-DA is that PLS-DA takes into account sample classification in calculating sample relation or correlation, therefore it is used to sharpen differences between samples and to help identify unknown samples.

PCA has been applied to many biological SIMS experiments. It has revealed spectral differences in brain tissue (Sjovall et al. 2004), differences between mouse embryo tissues (Wu et al. 2007), and identify cell specific biomarkers from different breast cancer cell types (Kulp et al. 2006). During data analysis it is important to keep in mind that topographical features can affect imaging and should be corrected for (Monroe et al. 2005). In addition when comparing SIMS ion spectra it is important to normalize to a ubiquitous and biologically significant molecule. Finally, when using MVA methods, sample and experimental considerations should be taken into account when preprocessing the data, since these can influence data output and interpretation (Wagner *et al.* 2004).

Future outlook for ToF-SIMS

In the past lipid biology has lacked a viable technique to visualize subcellular lipid heterogeneities. This has greatly limited lipids studies despite their biological

importance and association with disease and disorders. ToF-SIMS now allows biologists to address long-standing questions about lipid-lipid interactions and the role lipids play in human pathology. It has already been used to identify high amounts of non-esterified fatty acids as well as a heterogeneous distribution of lipids and vitamin E in atherosclerotic tissue (Mas *et al.* 2007, Malmberg *et al.* 2007). It has revealed lipid and vitamin E heterogeneities on human striated muscle samples from children affected with muscular dystrophy (Tahallah *et al.* 2008), and in identifying potential biomarkers from different human breast cancer cell types (Kulp et al. 2006). Therefore, some of the most likely applications of SIMS in biology are in studying lipid associated cardiovascular and brain diseases and disorders.

Most of the lipids detected to date using ToF-SIMS make up high concentrations in cells, therefore a challenge for SIMS will be to expand detection to lower concentration lipids and increase the diversity of small molecules detected. Continued advances with SIMS have addressed some of these issues, for example sample surface coating with Au and Ag enhances ionization of surface molecules, decreasing collection times and improving the ability to detect lower yield molecules (Altelaar *et al.* 2006, Nygren et al. 2004, Nygren et al. 2007, Sjovall et al. 2003).

A major advance in the adoption of SIMS in biology is the availability of softer ionization methods (i.e. Au, Bi, and C_{60}) (Ostrowski *et al.* 2005). In addition coupling SIMS with tandem mass spectrometry (MS/MS) will enhance identification of unknown molecules (Carado *et al.* 2008). Although polyatomic cluster ions have improved detection of higher molecular weight ion, the number of secondary ions is significantly decreased, resulting in longer collection times (Brunelle *et al.* 2005). Despite challenges and limitations with ToF-SIMS, it has already proven to be a valuable tool for biologists. Combining it with other techniques such as immunohistochemistry, MVA methods, and quantitative analytical methods, will allow for greater interpretation of biologically significant results.

METABOLOMICS TO STUDY SMALL MOLECULES

The ability to uncover biochemical differences between normal and diseased tissue or tissue exposed to an environmental stimulus can provide a detailed description

of the status and function of biochemical process during different cellular states. This process of monitoring changes in metabolites has led to the terms "metabonomics" and "metabolomics". In 1999 Jeremy Nicholson and colleagues formally defined metabonomics as "the quantitative measurement of the dynamic multiparametric metabolic response of living systems to pathophysiological stimuli or genetic modification" (Nicholson *et al.* 1999). Then in 2001 Oliver Fiehn defined metabolomics as a "comprehensive and quantitative analysis of all metabolites" in a system (Lindon *et al.* 2007). Although both terms are increasingly being used interchangeably, the term metabonomics is more prevalent in the field of NMR spectroscopy and when metabolic profiling may not include a comprehensive analysis of a system. On the other hand, metabolomics appears more prevalent among mass-spectrometry based techniques and when comprehensive analyses of metabolite changes is carried out. For this reason metabolomics will be used throughout this dissertation.

Techniques and methods for metabolomic profiling and data analysis

Three technologies have been widely used for metabolite analysis of biological tissues and fluids, each have associated advantages and disadvantages. One of most widely used methods in metabonomics is nuclear magnetic resonance (NMR). It is a nondestructive method providing information on molecular structure and relative concentration in complex mixtures. In addition to being a non-destructive method it requires little sample preparation, is high-throughput, and can detect a wide range of metabolites. The main disadvantage is a lack of sensitivity of low concentration metabolites, thus making NMR more widely used for easily attainable samples, such as biofluids (e.g. blood and urine) (Zhang *et al.* 2009, Fujiwara *et al.* 2009).

Gas chromatography mass spectrometry (GC-MS) has been widely used for metabolite analysis of biological tissue and is well suited for small sample volumes due to greater sensitivity over other methods. However, this method does suffer certain disadvantages, namely metabolite extraction is more laborious and polar metabolites are less detectable unless they are chemically derivatized (Wang 2008). Despite certain disadvantages GC-MS is well suited for the detection of a range of metabolites including: polar organics, amino acids, lipids, and sugars.

Metabolite analysis by liquid chromatography mass spectrometry (LC-MS) is an increasingly popular method for analysis with the advantage that compound derivatization is not required and some samples can be injected directly into the instrument (e.g. urine) (Gika *et al.* 2008). However, an advantage of GC-MS based metabolomics is that identification of unknown metabolites is easier due to more comprehensive databases (Lindon et al. 2007).

As with SIMS data analysis, multivariate statistical methods (e.g. PCA and PLS-DA) can be applied to metabolomic data collected using either NMR or mass spectrometry based methods. As stated above MVA methods allows one to more efficiently analyze all of the collected data at once, by reducing the complexity of the data to identify relationships between samples and identify key metabolites that exhibit significant variation between samples.

Metabolomic studies in brain

The global study of metabolites is a relatively new but rapidly growing field with the potential to identify major metabolic differences between a variety of biological conditions and samples. Its application in the study of brain neurochemistry will enhance our understanding of many central nervous system disorders, which have been identified as having biochemical abnormalities (Kaddurah-Daouk & Krishnan 2009). Moreover, it will complement genomic and protomic data used to uncover cellular and tissue changes under a variety of conditions (i.e. age, nutrition, toxicity, stimulus). Therefore such a global analysis is critical in identifying biomarkers that can accurately identify disease states, progression, and response to treatment, as well as in studying biochemical changes under a variety of environmental conditions.

Metabolomics can be applied as a valuable functional genomic tool capable of identifying biochemical differences in tissues afflicted with genetic disorders. In one such study different brain regions from wild type control mice and mice deficient in the expression of Vesicular Monoamine Transporter 2 (VMAT2), which is involved in sequestering monoamines into synaptic vesicles , were compared and mice deficient in VMAT2 showed deceased levels of taurine and creatine/phosphocreatine and increases in glutamate and N-acetyl aspartate, suggesting a complex biochemical alteration between

wild type and VMAT2 deficient mice (Salek *et al.* 2008). A number of other metabolomic studies have been carried out identifying differences between wild type and gene knockout or expression deficient animal models (Griffin *et al.* 2002, Griffin *et al.* 2004, Jones *et al.* 2005, Pears *et al.* 2005). These experiments demonstrate that metabolite profiling used in combination with MVA methods serve as viable tool for functional genomic phenotyping and biomarker identification.

Cellular diversity and complexity in the brain offers a significant challenge for metabolomic studies, an example of such complexity is shown in a study by Tsang, TM et al. in which rat brain stem, cerebellum, frontal cortex, and hippocampus were dissected and subjected to NMR analysis. The results showed that each brain region had a distinct metabolomic profile and by applying MVA methods (e.g. PSLDA) they were able to differentiate brain regions (Tsang *et al.* 2005). Not only was this study important in characterizing the metabolomic profile of different brain regions but serves to highlight the importance of careful sample dissection when carrying out metabolomic studies. Clearly, challenges exist in the analysis of brain tissue, however a number of studies have demonstrated its promise applied to neurobiology.

Future outlook for metabolomics

Development of new and improved technologies will be critical in obtaining a more complete picture of a cells and tissues metabolome. Many improvements will likely come from better separation and detection methods, and improved database and software analysis tools capable of better pattern recognition and peak identification. Enhanced statistical tools will also be critical in identifying biomarkers and reducing unwanted influences caused by internal (e.g. genetic makeup) and external (e.g. environment) factors.

One of the biggest challenges is to integrate and cross correlate genomic, proteomic, and metabolomic data to identify global differences between cells and tissues. The aim of systems biology is to integrate global analysis methods to generate complementary information and obtain a more accurate picture of the biochemical and transcriptomic states between samples (Watkins *et al.* 2002).

SUMMARY

The ability of songbirds to undergo learned vocal communication and the discovery that the regions involved in learning and memory are anatomically discreet interconnected brain areas makes them an attractive model to study brain development and molecular changes upon song exposure. The discovery that many small molecule binding and interacting molecules are associated with these brain areas and exhibit dynamic changes during development and learning and memory makes them of considerable interest in the study of the zebra finch brain. Lipids represent a specific class of small molecule that play a variety of cellular functions as well as being associated with neurological diseases and disorders. More importantly lipid and lipophilic interacting molecules show expression differences in the zebra finch song system. Advances with ToF-SIMS have now allowed for the detection and subcellular imaging of lipids on biological tissue, which traditionally have relied on crude sample dissection and detection providing no spatial distribution information.

Metabolomics is an increasingly important field of research uncovering global biochemical differences in cells and tissue after an environmental stimulus (i.e. song exposure) and in studying disease. Utilizing metabolomic methods coupled with statistical tools and harnessing information generated though genomic and proteomic studies one can study global changes using a systems biology approach. Genomic and proteomic studies focusing on the auditory lobule of the zebra finch have already identified changes upon song exposure. Therefore metabolomic studies focusing on AL combined with a global analysis using genomic, proteomic, and metabolomic data has the potential to significantly enhance our understanding of biochemical and cellular changes that occur during learning and memory.

QUESTIONS ADDRESSED IN THE DISSERTATION

Taking advantage of advances in Time of Flight – Secondary Ion Mass Spectrometry, metabolomics, and systems biology I seek to investigate the distribution and changes of small molecules in the zebra finch song system. My dissertation will address three overall topics:

1) Use ToF-SIMS to generate a high-resolution subcellular map of small molecules across a whole adult male sagittal brain section.

This chapter seeks to utilize advances in imaging mass spectrometry to detect and image a class of small molecules (e.g. lipids) to investigate their subcellular distribution in brain. Utilizing a whole adult male sagittal brain section, focusing on RA and HVC, will allow us to better understand differences in brain neurochemistry.

2) Does the ToF-SIMS chemical profile show age related differences in RA before innervation by HVC projection neurons (post hatch day 20), after innervation is complete (p40), and in adults? Do the different song nuclei exhibit unique ToF-SIMS chemical profiles? Do the song nuclei show significant differences in fatty acid distribution compared to the surrounding tissue?

The aim of this chapter is to expand on the investigations from chapter 2. I will use ToF-SIMS to collect small molecule chemical information and use MVA methods to analyze the chemical data. Immunohistochemistry will be used correlate chemical differences observed by ToF-SIMS from AreaX, LMAN, DLM, HVC, RA and the auditory lobule, to histological information.

3) Do zebra finches exhibit unique metabolic profiles under different song states (song vs. silence) and can I identify potential biomarkers unique to each song state? Can we identify specific metabolic pathways as changing after song stimulation using a systems biology approach?

This chapter aims to investigate metabolic changes upon song stimulation in the auditory lobule. It also aims to utilize metabolic data in combination with previously generated transcriptional data, to provide a more comprehensive picture of the dynamic cellular changes that take place during learning and memory.

FIGURES AND TABLES

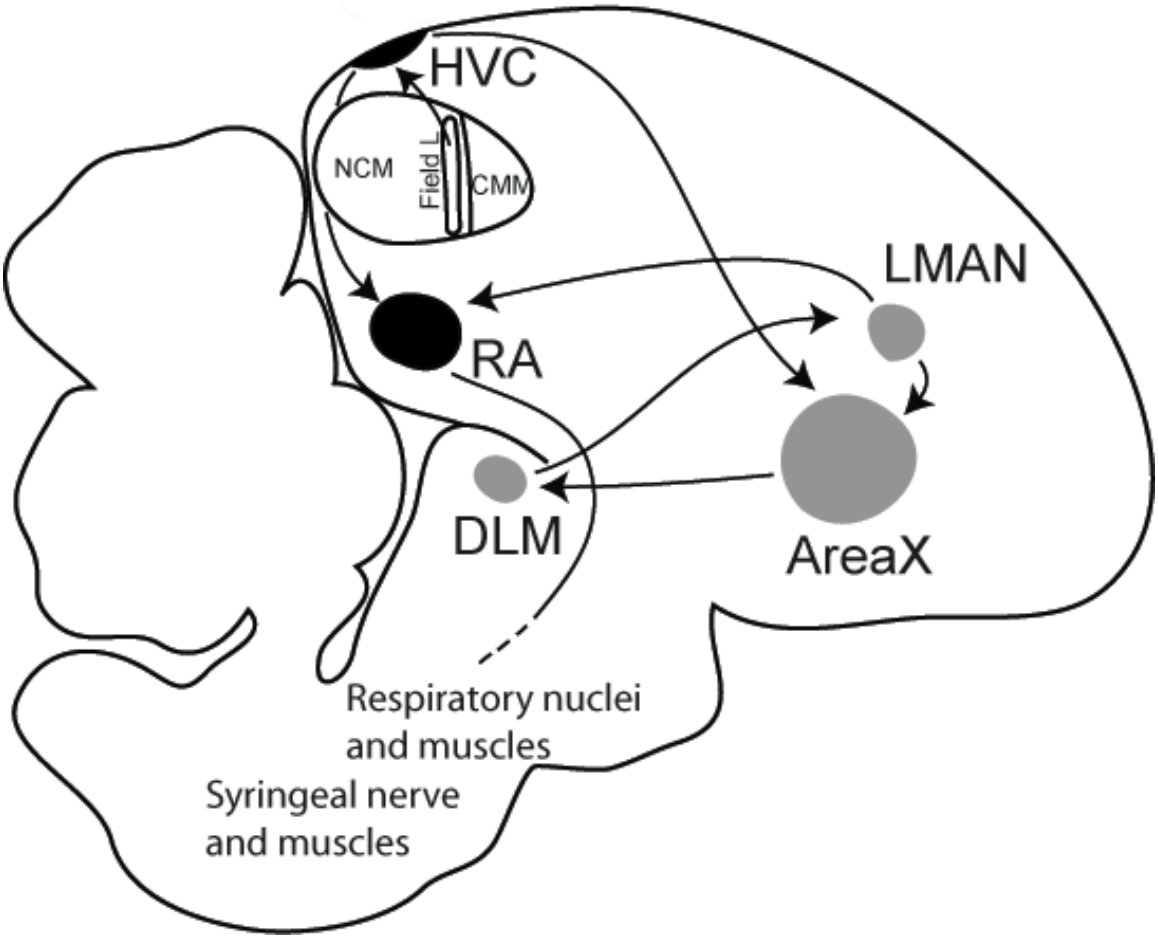

Figure 1.1. Schematic drawing of a sagittal section of an adult male zebra finch brain showing the major song nuclei and neuronal connections in the song system. The anterior forebrain pathway, in grey, is composed of AreaX, lateral magnocellular nucleus of the anterior nidopallium (LMAN), and the dorso-medial division of the medial thalamus (DLM). In white the auditory forebrain pathway includes Field L, caudal medial mesopallium (CMM), and the caudal medial nidopallium (NCM), and makes up the auditory lobule (AL). In black is the song motor pathway composed of the robust nucleus of the arcopallium (RA) and HVC.

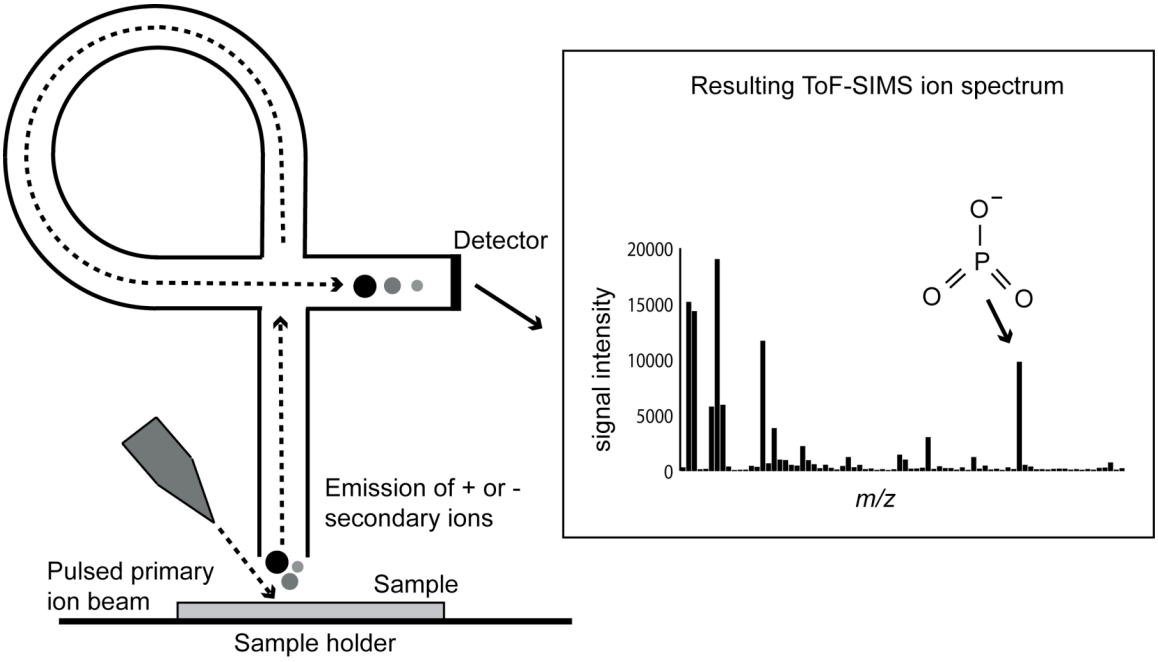

Figure 1.2. Illustration depicting Time of Flight – Secondary Ion Mass Spectrometry.

REFERENCES

Adamczyk, A., Kacprzak, M. and Kazmierczak, A. (2007) Alpha-synuclein decreases arachidonic acid incorporation into rat striatal synaptoneurosomes. Folia Neuropathol, 45, 230-235.

Ahmad, A., Murthy, M., Greiner, R. S., Moriguchi, T. and Salem, N., Jr. (2002) A decrease in cell size accompanies a loss of docosahexaenoate in the rat hippocampus. Nutr Neurosci, 5, 103-113.

Altelaar, A. F., Klinkert, I., Jalink, K., de Lange, R. P., Adan, R. A., Heeren, R. M. and Piersma, S. R. (2006) Gold-enhanced biomolecular surface imaging of cells and tissue by SIMS and MALDI mass spectrometry. Anal Chem, 78, 734-742.

Assayag, K., Yakunin, E., Loeb, V., Selkoe, D. J. and Sharon, R. (2007) Polyunsaturated fatty acids induce alpha-synuclein-related pathogenic changes in neuronal cells. Am J Pathol, 171, 2000-2011.

Berger, A., Mutch, D. M., German, J. B. and Roberts, M. A. (2002) Dietary effects of arachidonate-rich fungal oil and fish oil on murine hepatic and hippocampal gene expression. Lipids Health Dis, 1, 2.

Bilderback, T. R., Chan, J. R., Harvey, J. J. and Glaser, M. (1997) Measurement of the rate of myelination using a fluorescent analogue of ceramide. J Neurosci Res, 49, 497-507.

Boksa, P., Mykita, S. and Collier, B. (1988) Arachidonic acid inhibits choline uptake and depletes acetylcholine content in rat cerebral cortical synaptosomes. J Neurochem, 50, 1309-1318.

Bottjer, S. W. and Johnson, F. (1997) Circuits, hormones, and learning: vocal behavior in songbirds. J Neurobiol, 33, 602-618.

Bottjer, S. W., Miesner, E. A. and Arnold, A. P. (1984) Forebrain lesions disrupt development but not maintenance of song in passerine birds. Science, 224, 901-903.

Brunelle, A., Touboul, D. and Laprevote, O. (2005) Biological tissue imaging with time-of-flight secondary ion mass spectrometry and cluster ion sources. J Mass Spectrom, 40, 985-999.

Calderon, F. and Kim, H. Y. (2004) Docosahexaenoic acid promotes neurite growth in hippocampal neurons. J Neurochem, 90, 979-988.

Carado, A., Kozole, J., Passarelli, M., Winograd, N., Loboda, A., Bunch, J., Wingate, J., Hankin, J. and Murphy, R. (2008) Biological tissue imaging with a hybrid cluster SIMS quadrupole time-of-flight mass spectrometer. Applied Surface Science, 255, 1572-1575.

Chen, C. and Bazan, N. G. (2005) Lipid signaling: sleep, synaptic plasticity, and neuroprotection. Prostaglandins Other Lipid Mediat, 77, 65-76.

Christie, W. W. (1989) Gas chromatography and lipids : a practical guide. Oily, Ayr, Scotland.

Clayton, D. F. (1997) Role of gene regulation in song circuit development and song learning. J Neurobiol, 33, 549-571.

Clayton, D. F. and George, J. M. (1999) Synucleins in synaptic plasticity and neurodegenerative disorders. J Neurosci Res, 58, 120-129.

Clements, M. P., Bliss, T. V. and Lynch, M. A. (1991) Increase in arachidonic acid concentration in a postsynaptic membrane fraction following the induction of long-term potentiation in the dentate gyrus. Neuroscience, 45, 379-389.
Conway, C. J., Eddleman, W. R. and Simpson, K. L. (1994) Seasonal-Changes in Fatty-Acid Composition of the Wood-Thrush. Condor, 96, 791-794.
Dagai, L., Peri-Naor, R. and Birk, R. Z. (2009) Docosahexaenoic acid significantly stimulates immediate early response genes and neurite outgrowth. Neurochem Res, 34, 867-875.
Das, U. N. (2006) Essential fatty acids: biochemistry, physiology and pathology. Biotechnol J, 1, 420-439.
Davidson, W. S., Jonas, A., Clayton, D. F. and George, J. M. (1998) Stabilization of alpha-synuclein secondary structure upon binding to synthetic membranes. J Biol Chem, 273, 9443-9449.
Denisenko-Nehrbass, N. I., Jarvis, E., Scharff, C., Nottebohm, F. and Mello, C. V. (2000) Site-specific retinoic acid production in the brain of adult songbirds. Neuron, 27, 359-370.
Dong, S., Replogle, K. L., Hasadsri, L., Imai, B. S., Yau, P. M., Rodriguez-Zas, S., Southey, B. R., Sweedler, J. V. and Clayton, D. F. (2009) Discrete molecular states in the brain accompany changing responses to a vocal signal. Proc Natl Acad Sci U S A, 106, 11364-11369.
Doupe, A. J. and Kuhl, P. K. (1999) Birdsong and human speech: common themes and mechanisms. Annu Rev Neurosci, 22, 567-631.
Doupe, A. J. and Solis, M. M. (1997) Song- and order-selective neurons develop in the songbird anterior forebrain during vocal learning. J Neurobiol, 33, 694-709.
el-Husseini Ael, D. and Bredt, D. S. (2002) Protein palmitoylation: a regulator of neuronal development and function. Nat Rev Neurosci, 3, 791-802.
Ellis, C. E., Murphy, E. J., Mitchell, D. C., Golovko, M. Y., Scaglia, F., Barcelo-Coblijn, G. C. and Nussbaum, R. L. (2005) Mitochondrial lipid abnormality and electron transport chain impairment in mice lacking alpha-synuclein. Mol Cell Biol, 25, 10190-10201.
Ewing, A. G. (2006) Molecule specific imaging in biology: What are the challenges and the important applications? Applied Surface Science, 252, 6821-6826.
Fenton, W. S., Hibbeln, J. and Knable, M. (2000) Essential fatty acids, lipid membrane abnormalities, and the diagnosis and treatment of schizophrenia. Biol Psychiatry, 47, 8-21.
Fujiwara, M., Kobayashi, T., Jomori, T., Maruyama, Y., Oka, Y., Sekino, H., Imai, Y. and Takeuchi, K. (2009) Pattern recognition analysis for H-1 NMR spectra of plasma from hemodialysis patients. Analytical and Bioanalytical Chemistry, 394, 1655-1660.
George, J. M., Jin, H., Woods, W. S. and Clayton, D. F. (1995) Characterization of a novel protein regulated during the critical period for song learning in the zebra finch. Neuron, 15, 361-372.
Gika, H. G., Theodoridis, G., Extance, J., Edge, A. M. and Wilson, I. D. (2008) High temperature-ultra performance liquid chromatography-mass spectrometry for the metabonomic analysis of Zucker rat urine. J Chromatogr B, 871, 279-287.

Griffin, J. L., Cemal, C. K. and Pook, M. A. (2004) Defining a metabolic phenotype in the brain of a transgenic mouse model of spinocerebellar ataxia 3. Physiol Genomics, 16, 334-340.
Griffin, J. L., Muller, D., Woograsingh, R., Jowatt, V., Hindmarsh, A., Nicholson, J. K. and Martin, J. E. (2002) Vitamin E deficiency and metabolic deficits in neuronal ceroid lipofuscinosis described by bioinformatics. Physiol Genomics, 11, 195-203.
Grisham, W. and Arnold, A. P. (1995) A direct comparison of the masculinizing effects of testosterone, androstenedione, estrogen, and progesterone on the development of the zebra finch song system. J Neurobiol, 26, 163-170.
Grisham, W., Mathews, G. A. and Arnold, A. P. (1994) Local intracerebral implants of estrogen masculinize some aspects of the zebra finch song system. J Neurobiol, 25, 185-196.
Guerquin-Kern, J. L., Wu, T. D., Quintana, C. and Croisy, A. (2005) Progress in analytical imaging of the cell by dynamic secondary ion mass spectrometry (SIMS microscopy). Biochim Biophys Acta, 1724, 228-238.
Hartmann, T., Kuchenbecker, J. and Grimm, M. O. (2007) Alzheimer's disease: the lipid connection. J Neurochem, 103 Suppl 1, 159-170.
He, C., Qu, X., Cui, L., Wang, J. and Kang, J. X. (2009) Improved spatial learning performance of fat-1 mice is associated with enhanced neurogenesis and neuritogenesis by docosahexaenoic acid. Proc Natl Acad Sci U S A, 106, 11370-11375.
Herrmann, K. and Arnold, A. P. (1991) The development of afferent projections to the robust archistriatal nucleus in male zebra finches: a quantitative electron microscopic study. J Neurosci, 11, 2063-2074.
Holloway, C. C. and Clayton, D. F. (2001) Estrogen synthesis in the male brain triggers development of the avian song control pathway in vitro. Nat Neurosci, 4, 170-175.
Huesmann, G. R. and Clayton, D. F. (2006) Dynamic role of postsynaptic caspase-3 and BIRC4 in zebra finch song-response habituation. Neuron, 52, 1061-1072.
Igarashi, M., Ma, K., Gao, F., Kim, H. W., Greenstein, D., Rapoport, S. I. and Rao, J. S. (2009) Brain lipid concentrations in bipolar disorder. J Psychiatr Res.
Innis, S. M. (2008) Dietary omega 3 fatty acids and the developing brain. Brain Res, 1237, 35-43.
Jackson, S. N. and Woods, A. S. (2009) Direct profiling of tissue lipids by MALDI-TOFMS. J Chromatogr B Analyt Technol Biomed Life Sci, 877, 2822-2829.
Jarvis, E. D. (2004) Learned birdsong and the neurobiology of human language. Ann N Y Acad Sci, 1016, 749-777.
Jones, G. L. A. H., Sang, E., Goddard, C. et al. (2005) A functional analysis of mouse models of cardiac disease through metabolic profiling. Journal of Biological Chemistry, 280, 7530-7539.
Kaddurah-Daouk, R. and Krishnan, K. R. R. (2009) Metabolomics: A Global Biochemical Approach to the Study of Central Nervous System Diseases. Neuropsychopharmacol, 34, 173-186.
Kollmer, F. (2004) Cluster primary ion bombardment of organic materials. Applied Surface Science, 231-2, 153-158.

Konishi, M. and Akutagawa, E. (1985) Neuronal growth, atrophy and death in a sexually dimorphic song nucleus in the zebra finch brain. Nature, 315, 145-147.
Konishi, M. and Akutagawa, E. (1988) A critical period for estrogen action on neurons of the song control system in the zebra finch. Proc Natl Acad Sci U S A, 85, 7006-7007.
Kulp, K. S., Berman, E. S., Knize, M. G., Shattuck, D. L., Nelson, E. J., Wu, L., Montgomery, J. L., Felton, J. S. and Wu, K. J. (2006) Chemical and biological differentiation of three human breast cancer cell types using time-of-flight secondary ion mass spectrometry. Anal Chem, 78, 3651-3658.
Lindon, J. C., Nicholson, J. K. and Holmes, E. (2007) The handbook of metabonomics and metabolomics. Elsevier, Amsterdam ; Oxford.
London, S. E., Dong, S., Replogle, K. and Clayton, D. F. (2009) Developmental shifts in gene expression in the auditory forebrain during the sensitive period for song learning. Dev Neurobiol, 69, 437-450.
Maier, O., Oberle, V. and Hoekstra, D. (2002) Fluorescent lipid probes: some properties and applications (a review). Chem Phys Lipids, 116, 3-18.
Malmberg, P., Borner, K., Chen, Y., Friberg, P., Hagenhoff, B., Mansson, J. E. and Nygren, H. (2007) Localization of lipids in the aortic wall with imaging TOF-SIMS. Biochimica Et Biophysica Acta-Molecular and Cell Biology of Lipids, 1771, 185-195.
Margoliash, D. (1997) Functional organization of forebrain pathways for song production and perception. J Neurobiol, 33, 671-693.
Mas, S., Touboul, D., Brunelle, A., Aragoncillo, P., Egido, J., Laprevote, O. and Vivanco, F. (2007) Lipid cartography of atherosclerotic plaque by cluster-TOF-SIMS imaging. Analyst, 132, 24-26.
McCue, M. D., Amitai, O., Khozin-Goldberg, I., McWilliams, S. R. and Pinshow, B. (2009) Effect of dietary fatty acid composition on fatty acid profiles of polar and neutral lipid tissue fractions in zebra finches, Taeniopygia guttata. Comp Biochem Physiol A Mol Integr Physiol, 154, 165-172.
McQuaw, C. M., Sostarecz, A. G., Zheng, L., Ewing, A. G. and Winograd, N. (2006) Investigating lipid interactions and the process of raft formation in cellular membranes using ToF-SIMS. Applied Surface Science, 252, 6716-6718.
McQuaw, C. M., Zheng, L. L., Ewing, A. G. and Winograd, N. (2007) Localization of sphingomyelin in cholesterol domains by imaging mass spectrometry. Langmuir, 23, 5645-5650.
Mello, C. V. and Clayton, D. F. (1995) Differential induction of the ZENK gene in the avian forebrain and song control circuit after metrazole-induced depolarization. J Neurobiol, 26, 145-161.
Monroe, E. B., Jurchen, J. C., Lee, J., Rubakhin, S. S. and Sweedler, J. V. (2005) Vitamin E imaging and localization in the neuronal membrane. J Am Chem Soc, 127, 12152-12153.
Mooney, R. and Rao, M. (1994) Waiting periods versus early innervation: the development of axonal connections in the zebra finch song system. J Neurosci, 14, 6532-6543.

Moriguchi, T., Greiner, R. S. and Salem, N., Jr. (2000) Behavioral deficits associated with dietary induction of decreased brain docosahexaenoic acid concentration. J Neurochem, 75, 2563-2573.
Nicholson, J. K., Lindon, J. C. and Holmes, E. (1999) 'Metabonomics': understanding the metabolic responses of living systems to pathophysiological stimuli via multivariate statistical analysis of biological NMR spectroscopic data. Xenobiotica, 29, 1181-1189.
Nottebohm, F., Stokes, T. M. and Leonard, C. M. (1976) Central control of song in the canary, Serinus canarius. J Comp Neurol, 165, 457-486.
Nygren, H., Borner, K., Hagenhoff, B., Malmberg, P. and Mansson, J. E. (2005) Localization of cholesterol, phosphocholine and galactosylceramide in rat cerebellar cortex with imaging TOF-SIMS equipped with a bismuth cluster ion source. Biochim Biophys Acta, 1737, 102-110.
Nygren, H., Hagenhoff, B., Malmberg, P., Nilsson, M. and Richter, K. (2007) Bioimaging TOF-SIMS: High resolution 3D Imaging of single cells. Microscopy Research and Technique, 70, 969-974.
Nygren, H., Malmberg, P., Kriegeskotte, C. and Arlinghaus, H. F. (2004) Bioimaging TOF-SIMS: localization of cholesterol in rat kidney sections. FEBS Lett, 566, 291-293.
Ostrowski, S. G., Szakal, C., Kozole, J., Roddy, T. P., Xu, J. Y., Ewing, A. G. and Winograd, N. (2005) Secondary ion MS imaging of lipids in picoliter vials with a buckminsterfullerene ion source. Analytical Chemistry, 77, 6190-6196.
Ostrowski, S. G., Van Bell, C. T., Winograd, N. and Ewing, A. G. (2004) Mass spectrometric imaging of highly curved membranes during Tetrahymena mating. Science, 305, 71-73.
Pears, M. R., Cooper, J. D., Mitchison, H. M., Mortishire-Smith, R. J., Pearce, D. A. and Griffin, J. L. (2005) High resolution H-1 NMR-based metabolomics indicates a neurotransmitter cycling deficit in cerebral tissue from a mouse model of Batten disease. Journal of Biological Chemistry, 280, 42508-42514.
Pernber, Z., Richter, K., Mansson, J. E. and Nygren, H. (2007) Sulfatide with different fatty acids has unique distributions in cerebellum as imaged by time-of-flight secondary ion mass spectrometry (TOF-SIMS). Biochim Biophys Acta, 1771, 202-209.
Perrin, R. J., Woods, W. S., Clayton, D. F. and George, J. M. (2000) Interaction of human alpha-Synuclein and Parkinson's disease variants with phospholipids. Structural analysis using site-directed mutagenesis. J Biol Chem, 275, 34393-34398.
Pierce, B. J., McWilliams, S. R., O'Connor, T. P., Place, A. R. and Guglielmo, C. G. (2005) Effect of dietary fatty acid composition on depot fat and exercise performance in a migrating songbird, the red-eyed vireo. Journal of Experimental Biology, 208, 1277-1285.
Pinaud, R., Osorio, C., Alzate, O. and Jarvis, E. D. (2008) Profiling of experience-regulated proteins in the songbird auditory forebrain using quantitative proteomics. European Journal of Neuroscience, 27, 1409-1422.
Piomelli, D. (2005) The challenge of brain lipidomics. Prostaglandins Other Lipid Mediat, 77, 23-34.

Polymeropoulos, M. H., Lavedan, C., Leroy, E. et al. (1997) Mutation in the alpha-synuclein gene identified in families with Parkinson's disease. Science, 276, 2045-2047.
Reiner, A., Perkel, D. J., Bruce, L. L. et al. (2004) Revised nomenclature for avian telencephalon and some related brainstem nuclei. J Comp Neurol, 473, 377-414.
Rimbach, G., Minihane, A. M., Majewicz, J., Fischer, A., Pallauf, J., Virgli, F. and Weinberg, P. D. (2002) Regulation of cell signalling by vitamin E. Proc Nutr Soc, 61, 415-425.
Salek, R. M., Colebrooke, R. E., Macintosh, R., Lynch, P. J., Sweatman, B. C., Emson, P. C. and Griffin, J. L. (2008) A metabolomic study of brain tissues from aged mice with low expression of the vesicular monoamine transporter 2 (VMAT2) gene. Neurochem Res, 33, 292-300.
Sastry, P. S. (1985) Lipids of nervous tissue: composition and metabolism. Prog Lipid Res, 24, 69-176.
Schmidt, D., Jiang, Q. X. and MacKinnon, R. (2006) Phospholipids and the origin of cationic gating charges in voltage sensors. Nature, 444, 775-779.
Simons, K. and Toomre, D. (2000) Lipid rafts and signal transduction. Nat Rev Mol Cell Biol, 1, 31-39.
Sjovall, P., Lausmaa, J. and Johansson, B. (2004) Mass spectrometric imaging of lipids in brain tissue. Anal Chem, 76, 4271-4278.
Sjovall, P., Lausmaa, J., Nygren, H., Carlsson, L. and Malmberg, P. (2003) Imaging of membrane lipids in single cells by imprint-imaging time-of-flight secondary ion mass spectrometry. Analytical Chemistry, 75, 3429-3434.
Smith, S. B., McWilliams, S. R. and Guglielmo, C. G. (2007) Effect of diet composition on plasma metabolite profiles in a migratory songbird. Condor, 109, 48-58.
Sohrabji, F., Nordeen, E. J. and Nordeen, K. W. (1990) Selective impairment of song learning following lesions of a forebrain nucleus in the juvenile zebra finch. Behav Neural Biol, 53, 51-63.
Sublette, M. E., Russ, M. J. and Smith, G. S. (2004) Evidence for a role of the arachidonic acid cascade in affective disorders: a review. Bipolar Disord, 6, 95-105.
Suzuki, T. (2002) Lipid rafts at postsynaptic sites: distribution, function and linkage to postsynaptic density. Neurosci Res, 44, 1-9.
Tahallah, N., Brunelle, A., De La Porte, S. and Laprevote, O. (2008) Lipid mapping in human dystrophic muscle by cluster-time-of-flight secondary ion mass spectrometry imaging. J Lipid Res, 49, 438-454.
Tsang, T. M., Griffin, J. L., Haselden, J., Fish, C. and Holmes, E. (2005) Metabolic characterization of distinct neuroanatomical regions in rats by magic angle spinning H-1 nuclear magnetic resonance spectroscopy. Magnet Reson Med, 53, 1018-1024.
Ueda, K., Fukushima, H., Masliah, E. et al. (1993) Molecular cloning of cDNA encoding an unrecognized component of amyloid in Alzheimer disease. Proc Natl Acad Sci U S A, 90, 11282-11286.
Ulloth, J. E., Casiano, C. A. and De Leon, M. (2003) Palmitic and stearic fatty acids induce caspase-dependent and -independent cell death in nerve growth factor differentiated PC12 cells. J Neurochem, 84, 655-668.

Vates, G. E., Broome, B. M., Mello, C. V. and Nottebohm, F. (1996) Auditory pathways of caudal telencephalon and their relation to the song system of adult male zebra finches. J Comp Neurol, 366, 613-642.
Vickerman, J. C., Briggs, D. and SurfaceSpectra Ltd. (2001) ToF-SIMS : surface analysis by mass spectrometry. IM, Chichester.
Wagner, M. S., Graham, D. J., Ratner, B. D. and Castner, D. G. (2004) Maximizing information obtained from secondary ion mass spectra of organic thin films using multivariate analysis. Surf Sci, 570, 78-97.
Wang, F. (2008) Biomarker methods in drug discovery and development: Methods in pharmacology and toxicology. Humana Press, Totowa, NJ.
Watkins, S. M., Reifsnyder, P. R., Pan, H., German, J. B. and Leiter, E. H. (2002) Lipid metabolome-wide effects of the PPAR gamma agonist rosiglitazone. Journal of Lipid Research, 43, 1809-1817.
Wu, L., Lu, X., Kulp, K. S., Knize, M. G., Berman, E. S. F., Nelson, E. J., Felton, J. S. and Wu, K. J. J. (2007) Imaging and differentiation of mouse embryo tissues by ToF-SIMS. International Journal of Mass Spectrometry, 260, 137.
Yavin, E., Himovichi, E. and Eilam, R. (2009) Delayed cell migration in the developing rat brain following maternal omega 3 alpha linolenic acid dietary deficiency. Neuroscience, 162, 1011-1022.
Yehuda, S., Rabinovitz, S., Carasso, R. L. and Mostofsky, D. I. (1998) Fatty acids and brain peptides. Peptides, 19, 407-419.
Youdim, K. A., Martin, A. and Joseph, J. A. (2000) Essential fatty acids and the brain: possible health implications. Int J Dev Neurosci, 18, 383-399.
Zhang, S., Zheng, C., Lanza, I. R., Nair, K. S., Raftery, D. and Vitek, O. (2009) Interdependence of Signal Processing and Analysis of Urine H-1 NMR Spectra for Metabolic Profiling. Analytical Chemistry, 81, 6080-6088.
Zheng, L., McQuaw, C. M., Baker, M. J., Lockyer, N. P., Vickerman, J. C., Ewing, A. G. and Winograd, N. (2008) Investigating lipid-lipid and lipid-protein interactions in model membranes by ToF-SIMS. Applied Surface Science, 255, 1190-1192.
Zheng, L., McQuaw, C. M., Ewing, A. G. and Winograd, N. (2007) Sphingomyelin/phosphatidylcholine and cholesterol interactions studied by imaging mass spectrometry. Journal of the American Chemical Society, 129, 15730.

CHAPTER 2
LIPID IMAGING IN THE ZEBRA FINCH BRAIN WITH SECONDARY ION MASS SPECTROMETRY

Reprinted from International Journal of Mass Spectrometry, 260, Kensey R. Amaya, Eric B. Monroe, Jonathan V. Sweedler, David F. Clayton. Lipid imaging in the zebra finch brain with secondary ion mass spectrometry, 121-127, Copyright (2007), with permission from Elsevier.

ABSTRACT

Lipids have diverse functions in the nervous system, but the study of their anatomical distributions in the intact brain is rather difficult using conventional methodologies. Here we demonstrate the application of high resolution time-of-flight (ToF) secondary ion mass spectrometry (SIMS) to image various lipid components and cholesterol across an entire brain section prepared from an adult zebra finch (*Taeniopygia guttata*), with a spatial resolution of 2.3 μm, resulting in the formation of 11.5 megapixel chemical images. The zebra finch is a songbird in which specific neural and developmental functions have been ascribed to discrete "song control nuclei" of the forebrain. We have observed a relative increase of palmitic acid C16:0 and oleic acid C18:1 in song control nuclei versus the surrounding tissue, while phosphate (PO^{3-}), representative of phospholipids, was lower in these regions. Cholesterol was present at a high level only in the white matter of the optic tectum. More diffuse distributions were observed for stearic, arachidonic, linolenic, and palmitoleic acids. The presented results illustrate that SIMS imaging is a useful approach for assessing changes in lipid content during song circuit development and song learning.

INTRODUCTION

Lipids comprise a diverse array of molecular forms and are important in multiple aspects of brain development and brain function (Aveldano & Bazan 1973, Baker & Chang 1980, Bazan 2005, Gross *et al.* 2005, Sastry 1985, Suzuki 2002, Rosner 2003). Many lipids have complex regional and subcellular distributions, but approaches for

analyzing these distributions have been limited primarily to crude dissection and biochemical fractionation techniques (Roots & Johnston 1965), or fluorescent imaging techniques that require the chemical modification native lipids (Huster *et al.* 2001, Maier *et al.* 2002, Kuerschner *et al.* 2005) which may modify its biological properties (Maier et al. 2002, Kuerschner et al. 2005, Ishitsuka *et al.* 2004).

In recent years, mass spectrometric imaging has emerged as a discovery tool to uncover the distribution of small molecules in biological tissues. Time-of-flight secondary ion mass spectrometry (ToF-SIMS) eliminates the need for any chemical labeling, tissue homogenization, or analyte preselection, and can provide both chemical specificity and the spatial distributions of endogenous compounds on the surface of a biological sample. A chemical image is created by scanning a mass spectrometric data-acquisition point in a raster pattern across the tissue and collecting a complete mass spectrum for each individual location. This enables the construction of tens to hundreds of chemically specific images of both known and uncharacterized compounds from a single experiment. ToF-SIMS can yield a spatial resolution of a micron or better, and has been applied to elemental imaging of single cells (Clerc *et al.* 1997, Chandra *et al.* 2000) as well as molecular imaging in drug delivery systems, (Belu *et al.* 2000) kidney (Nygren *et al.* 2004), nervous tissue (Sjovall *et al.* 2004) and single neurons,(Monroe *et al.* 2005) rat pheochromocytoma (PC12) cells,(Roddy *et al.* 2002) leukocytes,(Sjovall *et al.* 2003) paramecia,(Colliver *et al.* 1997) *Tetrahymena,*(Ostrowski *et al.* 2004) and liposomes.(Cannon *et al.* 2000) Recent developments of gold and cluster ion sources have increased the mass range available for analysis using ToF-SIMS to an upper limit of >1000 Da.

In this work, we apply ToF-SIMS imaging to the study of fatty acid distribution within the brain of the zebra finch (*Taeniopygia guttata*), a songbird. The zebra finch is an important model for neural circuit development, neurogenesis, and learning and memory (for comprehensive reviews see (Zeigler 2004, Brenowitz *et al.* 1997)). A male zebra finch learns to sing during a critical period in juvenile development. Song production is under the control of an interconnected set of anatomically discrete, circumscribed nuclei in the telencephalon. These nuclei comprise the “song circuit” and are found only in songbirds. The output nucleus of the circuit, RA (robust nucleus of the

arcopallium), receives a major axonal projection from another nucleus (Nottebohm *et al.* 1976) known formally as HVC (Reiner *et al.* 2004). This projection is never completed in females of this species, who do not sing. Both RA and HVC are large and easy to visualize, even in unstained brain sections. Molecular genetic (Denisenko-Nehrbass *et al.* 2000, George *et al.* 1995) and cell culture (Holloway & Clayton 2001, Schlinger *et al.* 2001) analyses have suggested the potential involvement of various lipids and neurosteroids in the formation and function of the song circuit. Hence, the ability to identify and localize these small molecules within specific song nuclei would be of great benefit to further research.

Here we show the high resolution chemical imaging of a complete sagittal section of the songbird brain resulting in the creation of ion images, consisting of 11.5 megapixels each, for several fatty acids, as well as phosphate and cholesterol, at a spatial resolution of 2.3 μm. Ion images corresponding to palmitic acid (C16:0) and oleic acid (C18:1) show increased presence in the song nuclei HVC and RA while phosphate (PO^{3-}) was decreased in comparison to the surrounding tissue. Several other lipids and cholesterol also show interesting localizations across the tissue section. By combining high resolution chemical imaging with a tiling procedure to produce very large ion images, both gross morphological features and small-scale distribution patterns are observed.

MATERIALS AND METHODS

Brain collection and sectioning

Adult zebra finches, *Taeniopygia guttata* (>90 days of age), were sacrificed by decapitation and the brain removed. Brains were rapidly frozen on dry ice and stored at −80 °C until needed. A small drop of embedding media was used to affix the brain to the stage of a HM 550 ultramicrotome (Microm International, Walldorf, Germany) for sectioning. Tissues were not completely embedded in the media as this may have caused significant suppression of analyte signals acquired from the biological samples (Kruse & Sweedler 2003, Schwartz *et al.* 2003). Sections (20 μm, parasagittal plane with the posterior and anterior areas of the section ~1.5 mm and ~1.7 mm from the midline) were collected at −14 °C using a 7° sectioning angle. Sections containing the song nuclei HVC

and RA, from the brain hemisphere not in contact with the embedding material, were collected on glass slides and stored at −80 °C. Sections adjacent to those used for ToF SIMS analysis were collected and verified to contain the HVC and RA song nuclei via cresyl violet staining (Fig. 2.1). All presented figures are from a single animal although similar distribution patterns were observed in sections from two other animals.

Histological staining

Sections were stained for cell nuclei and nucleoli with cresyl violet. Sections were first fixed in a solution of 4% paraformaldehyde dissolved in 100 mM phosphate buffer (final pH ~7.2) for 5 min. Sections were then placed in 25mM phosphate buffered saline for 2 min followed by 2 min in ddH2O. Tissues were stained for 10 min in 0.1% cresyl violet and then dehydrated sequentially in 70%, 95%, and 100% ethanol and cleared for 5 min in Citrisolv (Fisher Scientific, Rochester, NY). Samples were then mounted with a cover slip using Permount.

ToF-SIMS analysis

Immediately prior to analysis, sections were removed from a −80 °C freezer and warmed under vacuum for 45 min and coated with a 1 nm deposition of Au using a Desk II TFC sputter coater (Denton Vacuum, Moorestown, NJ). ToF SIMS analyses were performed with a TRIFT ToF-SIMS mass spectrometer (Physical Electronics, Chanhassen, MN) equipped with a gold liquid metal ion cluster source operating at 22 keV. The Au^{2+} primary ion beam was randomly rastered in a 256 x 256 pixel region at 8 kHz with an 8 ns pulse-width in unbunched mode. Total ion doses were kept well below the static limit of $1x10^{13}$ primary ions cm^{-2} (~$3x10^{9}$ cm^{-2}). Negative secondary ions (*m/z* 0.1–2000) were collected for 194 individual 600 μm x 600 μm tiles located across the sample in an ordered raster pattern with a 2–15% overlap between tiles without charge compensation. Mass spectra were internally calibrated using the Au^{-}, Au^{2-}, and Au^{3-} peaks. Images of these ions showed a homogenous distribution across the sample, suggesting that no artifacts were created as a result of sample coating.

Image analysis and stitching

Ion images, assembled using WinCadence software (Physical Electronics) for each individual tile, were created for the following compounds: phosphate PO^{3-} (*m/z* 79.0), cholesterol (*m/z* 385.4), arachidonic acid C20:4 (*m/z* 303.2), palmitic acid C16:0 (*m/z* 255.2), palmitoleic acid C16:1 (*m/z* 253.2), stearic acid C18:0 (*m/z* 283.3), oleic acid C18:1 (*m/z* 281.2), linoleic acid C18:2 (*m/z* 279.23), and α-linolenic acid C18:3 (*m/z* 277.2). All images were created using the same relative intensity scale to enable the individual image tiles to be combined into an ion image for the entire tissue section. Individual ion images for each compound were combined using VLmerge (an opensource software produced by the Imaging Technology Group at the Beckman Institute, University of Illinois at Urbana Champaign) to produce an ion image consisting of ~11.5 megapixels for each compound. Slight fluctuations in ion yields were observed in several tiles due to fluctuations in primary ion current, although this effect did not inhibit analyses.

RESULTS

Tissue staining and morphology

A tissue section adjacent to the one used for ToF-SIMS analysis was stained using cresyl violet to enhance the visualization of gross histological structure (Fig. 2.1). The song nuclei HVC and RA characteristically stain more darkly than surrounding tissue. Also visible are striations corresponding to the lamina pallio-subpallialis (LPS), lamina frontalis superior (LFS), and the lamina mesopallialis (LaM). The morphological complexity of the tissue section allows for the analysis of many different features with ToF-SIMS within a single experiment.

Chemical imaging

Chemical images were produced for several compounds across the tissue section as outlined below. Each image is the reconstruction of 194 individual 256 x 256 pixel images at a spatial resolution of 2.3 μm. A partial mass spectrum from a single 600 μm x 600 μm tile, which is the sum of 65,536 individual mass spectra, is presented in Fig. 2.2. Mass spectra from each tile produced hundreds of signals over the collected mass range.

Many of these signals consisted of various fragment products formed during the desorption process while other components ionized intact and produced ion currents of adequate strength to allow for their imaging. Some ions had homogenous distributions across the tissue (not shown). Imaged ions were selected for detailed analysis based on their biological significance, strength of ion signal, and interesting distribution across the tissue section, and were identified on the basis of mass matches to previously reported fatty acid and cholesterol signals (Schwartz et al. 2003, Touboul *et al.* 2005).

Phosphate (PO^{3-})

The signal for phosphate (PO^{3-}, *m/z* 79.0), which is believed to be indicative of membrane phospholipids, is strong throughout the tissue and presents distinctive morphological details (Fig. 2.3A). The song nuclei HVC and RA are marked by a decrease in intensity compared to the surrounding tissue (Figs. 2.3A and 2.4B). The LPS, fasciculus prosencephali lateralis (FPL), LFS, entopallium (E), and LaM also show a decrease in the phosphate distribution.

Cholesterol

Cholesterol (*m/z* 385.4) is found to be present at the highest levels in the optic tectum (Fig. 2.3B). More precisely, the distribution corresponds to regions of white matter comprised largely of myelinated axons. Increased cholesterol in the white matter has previously been observed in mouse brain, where it is believed to be associated with myelin (Sjovall et al. 2004). In addition, cholesterol also appears to have an enhanced presence in another region enriched for fibers, the tract FPL (Szekely & Krebs 1996).

Arachidonic acid

The polyunsaturated fatty acid, arachidonic acid (C20:4, *m/z* 303.2), generates a weak but granular signal, distributed evenly across this section with no strong anatomical localization (Fig. 2.3C). There is a slight increase in the caudal forebrain not observed with the other lipids (suggesting possible biological significance as opposed to experimental artifact) and a slight relative decrease in RA.

C16 lipids

Signal corresponding to the 16-carbon saturated fatty acid, palmitic acid (C16:0, *m/z* 255.2), is increased in the song nuclei HVC and RA compared to the surrounding tissue (Figs. 2.3D and 2.4C), suggesting that palmitic acid is enriched in these nuclei. Moreover, close inspection reveals a relative increase along the dorsal external edge of RA, an area apparently corresponding to the "cup" of RA which receives a developmentally and functionally distinct set of inputs from HVC (Holloway & Clayton 2001, Mooney & Rao 1994, Konishi & Akutagawa 1985). Increased signal is also seen in E. The monounsaturated form, palmitoleic acid (C16:1, *m/z* 253.2), presents a similar distribution within the tissue section (Fig. 2.3E), although with a lower signal intensity. Several discrete points or lines of increased signal are observed around the rim of the section and are generally present in the other images. This artifact is due largely to an increased background signal along the edges of the tissue and from the substrate, as verified by observing the mass spectra from these regions.

C18 lipids

We analyzed signals for four, 18-carbon fatty acids of increasing unsaturation: stearic acid (C18:0, *m/z* 283.3), oleic acid (C18:1, *m/z* 281.2), linoleic acid (C18:2, *m/z* 279.2), and α- linolenic acid (C18:3, *m/z* 277.2). Interestingly, each of these compounds has a different distribution pattern. Stearic acid shows some enrichment in a region around the caudal edge of song nucleus RA, as well as in the dorsal telencephalon (superficial to LaM) (Fig. 2.3F). The monounsaturated fatty acid, oleic acid (C18:1), is present at a high level in regions identified as HVC, RA and E (Fig. 2.3G, see also Fig. 2.4D). The pattern is superficially similar to that for palmitic acid (Figs. 2.3D and 2.4C) but close inspection shows several differences—a complementary distribution within the center of E, no contrast along the lamina LaM and LFS, and less differentiation within the optic tectum. Linoleic acid (C18:2) localizes to several relatively small points of uncertain biological interpretation (Fig. 2.3H). Fig. 2.3I illustrates the distribution of the polyunsaturated lipid, α-linolenic acid (C18:3), and shows no strong localization in the brain section, although it is reduced in tectal layers that correspond to white matter.

DISCUSSION

Lipid distribution patterns and biological significance

The ability to relate specific chemical composition to anatomically defined morphological features in complex tissues represents one of the largest benefits of high-resolution chemical imaging approaches. In this study, multiple chemical images were produced from a single zebra finch brain section in its entirety, allowing the detection and comparison of the distribution of phosphate ion, cholesterol, and seven different lipids naturally present in the section. Analyses of similar sections from two other animals produced similar chemical images but are not shown here. The results reveal major differences in the distributions of these components.

Using the song nucleus RA as a focal point, some components are locally enriched, some locally impoverished, and others do not distinguish the nucleus from the surrounding tissue. RA is specifically enriched in three fatty acids—palmitate C16:0 (Fig. 2.4C), palmitoleate C16:1, and oleate C18:1 (Fig. 2.4D). Signals from phosphate (Fig. 2.4B) and arachidonic acid, however, are relatively decreased in RA. Palmitate is also relatively enriched in the "cup" structure along the dorsal edge, which may represent a projection terminus from HVC (Holloway & Clayton 2001).

The polyunsaturated fatty acids, linoleic C18:2 and α- linolenic acid C18:3, all have relatively low signal intensity and little or no significant spatial localization. Linoleic acid does, however, localize in the area identified as E. Low signal intensity may be indicative of low concentration or low negative ionization of these lipids under the SIMS process. This is the first report of any specific lipid content in the song control system, although prior studies have indicated significant roles for lipid binding proteins (Denisenko-Nehrbass et al. 2000, George et al. 1995) and steroid-synthesis enzymes (Holloway & Clayton 2001, Schlinger et al. 2001). This technique may make possible the systematic analysis of how lipids themselves may change in the song system in significant ways during song learning and circuit development.

Cholesterol is of particular interest for songbird neurobiology as it is a steroid precursor, and localized production of steroids within the brain appears to be important for development of the song control pathway in males. Might ToF-SIMS be used to identify and map the distribution of neurosteroids? These compounds are likely present in

much lower concentrations than cholesterol and may be below the detection level of ToF-SIMS. Continued improvements in the sensitivity of analyses and the observation of both positive and negative ions from a section may, however, help meet this challenge. Except for cholesterol, all imaged analytes may be found in tissue as covalently linked moieties in larger compounds. At the subcellular level, these analytes are expected to be present in cellular membranes but are not necessarily limited to the cell membrane. Free fatty acids may occur as intermediary metabolites but are also components of phospholipids (major components of cell membranes) and triglycerides (energy stores). The degree to which the presented signals are from free analytes, or are fragmentation products as a result of the desorption process, is not currently known. Phosphate, for instance, serves as a marker of phospholipids, although other cellular sources (e.g., nucleic acids) may also contribute. Cholesterol is considered a ubiquitous component of cell membranes, yet it shows one of the most restricted distributions we observed, virtually the inverse of phosphate. Conclusively identifying the source of a signal is difficult and was not performed in these experiments as the imaging is meant to serve as a discovery tool to uncover any lipid heterogeneities and to guide further, more directed studies into the underlying biology.

The complementary distributions of phosphate and cholesterol within the optic tectum are highlighted by a linescan analysis of the image (Fig. 2.5). As the linescan crosses a region of the brain that contains white matter, the cholesterol signal rises while the phosphate signal decreases. The opposite is true for regions of grey matter that are rich in cell bodies. Previous studies have noted the enrichment of cholesterol in white matter and have attributed this to the concentrations of cholesterol in myelin (Saher *et al.* 2005). Although linescans provide limited relative quantitative information, in this case from the optic tectum, further quantitation is hindered due to variability in ion yields across multiple tissue types and the low ion yields. Absolute quantitation for direct tissue samples is problematic for unlabeled compounds with MS in general, and in particular for SIMS, as many factors affect the ionization efficiency. However, relative quantitative comparisons of different regions may be performed by first normalizing ion images to a ubiquitous signal to remove any artifacts caused by sample preparation or topography (Monroe et al. 2005, Ostrowski et al. 2004). Extended periods of ion collection would

enable such relative comparisons but were not performed in this set of experiments.

Application of chemical imaging to tissue analysis

The chemical imaging of many compounds simultaneously and at high spatial resolution presents several challenges in regard to sample preparation, as well as other experimental considerations. In the experiments here, the tissue samples were flash-frozen immediately after dissection to minimize analyte redistribution. In addition, sample manipulations for the ToF-SIMS were kept to a minimum to prevent the loss and redistribution of analytes and to minimize the introduction of contaminants. With this conservative approach we appear to have achieved good reproducibility of results, as we observed similar distribution patterns for all studied compounds within the song nuclei RA and HVC of three separate birds.

Relatively abundant signals, such as those from the phosphate ion, produce images that can be magnified substantially to the point at which cellular-level detail begins to emerge (Fig. 2.6). In the reconstructed image of phosphate, the heterogeneous distribution is apparent across the tissue (Fig. 2.6A). When fewer and fewer tiles are included in the image (49 tiles in Fig. 2.6B and 9 in Fig. 2.6C), the broad features present in the FPL are more difficult to distinguish and identify. The small-scale fluctuations in phosphate signals are still observable in the single 600μm x 600μm image presented in Fig. 2.6D. Despite the low ion count and few pixels, the observed features appear to be single cells that have been sectioned within the tissue. This conclusion is based on the size and the characteristic phosphate signal that arises from the phospholipids in the cellular membrane. Although challenging, the high-resolution megapixel chemical imaging of entire tissue sections allows for not only the observation of gross chemical distributions and morphology but also fine details that would not be visible at lower resolutions.

For analytes present in only small quantities such as arachidonic acid, detection might be improved by using a larger beam diameter or higher primary ion current to desorb more analyte molecules per mass spectrum – but at the expense of reduced spatial resolution and by extending the period of data acquisition to more closely approach the static limit. Applications of higher mass cluster ion sources may also further improve the

molecular imaging of intact lipids in the songbird brain.

The high-resolution chemical imaging of a complete sagittal section of the brain from the zebra finch, *Taeniopygia guttata*, reveals varied distributions of C16 and C18 saturated and mono-unsaturated fatty acids. The localizations of palmitic, palmitoleic, and oleic acids in the song nuclei are particularly interesting as these nuclei are intensively studied focal points for research into both neural development and adult plasticity. The results demonstrate the creation of chemical tissue maps that reach into the megapixel range with regard to the number of obtained mass spectra. Thus, the distribution of a large number of chemical components may be studied on both the gross morphological and micron level spatial scales within a single experiment.

ACKNOWLEDGMENTS

I would like to thank Charles Conway for assistance with the image stitching and Timothy Spila for technical assistance with the ToF-SIMS. This material is based upon work supported by the Initiative for Future Agriculture and Food Systems (grant no. 2001-52100-11527) from the USDA Cooperative State Research, Education and Extension service (D.F.C.), and the NIH through award nos. P30DA018310 to the UIUC Neuroproteomics Center on Cell to Cell Signaling, and R01 DA017940 (J.V.S.). This work was carried out in the Center for Microanalysis of Materials, University of Illinois, which is partially supported by the US Department of Energy under grant DEFG02-91-ER45439. K.A. was supported by an Agricultural Genome Sciences and Public Policy Graduate Fellowship and by NIH R01 MH061994 (subcontract to D.F.C., PI: Barney Schlinger, UCLA).

FIGURES AND TABLES

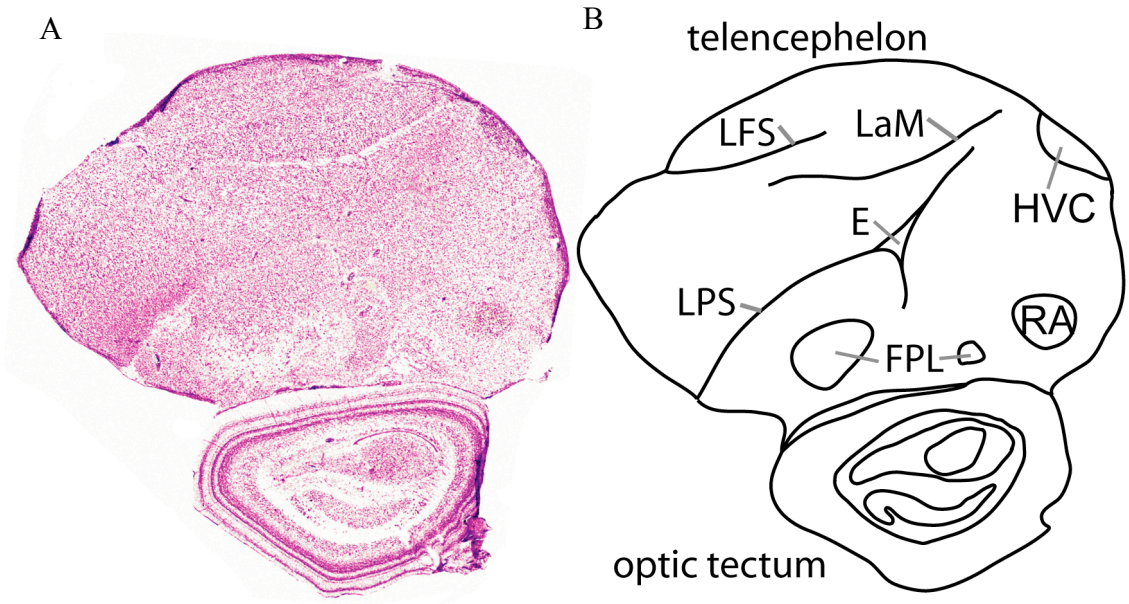

Figure 2.1. Morphological features are identified via (A) the cresyl violet staining of a section adjacent to that used for ToF-SIMS analysis. (B) A schematic representation illustrating the complex morphology of the imaged tissue section that contains the robust nucleus of the archistriatum (RA), high vocal center (HVC), fasciculus prosencephali lateralis (FPL), entopallium (E), lamina palliosubpallialis (LPS), lamina mesopallialis (LaM), and lamina frontalis superior (LFS).

Reproduced with permission from Elsevier.

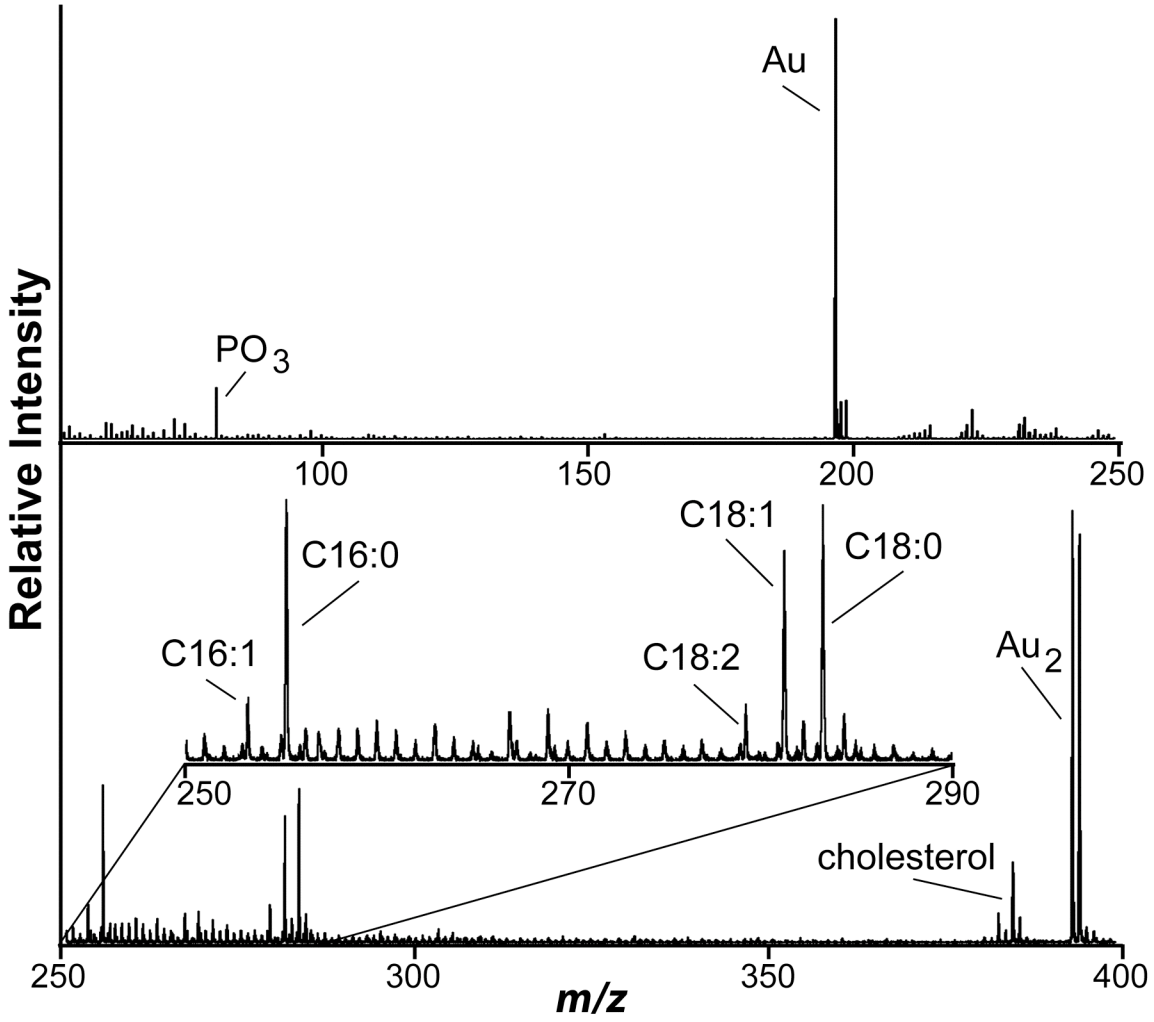

Figure 2.2. Mass spectrum from a single 600 μm x 600 μm region of the songbird brain at the junction between the optic tectum and telencephalon illustrating many of the imaged lipid signals, as well as cholesterol, and both Au^- and Au^{2-}.

Reproduced with permission from Elsevier.

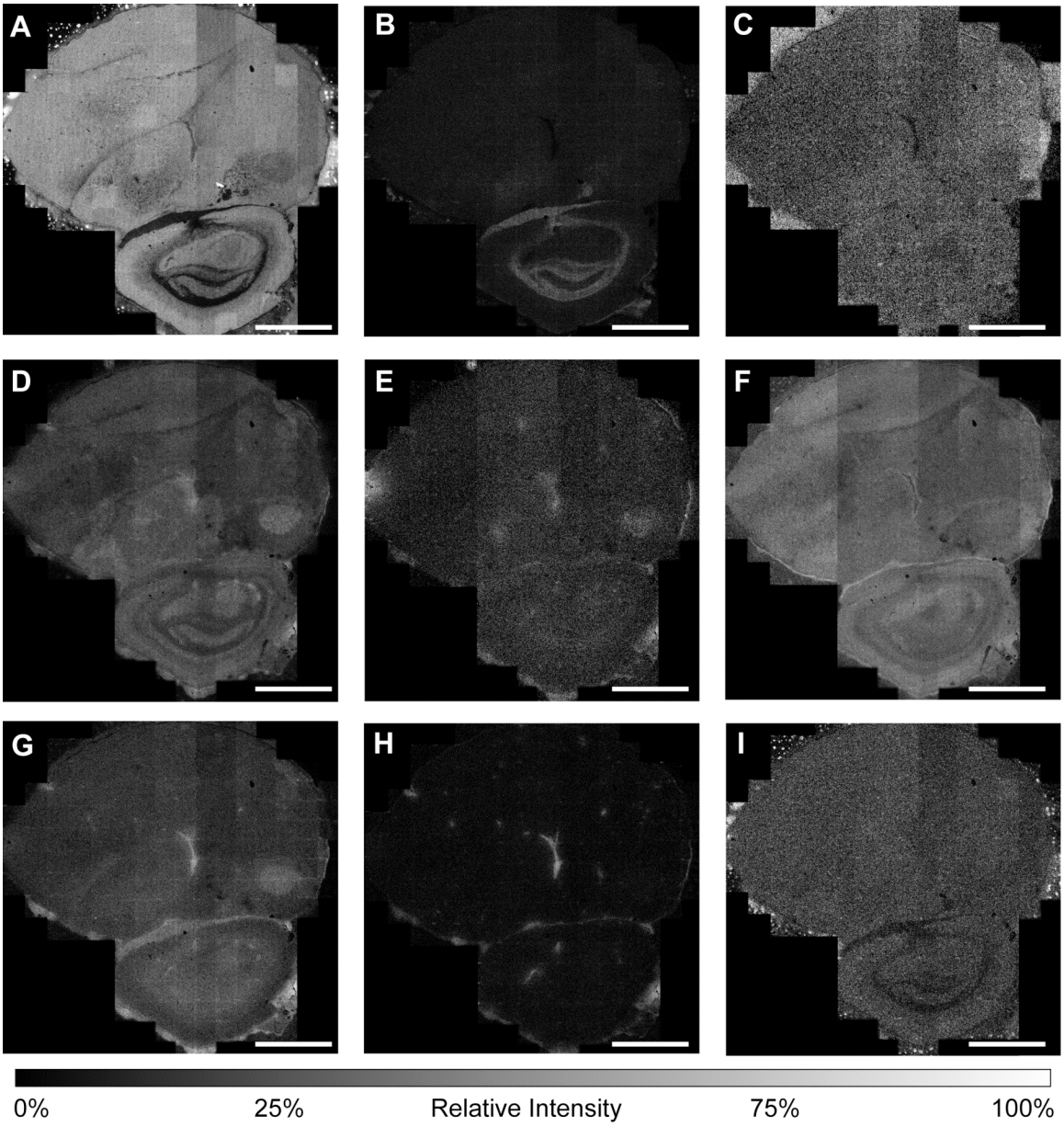

Figure 2.3. Selected ion images from the songbird brain. Each ion image consists of ~11.5 million pixels within the tissue section and is the combination of 194 individual 600 μm x 600 μm ion images prepared on the same relative intensity scale. Ion images are (A) phosphate PO^{3-} (*m/z* 79.0); (B) cholesterol (*m/z* 385.4); (C) arachidonic acid C20:4 (*m/z* 303.2); (D) palmitic acid C16:0 (*m/z* 255.2); (E) palmitoleic acid C16:1 (*m/z* 253.2); (F) stearic acid C18:0 (*m/z* 283.3); (G) oleic acid C18:1 (*m/z* 281.2); (H) linoleic acid C18:2 (*m/z* 279.23); and (I) α-linolenic acid C18:3 (*m/z* 277.2). Scale bars = 2 mm.

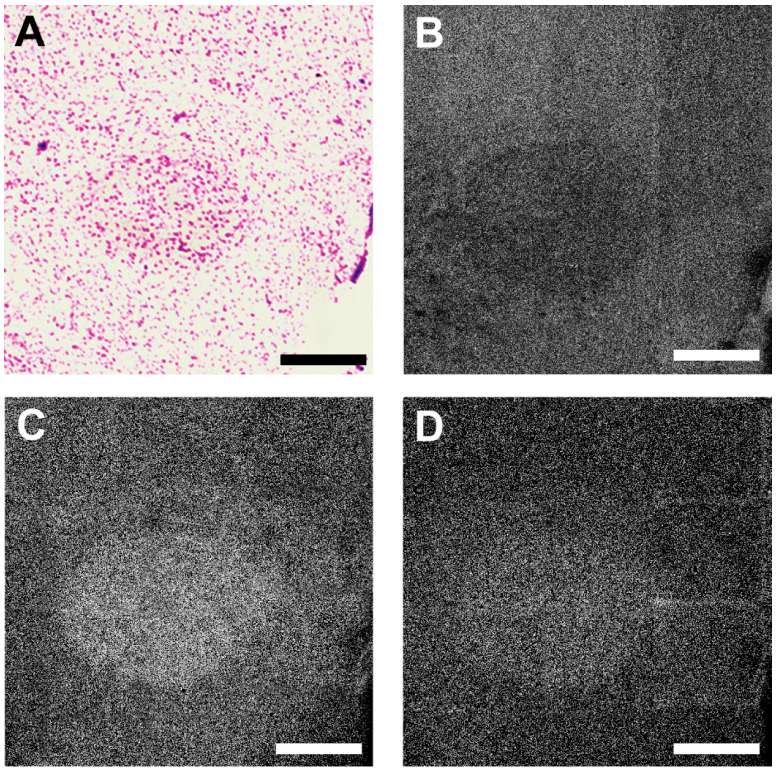

Figure 2.4. Selected images of the region including the song nucleus RA. (A) Cresyl violet histological stain of section adjacent to the one in B–D; (B) phosphate (PO^{3-}, *m/z* 79); (C) palmitic acid C16:0 (*m/z* 255); and (D) oleic acid C18:1 (*m/z* 281). Scale bars = 500 μm.

Reproduced with permission from Elsevier.

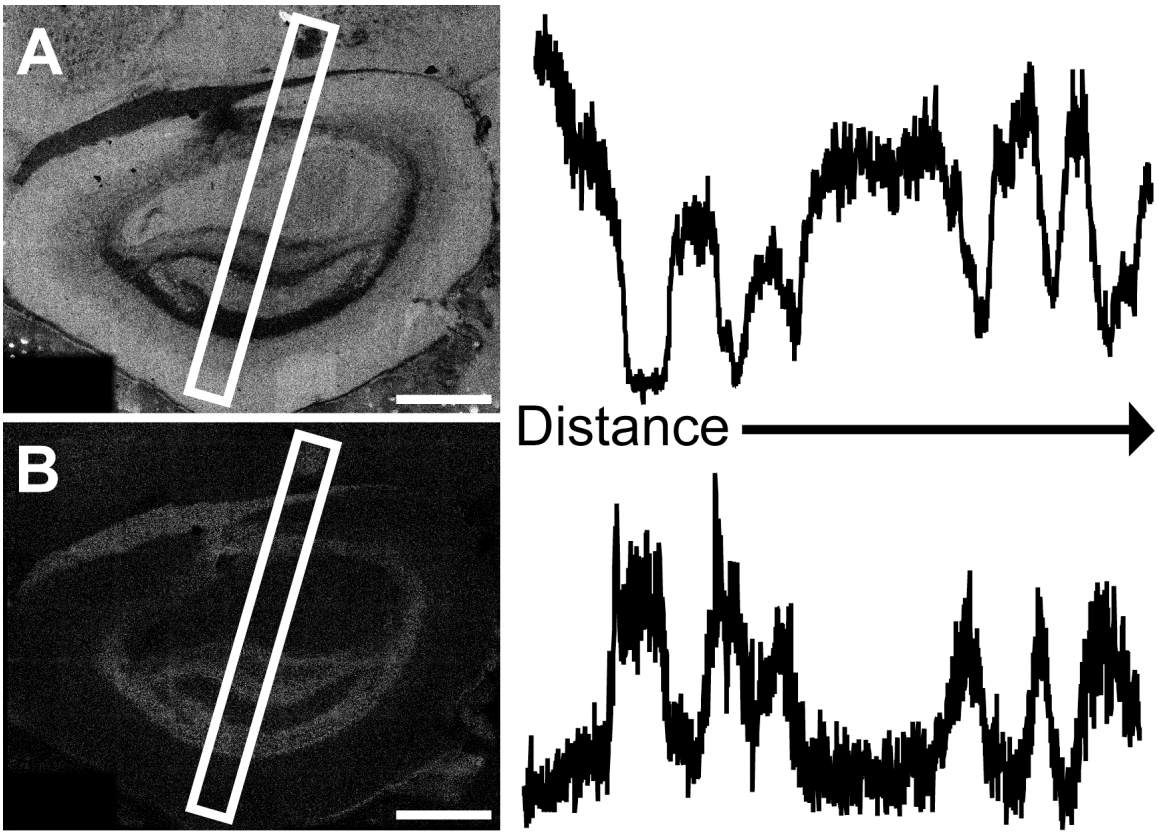

Figure 2.5. Linescans of (A) phosphate PO3− (*m/z* 79.0) and (B) cholesterol (*m/z* 385.4) from the optic tectum illustrate the complementary distribution of these two compounds. Linescans begin in the lower portion of the midbrain and extend up and to the right as outlined in the ion images. Scale bars = 1 mm.

Reproduced with permission from Elsevier.

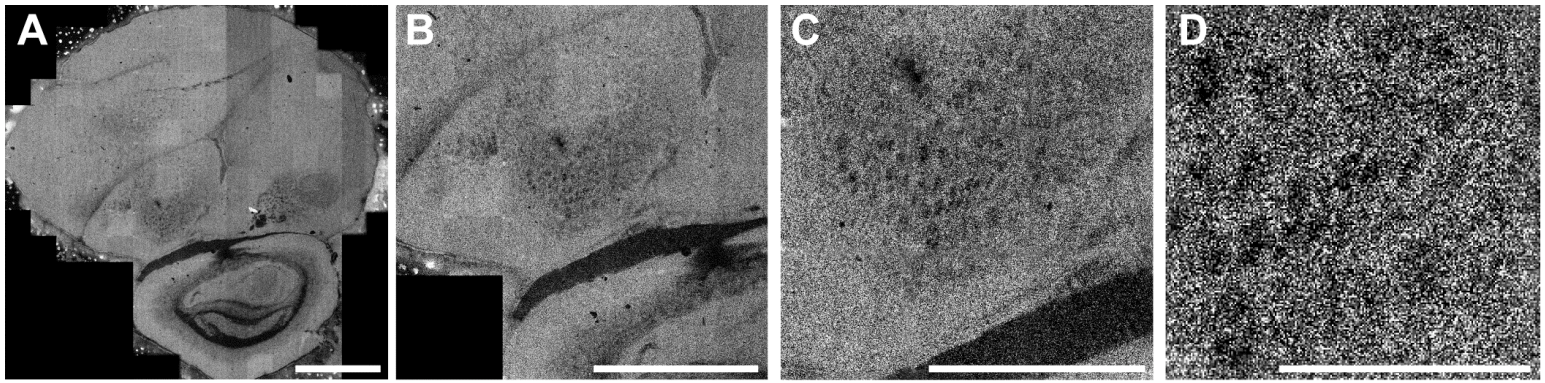

Figure 2.6. Sequential zoom of the phosphate ion image (*m/z* 79.0) in (A) the full tissue image with all 194 tiles (scale bar = 2 mm); (B) 49 central tiles (scale bar = 2 mm); (C) 9 tiles (scale bar = 1 mm); and (D) a single tile (scale bar =500 μm). The increasing levels of zoom reduce the overall image contrast from that observed in the larger images, but also allow the visualization of smaller features within the sample, including what appear to be the outline of individual cells.

REFERENCES

Aveldano, M. I. and Bazan, N. G. (1973) Fatty-Acid Composition and Level of Diacylglycerols and Phosphoglycerides in Brain and Retina. Biochim Biophys Acta, 296, 1-9.

Baker, R. R. and Chang, H. Y. (1980) The Incorporation of Radioactive Fatty-Acids into the Phospholipids of Nerve-Cell-Body Membranes Invivo - Evidence for Highly Labeled Neuronal Nuclei. Biochemical Journal, 188, 153-161.

Bazan, N. G. (2005) Lipid signaling in neural plasticity, brain repair, and neuroprotection. Mol Neurobiol, 32, 89-103.

Belu, A. M., Davies, M. C., Newton, J. M. and Patel, N. (2000) TOF-SIMS characterization and imaging of controlled-release drug delivery systems. Anal Chem, 72, 5625-5638.

Brenowitz, E. A., Margoliash, D. and Nordeen, K. W. (1997) An introduction to birdsong and the avian song system. J Neurobiol, 33, 495-500.

Cannon, D. M., Pacholski, M. L., Winograd, N. and Ewing, A. G. (2000) Molecule Specific Imaging of Freeze-Fractured, Frozen-Hydrated Model Membrane Systems Using Mass Spectrometry. J. Am. Chem. Soc., 122, 603-610.

Chandra, S., Smith, D. R. and Morrison, G. H. (2000) Subcellular imaging by dynamic SIMS ion microscopy. Anal Chem, 72, 104A-114A.

Clerc, J., Fourre, C. and Fragu, P. (1997) SIMS microscopy: methodology, problems and perspectives in mapping drugs and nuclear medicine compounds. Cell Biol Int, 21, 619-633.

Colliver, T. L., Brummel, C. L., Pacholski, M. L., Swanek, F. D., Ewing, A. G. and Winograd, N. (1997) Atomic and molecular imaging at the single-cell level with TOF-SIMS. Anal Chem, 69, 2225-2231.

Denisenko-Nehrbass, N. I., Jarvis, E., Scharff, C., Nottebohm, F. and Mello, C. V. (2000) Site-specific retinoic acid production in the brain of adult songbirds. Neuron, 27, 359-370.

George, J. M., Jin, H., Woods, W. S. and Clayton, D. F. (1995) Characterization of a novel protein regulated during the critical period for song learning in the zebra finch. Neuron, 15, 361-372.

Gross, R. W., Jenkins, C. M., Yang, J., Mancuso, D. J. and Han, X. (2005) Functional lipidomics: the roles of specialized lipids and lipid-protein interactions in modulating neuronal function. Prostaglandins Other Lipid Mediat, 77, 52-64.

Holloway, C. C. and Clayton, D. F. (2001) Estrogen synthesis in the male brain triggers development of the avian song control pathway in vitro. Nat Neurosci, 4, 170-175.

Huster, D., Muller, P., Arnold, K. and Herrmann, A. (2001) Dynamics of membrane penetration of the fluorescent 7-nitrobenz-2-oxa-1,3-diazol-4-yl (NBD) group attached to an acyl chain of phosphatidylcholine. Biophys J, 80, 822-831.

Ishitsuka, R., Yamaji-Hasegawa, A., Makino, A., Hirabayashi, Y. and Kobayashi, T. (2004) A lipid-specific toxin reveals heterogeneity of sphingomyelin-containing membranes. Biophys J, 86, 296-307.

Konishi, M. and Akutagawa, E. (1985) Neuronal growth, atrophy and death in a sexually dimorphic song nucleus in the zebra finch brain. Nature, 315, 145-147.

Kruse, R. and Sweedler, J. V. (2003) Spatial profiling invertebrate ganglia using MALDI MS. J Am Soc Mass Spectr, 14, 752-759.
Kuerschner, L., Ejsing, C. S., Ekroos, K., Shevchenko, A., Anderson, K. I. and Thiele, C. (2005) Polyene-lipids: a new tool to image lipids. Nat Methods, 2, 39-45.
Maier, O., Oberle, V. and Hoekstra, D. (2002) Fluorescent lipid probes: some properties and applications (a review). Chem Phys Lipids, 116, 3-18.
Monroe, E. B., Jurchen, J. C., Lee, J., Rubakhin, S. S. and Sweedler, J. V. (2005) Vitamin E imaging and localization in the neuronal membrane. J Am Chem Soc, 127, 12152-12153.
Mooney, R. and Rao, M. (1994) Waiting periods versus early innervation: the development of axonal connections in the zebra finch song system. J Neurosci, 14, 6532-6543.
Nottebohm, F., Stokes, T. M. and Leonard, C. M. (1976) Central control of song in the canary, Serinus canarius. J Comp Neurol, 165, 457-486.
Nygren, H., Malmberg, P., Kriegeskotte, C. and Arlinghaus, H. F. (2004) Bioimaging TOF-SIMS: localization of cholesterol in rat kidney sections. FEBS Lett, 566, 291-293.
Ostrowski, S. G., Van Bell, C. T., Winograd, N. and Ewing, A. G. (2004) Mass spectrometric imaging of highly curved membranes during Tetrahymena mating. Science, 305, 71-73.
Reiner, A., Perkel, D. J., Bruce, L. L. et al. (2004) Revised nomenclature for avian telencephalon and some related brainstem nuclei. J Comp Neurol, 473, 377-414.
Roddy, T. P., Cannon, D. M., Jr., Ostrowski, S. G., Winograd, N. and Ewing, A. G. (2002) Identification of cellular sections with imaging mass spectrometry following freeze fracture. Anal Chem, 74, 4020-4026.
Roots, B. I. and Johnston, P. V. (1965) Lipids Of Isolated Neurons. Biochem J, 94, 61-63.
Rosner, H. (2003) Developmental expression and possible roles of gangliosides in brain development. Prog Mol Subcell Biol, 32, 49-73.
Saher, G., Brugger, B., Lappe-Siefke, C., Mobius, W., Tozawa, R., Wehr, M. C., Wieland, F., Ishibashi, S. and Nave, K. A. (2005) High cholesterol level is essential for myelin membrane growth. Nature Neuroscience, 8, 468-475.
Sastry, P. S. (1985) Lipids of nervous tissue: composition and metabolism. Prog Lipid Res, 24, 69-176.
Schlinger, B. A., Soma, K. K. and London, S. E. (2001) Neurosteroids and brain sexual differentiation. Trends Neurosci, 24, 429-431.
Schwartz, S. A., Reyzer, M. L. and Caprioli, R. M. (2003) Direct tissue analysis using matrix-assisted laser desorption/ionization mass spectrometry: practical aspects of sample preparation. J Mass Spectrom, 38, 699-708.
Sjovall, P., Lausmaa, J. and Johansson, B. (2004) Mass spectrometric imaging of lipids in brain tissue. Anal Chem, 76, 4271-4278.
Sjovall, P., Lausmaa, J., Nygren, H., Carlsson, L. and Malmberg, P. (2003) Imaging of membrane lipids in single cells by imprint-imaging time-of-flight secondary ion mass spectrometry. Anal Chem, 75, 3429-3434.
Suzuki, T. (2002) Lipid rafts at postsynaptic sites: distribution, function and linkage to postsynaptic density. Neurosci Res, 44, 1-9.

Szekely, A. D. and Krebs, J. R. (1996) Efferent connectivity of the hippocampal formation of the zebra finch (Taenopygia guttata): An anterograde pathway tracing study using Phaseolus vulgaris leucoagglutinin. Journal of Comparative Neurology, 368, 198-214.

Touboul, D., Brunelle, A., Halgand, F., De La Porte, S. and Laprevote, O. (2005) Lipid imaging by gold cluster time-of-flight secondary ion mass spectrometry: application to Duchenne muscular dystrophy. J Lipid Res, 46, 1388-1395.

Zeigler, H. P. (2004) Introduction. Annals of the New York Academy of Sciences, 1016, xv-xviii.

CHAPTER 3

SMALL MOLECULE ANALYSIS AND IMAGING FATTY ACIDS IN THE ZEBRA FINCH SONG SYSTEM USING TIME OF FLIGHT – SECONDARY ION MASS SPECTROMETRY

ABSTRACT

Lipids play many essential roles in the brain with functions in cell signaling, potentiation, and signal transduction. Additionally they are important in learning in memory and increasingly associated with diseases such as Alzheimer's and Parkinson's. The zebra finch (*Taeniopygia guttata*), a songbird, is an established animal model in which the neuronal and developmental functions of the brain are well characterized and have been ascribed to anatomically discreet regions "song nuclei". In this study we image the subcellular distribution of essential and non-essential fatty acids across these brain regions using Time of Flight – Secondary Ion Mass Spectrometry (ToF-SIMS). Imaging by ToF-SIMS reveals locally enriched and depressed levels of omega-3 and -6 fatty acids as well as nonessential fatty acids in areas corresponding to the song nuclei. We use Principle Component Analysis (PCA) to show chemical differences between functionally distinct (e.g. robust nucleus of the arcopallium "RA" and auditory lobule "AL") and tissue specific brain areas (e.g. dorsolateral thalamic nucleus "DLM" and AreaX), as well as between song nuclei from post hatch day 20 and adult male birds. The results demonstrate the use of ToF-SIMS to study a class of small molecule that has remained difficult to study and its potential impact towards our understanding of learning and memory, and brain chemistry and disease.

INTRODUCTION

Lipids are one of the primary components of cell membranes, and have especially important functions in brain with roles in maintenance of electrochemical gradients (Saum *et al.* 1981, Schmidt *et al.* 2006) and synaptic organization (Suzuki 2002). In addition, lipids have been increasingly associated with important neurodegenerative disease such as Alzheimer's (Hartmann *et al.* 2007) and Parkinson's disease (Israeli &

Sharon 2009), and mental disorders such as schizophrenia (Fenton *et al.* 2000) and epilepsy (Cole-Edwards & Bazan 2005). Essential fatty acids have been of particular focus demonstrating their importance in cognitive function (Moriguchi *et al.* 2000), inflammatory and immunological responses (Simopoulos 2002), and disease. Non-essential fatty acids, those capable of being synthesized de-novo by the body have also been shown to play important cellular roles as post-translational modifications (Gubitosi-Klug *et al.* 2005) and in maintenance of proper membrane fluidity (Leekumjorn *et al.* 2009).

Efforts to study lipids in a biologically complex tissue such as the brain have typically relied on crude dissection, homogenization, and detection. However, these methods do not provide information pertaining to their cellular or subcellular distribution. Advances in chemically labeling lipids with fluorophores have been successful, however they adversely affect lipid-lipid and lipid-protein interactions (Maier *et al.* 2002). Time of Flight – Secondary ion mass spectrometry (ToF-SIMS) is a surface analysis tool that allows for subcellular imaging (lateral resolution of ~1 μm) of small molecules <1,000 *m/z* in biologically complex tissues such as the brain. The strength of ToF-SIMS is that no homogenization, analyte preselection, or chemical labeling is required. The technology has been shown to be a robust tool for the detection and imaging of lipids on a diverse array of tissues such as muscle (Tahallah *et al.* 2008), nervous system (Pernber *et al.* 2007), and kidney (Nygren *et al.* 2004). Subcellular imaging with ToF-SIMS has also revealed significant localization of other lipophilic molecules such as vitamin E in isolated neurons from *Aplysia californica* (Monroe *et al.* 2005).

The zebra finch (*Taeniopygia guttata*), a songbird, is an important model for neuronal circuitry development, neurogenesis, and learning and memory. A distinctive feature of the songbird brain is the presence of several large, discrete anatomical nuclei that are dedicated to the learning and production of song. These nuclei are interconnected into a "song control circuit" which is completed during a critical period in juvenile development, and only in males (females do not produce learned vocalizations). A young male zebra finch learns to sing by copying the song of an adult tutor during this critical period. With sexual maturity, male song learning ceases. The song control circuit is organized into two major pathways: 1) the "anterior forebrain pathway" (AFP), necessary

for learning to copy a song, and 2) the song motor-control pathway, necessary for vocalization (Brenowitz *et al.* 1997), as shown in Figure 3.1. These two pathways converge at the robust nucleus of the arcopallium (RA), which provides the output of the circuit onto the motor neurons that drive the respiratory and syringeal muscles responsible for singing. Additionally, a third region of the forebrain the auditory lobule (AL), composed of the caudal medial nidopallium (NCM) and the caudal medial mesopallium (CMM), has been implicated in recognition and memory of song auditory patterns (Mello *et al.* 1995). These various brain regions of the zebra finch song system have been studied intensively for their physiological and developmental properties (Clayton 1997), and they form a valuable reference set for studies of molecular composition in the brain (Lovell *et al.* 2008).

Several observations suggest important roles for lipids and fatty acids in song system development and function. One of the first genes shown to be developmentally regulated within the song control circuit encodes the ortholog of alpha-synuclein (originally referred to as synelfin), a lipid-binding protein subsequently implicated in Parkinson's Disease and other neurodegenerative diseases (Clayton & George 1999). Lipophilic molecules including retinoic acid (Jeong *et al.* 2005, Denisenko-Nehrbass *et al.* 2000b) and sex steroids (London *et al.* 2006) are synthesized in or near several of the song control nuclei and are necessary for song learning and song circuit development. Yet virtually nothing is known about the lipid and fatty acid composition of the song system.

Here we expand upon the results from chapter one, increasing the number of fatty acids identified by ToF-SIMS, and by including song nuclei RA, HVC, lateral magnocellular nucleus of the nidopallium (LMAN), dorsolateral thalamic nucleus (DLM), AreaX, and the auditory forebrain (NCM/CMM) in our analysis. These results reveal a complex distribution of fatty aids across different song nuclei in the male zebra finch brain, setting the basis for more targeted future studies to address a potential functional importance of these fatty acids in these areas critical to song learning and memory.

MATERIALS AND METHODS

Tissue preparation and staining

All animal procedures were conducted under procedures approved by the University of Illinois Institutional Animal Care and Use Committee. Male zebra finches were sacrificed by decapitation, the brain removed, and rapidly frozen on dry ice. Post-hatch day 20 birds were sexed postmortem by gonadal identification. Parasagittal sections, 16 μm in thickness, were collected beginning at 2.5 mm to the midline (~5.6 mm). Sections were alternatively placed on either a glass slide, for histological staining, or glass cover slip, for ToF-SIMS and immunohistochemical analysis. Sections were stored at -80 ^{o}C for no more then 3 weeks. Histological staining, by cresyl violet, was carried out as previously described (Amaya et al. 2007). Sections containing the song nuclei RA, HVC, LMAN, Area X, DLM, and AL were identified and the adjacent sections were used for ToF-SIMS or immunohistochemical analysis.

ToF-SIMS and image analysis

Sections were removed from -80 ^{o}C and immediately vacuum dried (~15 min) at room temperature. Dried sections were placed in a Desk II TFC sputter coater (Denton Vacuum, Moorestown, NJ) equipped with a gold target and ~10Å was deposited on sample surface to improve ionization of surface molecules (Altelaar et al. 2006). ToF-SIMS analysis was performed with a TRIFT ToF-SIMS mass spectrometer (Physical Electronics, Chanhassen, MN) equipped with a gold liquid metal ion source. Primary ion beam used Au_1 running at 22 keV, 2nAmp, and the primary ion dose was kept below the static limit of 1 x 10^{13} primary ions cm^{-2}. Mass spec images were collected using the built in mosaic function (Wincadence, Physical Electronics, Chanhassen, MN) (excluding HVC). Images of 1 x 1 mm were composed of 16 steps, each 250 x 250 μm, areas of 1.5 x 1.5 mm were composed of 16 steps, 375 x 375 μm each. Images containing HVC and AL were stitched as previously described (Amaya et al. 2007). All images were convolved once using the software default settings. Positive identification of molecules relied on purchased pure chemicals that were subjected to ToF-SIMS analysis (Table 3.1).

Principle Component Analysis (PCA)

For multivariate statistical analysis, mass spectra from the song nuclei were collected by using the region of interest function (ROI) (Wincadence, Physical Electronics, Chanhassen, MN). Spectra were box binned and normalized to carbon (*m/z* 12) a ubiquitous biologically significant ion. Contaminating peaks and peaks < *m/z* 50 were excluded from data analysis. PCA was carried out using PLS_Tool box (Eigenvector Research, Inc. Wenatchee, WA), data was preprocessed by autoscaling and transformed to a logarithmic scale ($\log_{10}$) to ensure high intensity peaks were not over represented (Wagner *et al.* 2004).

Immunohistochemistry

Sections were removed from -80 ^{o}C and fixed with 4% paraformaldehyde (pH 7.3) for 5 min and washed three times with 0.025M PBS (pH 7.0) 5min each time. Tissue was blocked for 1 hour at room temperature in a humid chamber with Image-iT FX signal enhancer (I36933, Invitrogen, Carlsbad, CA), followed by a TBS-TX (50 mM Tris HCl pH 7.4, 150 mM NaCl, and 0.1% Triton-X-100) wash (5 min, x3). A second blocking step with TBS-TX plus 10% normal donkey serum was done followed by a TBS-TX wash step.

Sections were then incubated with primary antibodies against the neuronal marker, NeuN 1:500, (MAB377, Millipore, Billerica, MA) and myelin basic protein, MBP 1:75, (AB9348, Millipore, Billerica, MA) at room temperature in a humid chamber. After 1hr tissue was washed with TBS-TX and incubated 1hr with the secondary antibodies Alexa 488 (A-21202, Invitrogen, Carlsbad, CA) and Alexa 546 (A11040, Invitrogen, Carlsbad, CA) diluted 1:500, followed by a TBS-TX wash. Cell nuclei were stained with DAPI (12 μg/mL) 5min, washed with TBS-TX, and cover slip mounted with ProLong Gold (P36934, Invitrogen, Carlsbad, CA). Slides were then analyzed under a Zeiss Axiovert 200M (Carl Zeiss Microimaging, Inc. Thornwood, NY) fluorescence microscope on site at the Institute for Genomic Biology core facilities.

RESULTS

Distribution of essential fatty acids across RA

The omega-3 and -6 fatty acids eicosapentaenoic acid (*m/z* 301; C20:5) and arachidonic acid (*m/z* 303; C20:4) (respectively) show relative decreased levels in RA compared to the surrounding tissue (Fig. 3.2C and D). Their highest levels are present in the nidopallium. We believe these represent unique chemical species since both FAs are detected by GC-MS, standards subjected to ToF-SIMS exhibited minimal fragmentation, and chemical distribution is not identical (data not shown). In contrast, the omega-3 FA DHA (m/z 327; C22:6) shows increased relative levels in RA compared to surrounding tissue, as do the FAs linoleic acid (m/z 279; C18:2) and 11,14-eicosadienoic acid (m/z 307; C20:2) (Fig. 3.2B, E, and F). The FA α-linolenic acid (m/z 277; C18:3) shows no significant difference in spatial distribution across the image (data not shown).

Histological and lipid analysis across RA

Cresyl violet staining shows a well-defined song nucleus RA, and we are able to identify key structural brain regions, the arcopallium and nidopallium (Fig. 3.3B). The adjacent section was immunohistochemically labeled with the neuronal marker, NeuN (green) showing robust labeling of RA and significant labeling in the nidopallium, but little to no staining in the surrounding arcopallium (Fig. 3.3C). Myelin labeling (red) shows a clear demarcation and a more intense overall labeling of RA compared to the arcopallium or nidopallium (Fig. 3.3C). Punctate areas of intense labeling in the anterior part of the arcopallium likely correspond to FPL fiber tracks, and striations in the nidopallium are neuronal projections that connect HVC and RA. Labeling of cell nuclei with DAPI (blue) shows no discernable difference in cell density across the image. A ToF-SIMS image showing the distribution of palmitic acid (C16:0) shows a clear difference in relative concentration across the different brain areas (Fig. 3.3D).

Using the region of interest (ROI) function we measure the relative FA and cholesterol levels between RA, the arcopallium, and the nidopallium (Fig. 3.3F). Increased levels for ten of the fifteen FAs are observed in RA compared to the arcopallium and nidopallium. Arachidonic acid (C20:4) and EPA (C20:5) are the only FAs that show the greatest relative concentration in the nidopallium. Cholesterol,

pentadecanoic acid (C15:0), and adrenic acid (C22:4) show slight increases in the arcopallium compared to RA and the nidopallium, while 8,11,14-Eicosatrienoic (C20:3) acid shows little difference across the three brain regions (Fig. 3.3F).

Distribution of DHA and AA in HVC, AreaX, LMAN, and DLM

Cresyl violet stained tissue sections show overall cellular distribution and location of the song nuclei exhibited by a more intense cellular labeling (Fig. 3.4B, G, L, and Q). Adjacent sections subjected to immunohistochemistry show little difference in cell density (DAPI), however general neuronal staining (NeuN) shows increased labeling for neurons in the song region (Fig. 3.4C, H, M, and R). Staining against myelin (MBP) shows a slight increase in background staining in LMAN and DLM, a slight decrease in AreaX, and little change in HVC compared to surrounding tissue areas (Fig. 3.4C, H, M, and R). The adjacent sections that were used for IHC were subjected to ToF-SIMS analysis. The omega-3 fatty acid, DHA shows a significant increase in its relative concentration in the areas corresponding to HVC, LMAN and DLM compared to surrounding tissue (Fig. 3.4I, N, and S), while AreaX shows no observable difference in the distribution across the image (Fig. 3.4D). SIMS imaging of the omega-6 fatty acid AA shows a significant decrease in signal in AreaX, DLM, and LMAN (Fig. 3.4E, J, and T) but only a slight relative decrease in HVC compared to surrounding tissue (Fig. 3.4O).

Linescan analysis of LMAN

ToF-SIMS imaging of LMAN shows a unique distribution of the monounsaturated fatty acid oleic acid (OA, C18:1) *m/z* 281 and the saturated fatty acid stearic acid (C18:0) *m/z* 283 (Fig. 3.5A and B). Comparing the relative signal intensity of oleic acid and stearic acid by linescan analysis, moving across the images from the upper left to the lower right, shows the changes in FA distribution (Fig. 3.5C). Oleic acid (red line) shows a significant increase in relative signal intensity in the area corresponding to the song nucleus. Stearic acid (blue line) shows two spots of maximum signal intensity extending over an area of ~150 μm (Fig. 3.5C). Both areas of increased stearic acid signal are immediately adjacent to the increased oleic acid signal. The area corresponding to LMAN, peak oleic acid signal, shows that the relative stearic acid level is similar to the

surrounding background tissue signal (Fig. 3.5C). Comparing the two images it appears the increased stearic acid signal encircles the increased oleic acid signal (Fig. 3.5A and B).

Fatty acid distribution across the auditory lobule

Cresyl violet staining of the auditory lobule (AL) shows fewer cells but larger ones in NCM and CMM (Fig. 3.6B). In contrast area corresponding to Field L has appears to have a higher cellular density can composed of smaller cells. Immunohistochemical analysis shows a similar distribution by DAPI staining and NeuN staining (Fig. 3.6C). Interestingly staining against myelin basic protein shows increased labeling in Field L area and the dorsal area of NCM (Fig. 3.6C). ToF-SIMS imaging reveals the saturated FA, palmitic acid with local enrichment along the laminal striation separating CMM from Field L and NCM, and CMM with a relative decrease in concentration (Fig. 3.6D). The mono-unsatruated FA oleic acid shows increased relative concentration in the caudal part of NCM and anterior part of CMM with decreased levels in Field L (Fig. 3.6E). However the saturated FA, stearic acid shows a localized increase in Field L compared to the surrounding AL tissue (Fig. 3.6F). The essential fatty acids DHA and EPA show increased relative levels in NCM and CMM, and locally depressed levels in the area corresponding to Field L (Fig. 3.6G and H). Increased relative levels of AA and EPA are also observed in the gray matter area of the cerebellum compared to white matter region.

Discrimination of song nuclei by PCA

Comparing ToF-SIMS spectra of the major song nuclei in the song system by PCA shows that PC1 (x-axis) captures 55% of the variation in the data (Fig. 3.7). Much of the variation is between the chemical profiles of NCM/CMM and RA along with one spectrum from LMAN (Fig. 3.7A). Analysis of the corresponding loadings plot reveals that NCM/CMM have greatest association (increased relative amount) with *m/z* 79.96 (phosphate), *m/z* 122.00 (ethanolamine), and unknown peaks (*m/z* 80.97, 152.91, 134.04) (Fig. 3.7B). The same loadings plot shows that RA and one LMAN spectrum have a relative increase in peaks corresponding to FAs *m/z* 255.23 (palmitic acid), *m/z* 227.36 (myristic acid), *m/z* 309.28 (11-eicosenoic acid), and *m/z* 327.23 (DHA) compared to

NCM/CMM. Spectra from the other song nuclei show little variation in relation to NCM/CMM and RA based on their position near the x-axis. PC2 (y-axis) accounts for 16.44% of the variation and captures major differences between AreaX and the song nuclei DLM, along with some spectra from RA and LMAN (Fig. 3.7A). Much of the difference is captured by an unknown peak, *m/z* 124.02, showing relative abundance in AreaX. Other peaks highly associated with AreaX include *m/z* 564.55, *m/z* 163.04, *m/z* 152.91, *m/z* 62.97, *m/z* 79.96 (phosphate) and *m/z* 122.00 (ethanolamine) (Fig. 3.7B). Along PC2 of the corresponding loadings plot shows that peaks corresponding to fatty acids *m/z* 327.23 (DHA), *m/z* 309.28 (11-eicosenoic acid), *m/z* 283.27 (stearic acid), and *m/z* 281.25 (oleic acid) show higher relative levels in DLM, and some spectra from RA and LMAN compared to AreaX (Fig. 3.7). Spectra from NCM, CMM, HVC, and some RA and DLM tissue show little variation compared to DLM and AreaX based on their proximity to the y-axis (Fig. 3.7A).

Developmental change in RA

We examined male birds at three different ages, corresponding to just before onset of the critical period for song learning and circuit maturation (post-hatch day 20, p20), the peak of the critical period (p40) and adulthood (>p90). Principle component analysis comparing RAs from three male birds at each age shows significant separation between adult and p20 RAs (Fig. 3.8A). Most of the age-related separation is along PC2, accounting for 21.26% of the total variation in the spectral data, while PC1 accounts for 66.25% of the variation and appears to capture inherent biological variation (Fig. 3.8A). Analysis of the corresponding loadings plot for PC2 reveals that phosphate (*m/z* 79.96), an unknown (*m/z* 124.01), and a peak representing phosphothanolamine (m/z 122.00) are the major peaks associated (increased relative abundance) with RA from p20 birds compared to adults (Fig. 3.8B). The loadings plot also shows that RAs from adult birds show greatest association (relative abundance) with high molecular peaks m/z 800's, along with some FA's including: DHA (m/z 327.24), 11-eicosanoic acid (m/z 309.28), and stearic acid (m/z 283.27), in addition to a peak corresponding to vitamin E (m/z 429.33) (Fig. 3.8B).

Developmental change of the song nuclei

Examination of the ToF-SIMS spectra are evaluated for the song nuclei RA, HVC, NCM, CMM, AreaX, LMAN, DLM from p20 and adult male zebra. ToF-SIMS spectra for each song nuclei were collected from three different birds and subjected to PCA analysis (Fig. 3.9). Principle component 2 (PC2) captures 14% of the variance in the spectra and separates p20 song nuclei from adults (Fig. 3.9A). The corresponding loadings plot shows that higher molecular weight molecules specifically *m/z* 660.84 and 662.85 have higher relative amount in adult song nuclei compared to those for p20 birds (Fig. 3.9B). In contrast lower *m/z* peaks 95.98, 66.01, and 68.02 are associated with song nuclei from p20 birds.

DISCUSSION

The results presented here demonstrate ToF-SIMS as a valuable tool used to uncover chemical heterogeneity and the subcellular distribution of fatty acids in functionally relevant areas in the zebra finch brain.

ToF-SIMS is a highly sensitive surface analysis method relaying on the bombardment of a primary ion to analyze the top few monolayers of a samples surface (Sodhi 2004). Topographical differences can affect the sputtering of secondary ions (McDonnell *et al.* 2005) and imaging. Cryosectioning prevents most of these topographical problems, however, we do observe small localized areas of high signal intensity in some images, most notably from linoleic acid C18:2 (*m/z* 279) along the brain tissue border (Fig. 3.10). These areas are minimal, easily identifiable, and did not affect the overall quality or analysis of the images.

Chemical fragmentation using ToF-SIMS is another common issue that has been addressed in part by using cluster ions (Brunelle *et al.* 2005) and higher molecular weight primary ions (Fletcher *et al.* 2006). The majority of the fatty acids detected in this study are likely lipids that have been fragmented upon impact by the primary ion. To demonstrate this we used a pure standard of phosphatidylethanolamine and subjected it to ToF-SIMS analysis (Fig. 3.11). Efforts to correlate esterified to FFA using ToF-SIMS is further complicated due to differences in molecular ionization and the effects surrounding compounds have on ionization in chemically complex samples like the brain (Ostrowski

et al. 2005). Despite limitations we are confident that the chemical differences observed accurately represent heterogeneous distribution differences across brain areas.

Our focus on RA to image the distribution of essential fatty acids was in part based on the fact RA is enriched in glutamatergic projection neurons as well as GABAergic neurons (Pinaud & Mello 2007), is enriched in synaptic connections, and its neurons are metabolically active. Essential fatty acids specifically DHA has been shown to be enriched in metabolically active brain areas such as the mammalian basal ganglia and gray matter (Diau *et al.* 2005). In addition, regions with increased synaptic vesicles (McGee *et al.* 1994), and nerve growth cones (Martin & Bazan 1992) have exhibitive increased DHA levels. It is hypothesized the highly unsaturated nature of DHA provides significant membrane fluidity required for proper brain function (Bourre et al. 1992) and neuronal development (Calderon & Kim 2004).

The observed decrease in relative signal of AA and EPA in RA proposes an interesting series of questions and areas of investigation. We hypothesize that lower EPA levels in RA may be a result of increased synthesis of EPA to DHA in order to maintain higher relative levels of DHA in RA. Arachidonic acid, a cell signaling molecule plays a role in long-term potentiation (Williams et al. 1989), but is well known for its pro-inflammatory effects as a precursor in eicosanoid synthesis (Simopoulos 2002) and its association with the alpha-synuclin protein in Parkinsons's patients (Ellis *et al.* 2005). Curiously, in RA the mRNA encoding the alpha-synuclein zebra finch protein homolog shows decreased transient expression in RA compared to the surrounding tissue (George *et al.* 1995).

Imaging by ToF-SIMS poses a challenge since a minimum number of counts per pixel is typically required to observe chemical differences across images (Brunelle et al. 2005).This limited our ability to image a subset of detectable molecules. Because RA presented us with tissue heterogeneity we measured the relative concentration of identifiable FAs and cholesterol across these brain regions. Overall, we observe an increase in relative FA concentration in RA compared to the surrounding brain areas, but do not observe any apparent correlation between FA distribution and histological results. However, a pattern does emerge in which the highly unsaturated 20-carbon length FAs have relative decreased concentration in RA compared to the arcopallium and

nidopallium, but increasing saturation results in increased C20 FA concentration in RA (Fig. 3.3F).

Arachidonic acid and DHA are two well-studied FAs and have shown important functional roles in the brain, this prompted us to image their distribution across HVC, LMAN, DLM, and AreaX. Overall AA exhibited a decrease in relative distribution in the area corresponding to the song nuclei as was shown in RA. However, AreaX did not show a corresponding increase in DHA as the other song nuclei show. AreaX is unique compared to the other song regions because it is located in the striatum proper of the basal ganglia containing both striatial and pallidal neurons mostly small γ-aminobutyric acid (GABA)ergic spiny neurons and fewer large GABAergic neurons (Farries & Perkel 2002, Reiner *et al.* 2004, Grisham & Arnold 1994, Carrillo & Doupe 2004). Differences in distribution for essential and non-essential fatty acids may reflect cellular differences in AreaX compared to other song regions.

In addition to the HVC-RA pathway another pathway connects to RA, the DLM-LMAN-RA pathway. During development of the connecting pathways LMAN undergoes dynamic cellular rearrangement. Behaviorally, impairment of DLM or LMAN affects a juvenile birds ability to learn song but not song it has already learned, in comparison impairment of RA affects vocal production during learning and already learned song. The DLM-LMAN-RA pathway is composed of two parallel pathways, one that to the LMAN "core", composed of magnocellular neurons; the other pathway connecting to the LMAN "shell", composed of parvicellular neurons (Johnson *et al.* 1995). Our results of ToF-SIMS imaging of LMAN appear to show differential distribution of fatty acids between the LMAN "core" and "shell" where stearic acid has a higher relative concentration in the LMAN "shell" compared to the LMAN "core". The ability to image fatty acid differences in a functionally relevant brain region and across small areas provides a unique insight into brain neurochemistry. These results reveal potential functional relevance of these fatty acids in neuronal function of LMAN.

Although not considered part of the song control system the auditory lobule AL, composed of CMM and NCM, is involved in the auditory processing of birdsong (Mello 2002). The AL exhibited a unique distribution of fatty acids not observed in the other song nuclei. The most striking difference in fatty acid distribution is for AA and EPA

showing the highest relative levels in the caudal part of NCM, with much lower levels in Field L area. We show that the AA levels are statistically higher in NCM compared to AA levels in other song regions (Table 3.2). Curiously, in the zebra finch AL the receptors for retinoic acid show a similar expression pattern (Jeong *et al.* 2005). Retinoic acid production in the song control system is necessary for normal song maturation (Denisenko-Nehrbass *et al.* 2000a), and in mice it has a role in neuronal plasticity and learning and memory (Krezel *et al.* 1998, Cocco *et al.* 2002). In addition to AA and EPA the AL showed differential distribution of palmitic acid, stearic acid, and oleic acid (Fig. 3.6D-F). The differential distribution of FAs adds to previous evidence that the auditory caudomedial telencephalon is composed of distinct cellular populations with distinct molecular, anatomical, and physiological properties.

Comparing the distribution of essential and non-essential fatty acids across the song nuclei most fatty acids appear to have a increased relative levels compared to surrounding tissue. The most noticeable difference is AreaX which may be due to its presence in the stiatum and its cellular composition, in addition to the fatty acids EPA and AA (Fig. 3.10 and 3.12).

PCA was applied to the ToF-SIMS spectra to identify chemical differences between song nuclei. Principle component 1 (PC1) captures 55% of the spectral variation and reveals chemical differentiation of the song nuclei based on their function in the song system. NCM/CMM, a sensory region, shows significant variation with RA, involved in motor function. Regions involved in both motor and sensory function cluster between RA and NCM/CMM representing less spectral variation. Decreased association of RA, compared to NCM/CMM, with phosphate and ethanolamein may suggest relative increase in sphingomyelin and glycosphingolipids (Isaac *et al.* 2006, Sastry 1985).

PC2 (y-axis) reveals an interesting pattern of distributions based on brain structure. The song nucleus Area X located in the striatum proper of the basal ganglia contains both striatial and pallidal neurons and mostly small γ-aminobutyric acid (GABA)ergic spiny neurons with fewer large GABAergic neurons (Farries & Perkel 2002, Reiner *et al.* 2004, Grisham & Arnold 1994, Carrillo & Doupe 2004). This region shows major chemical differences with DLM, located in the thalamic area of the brain. The corresponding loadings plot reveals a relative decrease in DHA and 11-eicosenoic

acid, in DLM compared to AreaX. The remaining song nuclei, all in the pallial tissue of the telencephalon, which is thought to share a common origin with the mammalian cortex (Farries & Perkel 2002) are composed of glutamatergic projection neurons, they cluster between AreaX and DLM. The ability to identify chemical signatures in biologically complex tissue such as the brain, correlating molecules to functionally relevant and tissue specific brain regions, and imaging their distribution represents a significant advance in the study of brain neurochemistry with applications in the study of neurological disorders and diseases.

RA receives a major projection from HVC, in males but not females at around post-hatch day 30, at which point juvenile males begin to vocalize and rehearse their learned conspecific male tutor song. We use ToF-SIMS and PCA to measure and observe chemical differences immediately before and after innervation of RA and after development of the song system is complete. RA is of interests because development of the pathway has been shown to be under the strong influence of neurosteroids, specifically 17β-estadiol (Holloway & Clayton 2001). RA undergoes changes that includes, a decrease in cell density, an increase in neuron soma size along with the volume of RA (Konishi & Akutagawa 1985). The transient expression of the lipid binding protein α-synuclein is also observed during development (George et al. 1995).

PC1 captures most of the variation (66%) representing biological variation. However, PC2 (y-axis) successfully separates RAs from p20 birds from those of adults. Interestingly RAs from p40 birds represent a sort of chemical transition from p20 to adult. The corresponding loadings plot shows high molecular weights ions *m/z* ~800-860 with relative increase in the adult RA. Although we have not positively identified these peaks they may represent esterified lipids such as triglycerides and glycosphingolipids (Pernber et al. 2007, Touboul *et al.* 2005). Vitamin E (*m/z* 429.33) and fatty acids DHA (m/z 327.24), 11-eicosanoic acid (m/z 309.28), and stearic acid (m/z 283.27) all show relative increases in adult RA compared to RAs from p20 birds.

RA from p20 birds is identified by an unknown peak at *m/z* 124.01, in addition peaks identified as phosphate (*m/z* 79.96) and ethanolamine (*m/z* 122.00) show relative increases in p20 RAs compared to adults. These results may suggest a relative increase in other lipids such as sphingomyelin in RA after the day 30 as the neuronal projections

connecting the HCV-RA pathway develop. Myelination has been shown to take place around post-hatch day 50 (Clayton 1997), to verify these results IHC using sections from p20 birds showed no staining using the MBP antibody (data not shown). Other ions showing significant association with p20 RAs include *m/z* 80.94, 62.97, 94.01, 146.04, these represent lower molecular weights molecules and likely constitute fragmentation ions of larger molecules, making their identification difficult. Appling PCA to ToF-SIMS data demonstrates we can successfully identify molecular ions, many of which are lipid associated or lipophilic, that show age related changes before and after a major developmental change in RA.

The results presented here demonstrate that subcellular imaging of fatty acids and other small molecules by ToF-SIMS in biologically complex samples, such as the brain, opens significant avenues in the study of brain neurochemistry and disease. Moreover, we demonstrate that combining ToF-SIMS with a multivariate statistical method such as PCA can successfully identified unique chemical signatures that are associated with functionally distinct and tissue specific brain areas, and show developmental changes in specific brain areas of the zebra finch. These studies represent the initial stage to map the distribution of potentially functionally significant small molecules in the zebra finch brain. Future studies focusing on the identification of unknown peaks in the ToF-SIMS spectra will significantly aid our understanding of small molecule heterogeneities across the zebra finch song system.

ACKNOWLEDGMENTS

I would like to thank Timothy Spila for his assistance with the ToF-SIMS. This investigation was supported by the National Institutes of Health under Ruth L. Kirschstein National Research Service Award F31 NS060179-01A1. Research was carried out in part in the Frederick Seitz Materials Research Laboratory Central Facilities, University of Illinois, which are partially supported by the U.S. Department of Energy under grants DE-FG02-07ER46453 and DE-FG02-07ER46471.

FIGURES AND TABLES

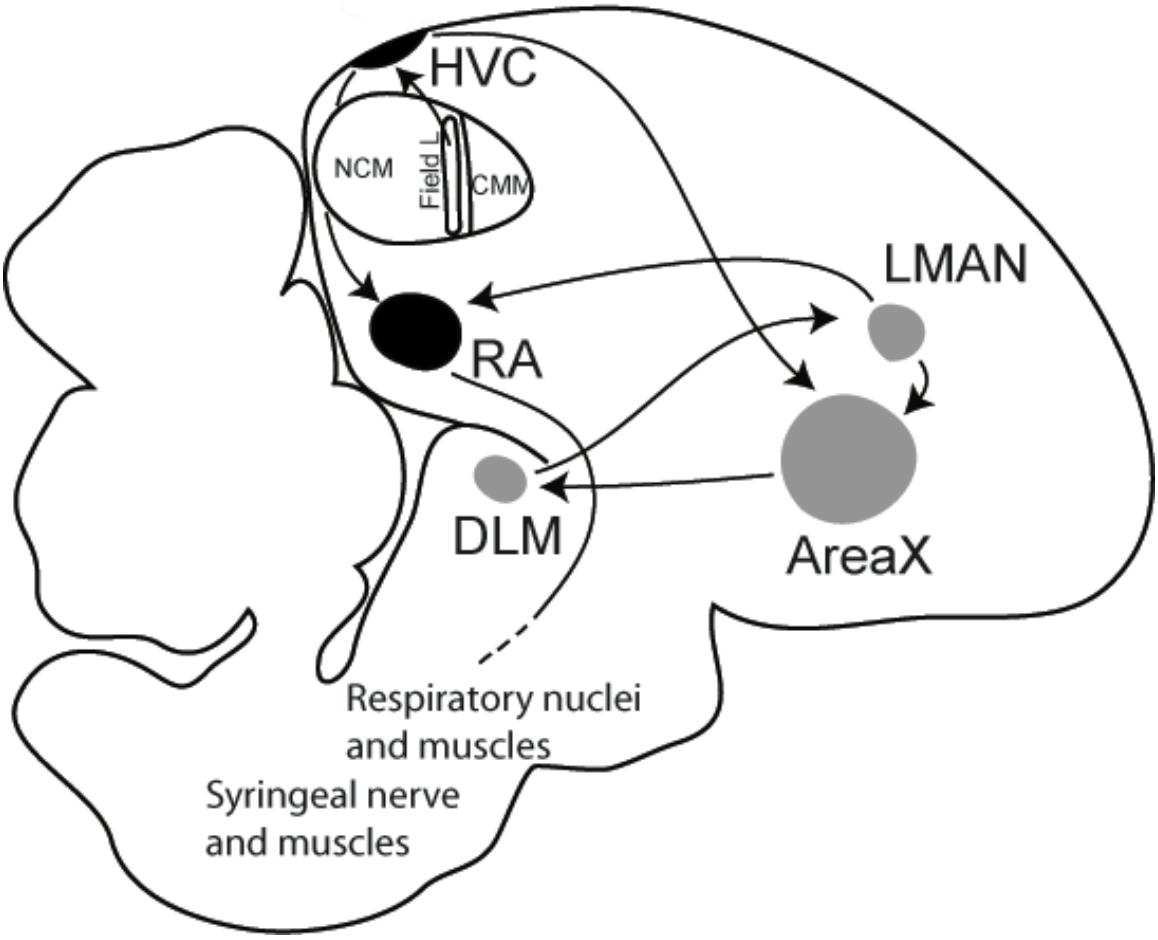

Figure 3.1. Schematic drawing of a sagittal section of an adult male zebra finch brain showing the major song nuclei and neuronal connections of the song system. The anterior forebrain pathway, in grey, is composed of AreaX, lateral magnocellular nucleus of the anterior nidopallium (LMAN), and the dorso-medial division of the medial thalamus (DLM). In white the auditory pathway includes Field L, caudal medial mesopallium (CMM), and the caudal medial nidopallium (NCM), which make up the auditory lobule (AL). In black is the song motor pathway composed of the robust nucleus of the arcopallium (RA) and HVC.

Lipid	Ion	Calculated	Measured	Designation
Phosphate	PO_2^-	62.97	62.97	molecular ion
Phosphate	PO_3^-	78.97	78.96	molecular ion
PE	$C_2H_5NO_3P^-$	122.04	122.00	head group
PE	$C_2H_7NO_4P^-$	140.05	140.02	head group
C14:0	$C_{14}H_{27}O_2^-$	227.36	227.20	[M-H]-
C15:0	$C_{15}H_{29}O_2^-$	241.39	241.22	[M-H]-
C16:1	$C_{16}H_{29}O_2^-$	253.40	253.22	[M-H]-
C16:0	$C_{16}H_{31}O_2^-$	255.42	255.23	[M-H]-
C17:0	$C_{17}H_{33}O_2^-$	269.44	269.24	[M-H]-
C18:2	$C_{18}H_{31}O_2^-$	279.44	279.24	[M-H]-
C18:1	$C_{18}H_{33}O_2^-$	281.45	281.24	[M-H]-
C18:0	$C_{18}H_{35}O_2^-$	283.47	283.28	[M-H]-
C20:5	$C_{20}H_{29}O_2^-$	301.44	301.22	[M-H]-
C20:4	$C_{20}H_{31}O_2^-$	303.46	303.22	[M-H]-
C20:3	$C_{20}H_{33}O_2^-$	305.47	305.22	[M-H]-
C20:2	$C_{20}H_{35}O_2^-$	307.49	307.26	[M-H]-
C20:1	$C_{20}H_{37}O_2^-$	309.51	309.31	[M-H]-
C22:6	$C_{22}H_{31}O_2^-$	327.48	327.23	[M-H]-
C22:4	$C_{22}H_{33}O_2^-$	329.50	331.27	[M-H]-
Cholesterol	$C_{27}H_{43}O^-$	383.63	383.31	[M-3H]-
Cholesterol	$C_{27}H_{45}O^-$	385.65	385.35	[M-H]-
Cholesterol	$C_{27}H_{46}O^-$	386.65	386.36	[M]-

Table 3.1. Peak assignment for standards used in ToF-SIMS analysis using negative ion detection.

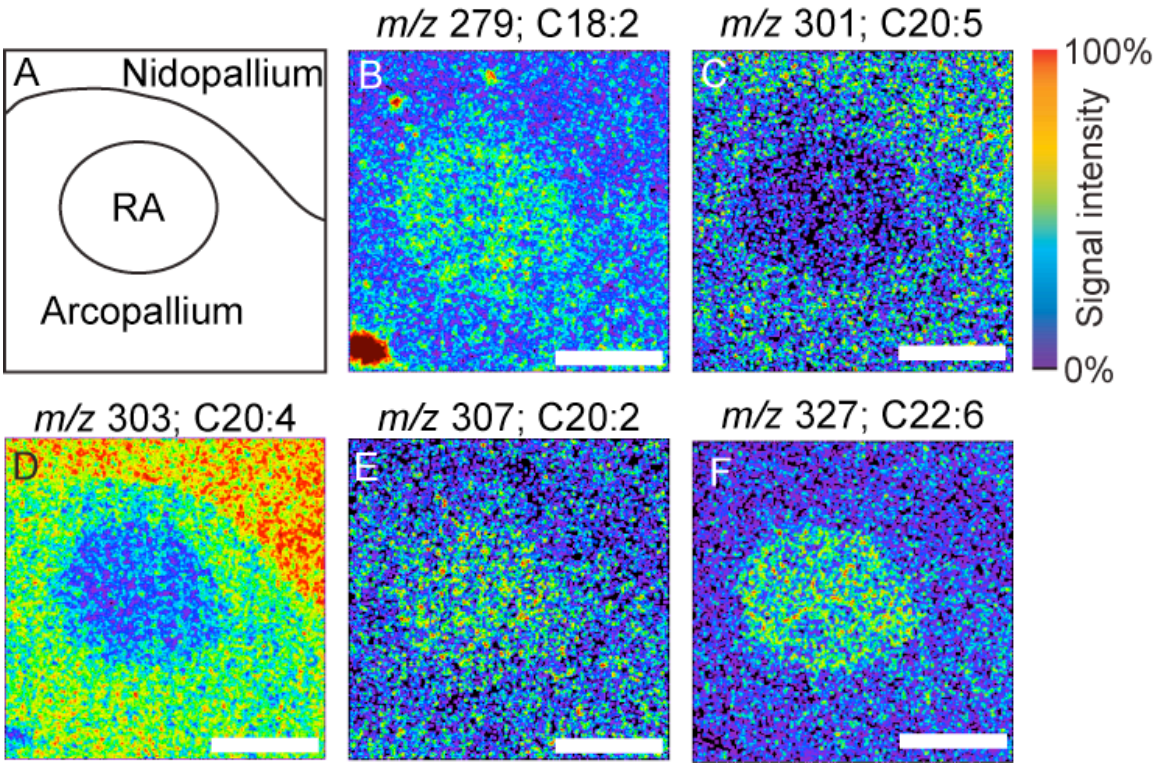

Figure 3.2. ToF-SIMS images showing the distribution of omega-3 and -6 fatty acids across RA. Illustration showing brain features in the section across RA (A). ToF-SIMS images showing the distribution of linoleic acid (C18:2) (B), eicosapentaenoic acid (C20:5) (C), arachidonic acid (C20:4) (D), 11,14-eicosadienoic acid (C20:2) (E), and docosahexaenoic acid (C22:6) (F). Scale bar = 500 μm

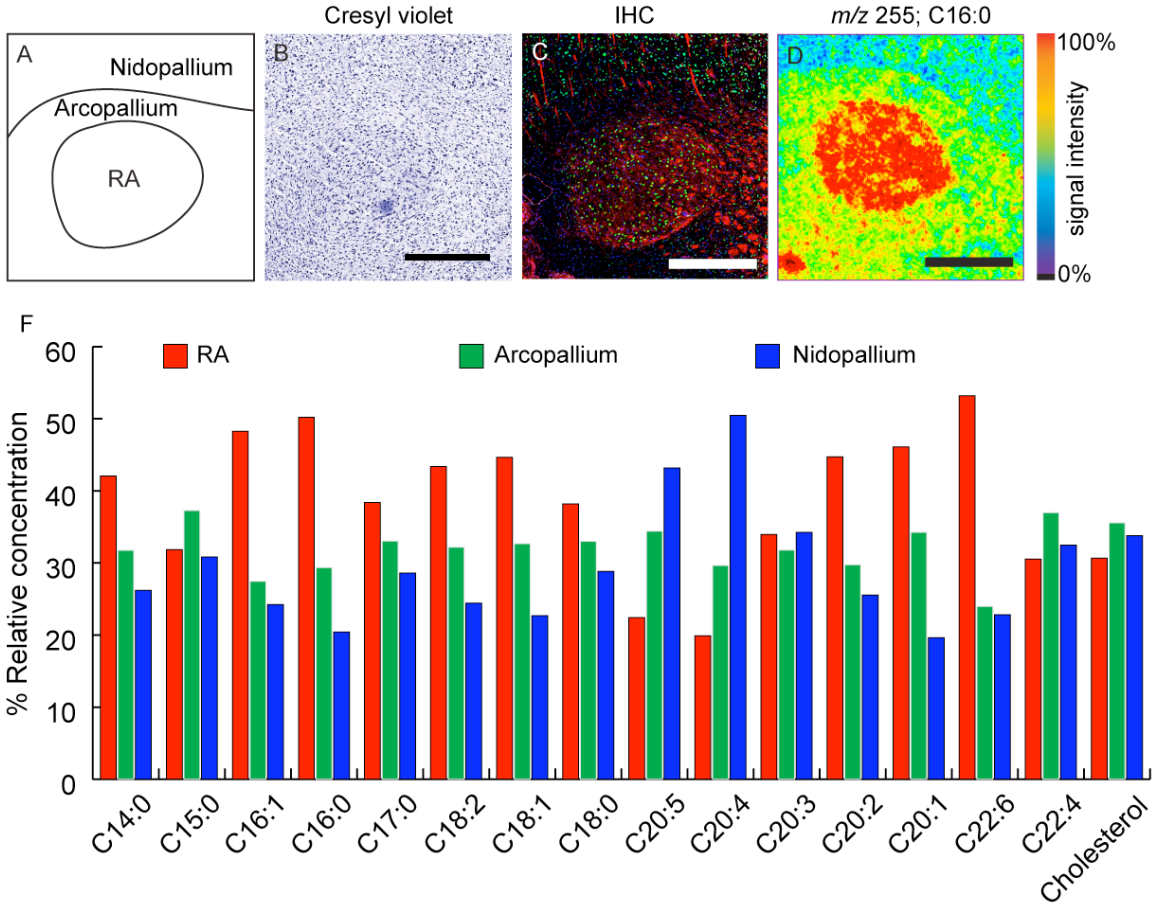

Figure 3.3. Relative FA concentration across the image of RA. Illustration showing anatomical features across RA (A), cresyl violet stained section showing cell distribution (B), IHC showing cell distribution with DAPI (blue), neuronal distribution NeuN (green), myelin basic protein (red) (C). ToF-SIMS image showing the distribution of palimitic acid (C16:0) across RA (D). The graph compares the relative concentration of different fatty acids in RA(red), the arcopallium (green), and nidopallium (blue) (F). Spectra were collected by ROI, normalized to the carbon ion, and expressed as a percentage of the total from the different brain areas. Scale = 500 μm

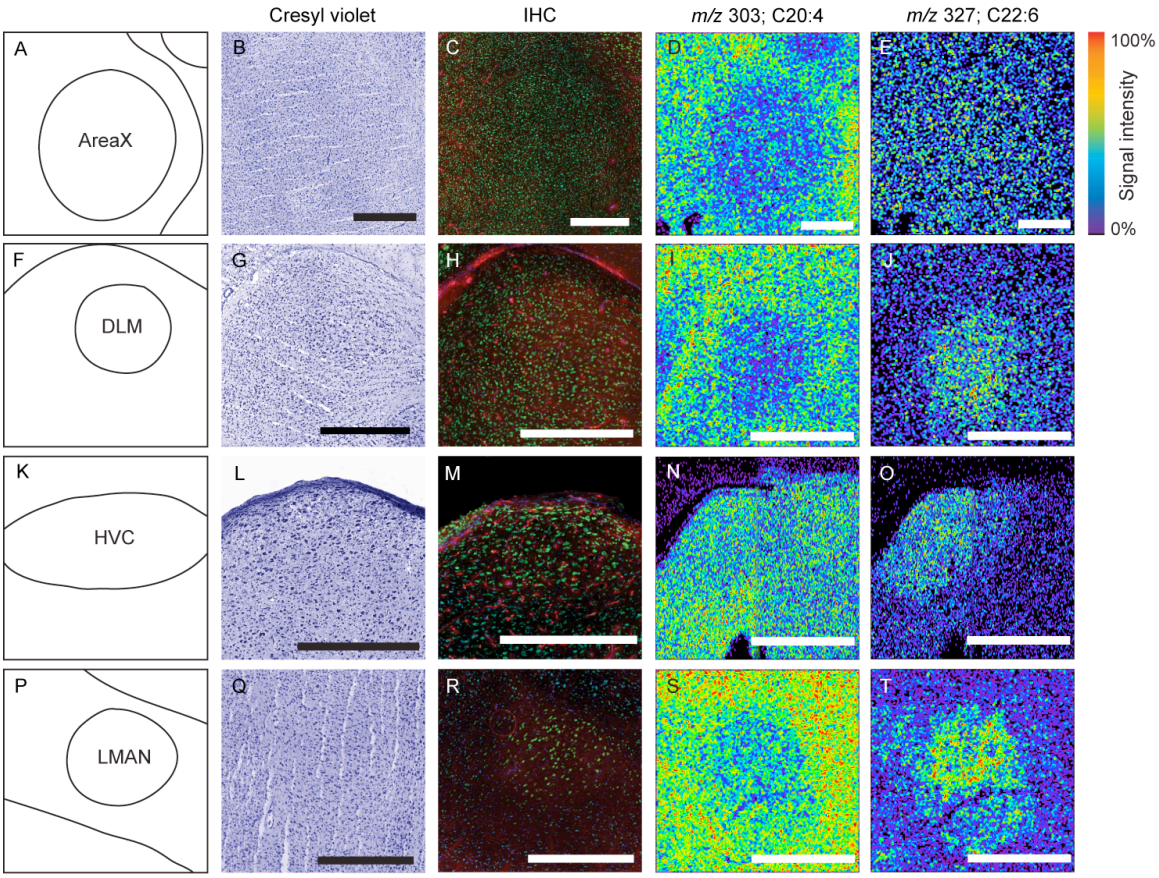

Figure 3.4. Anatomical analysis across AreaX, DLM, HVC, and LMAN and distribution of AA and DHA. Illustration showing brain features in the sections across the auditory lobule (A). Cresyl violet stained sections (B, G, L, and Q). Adjacent section used for immunohistochemistry (C, H, M, and R) NeuN (green), myelin basic protein (red), cell nuclei (blue). Adjacent section used for ToF-SIMS analysis showing the distribution of arachidonic acid (C20:4) (D, I, N, and S) and docosahexaenoic acid (C22:6) (E, J, O, and T). Scale bar = 500 μm

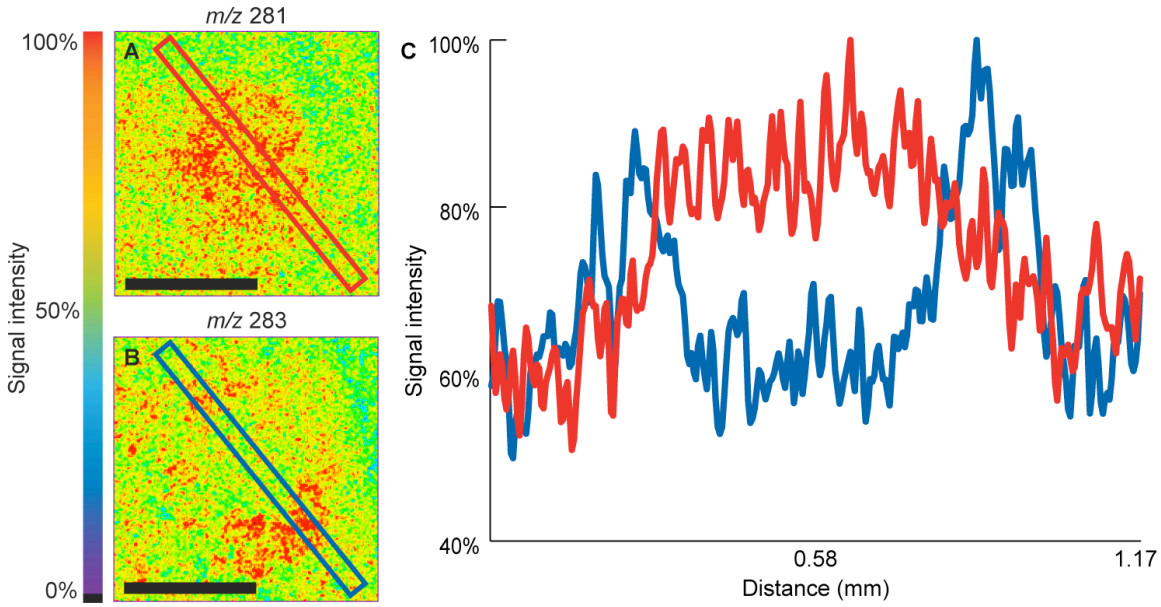

Figure 3.5. Line scan analysis of LMAN. ToF-SIMS images showing the distribution of *m/z* 281 oleic acid (C18:1) (A) and *m/z* 283 stearic acid (C18:0) (B). Line scan shows the relative intensity of the molecules across the images from the top left to the bottom right (C). Scale bar = 500 μm

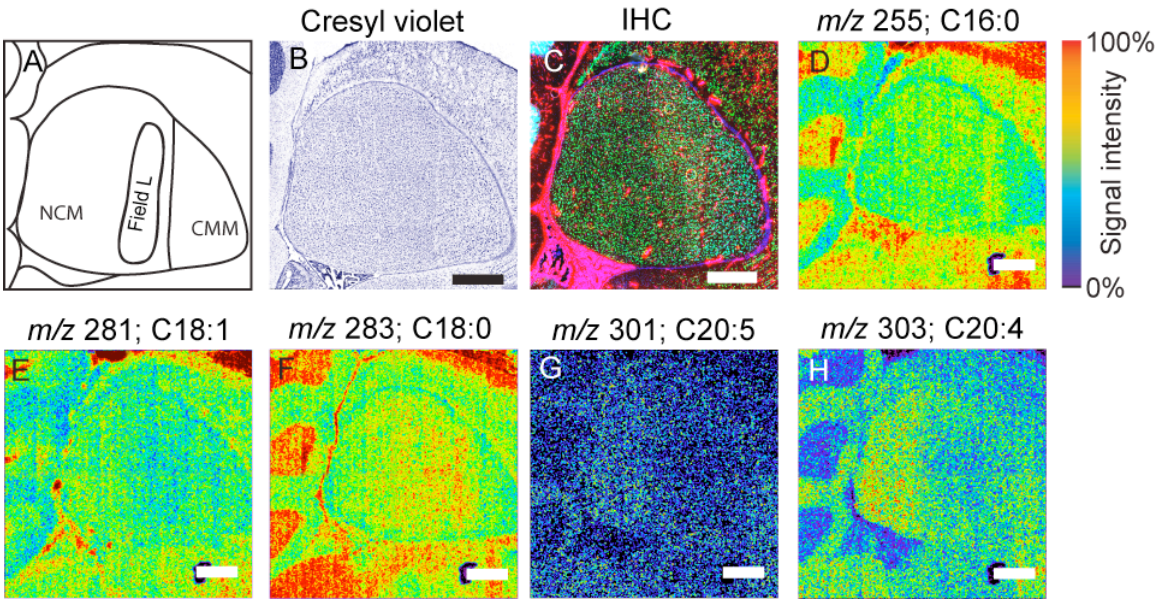

Figure 3.6. FA distribution across the auditory lobule. Illustration showing brain features in the section across the auditory lobule (A). Cresyl violet stained section (B). Adjacent stained section used for immunohistochemistry NeuN (green), myelin basic protein (red), cell nuclei (blue) (C). Adjacent section used for ToF-SIMS analysis showing the distribution of palmitic acid (C16:0) (D), oleic acid (C18:1) (E), stearic acid (C18:0) (F), eicosapentaenoic acid (C20:5) (G), and arachidonic acid (C20:4) (H). Scale bar = 500 μm

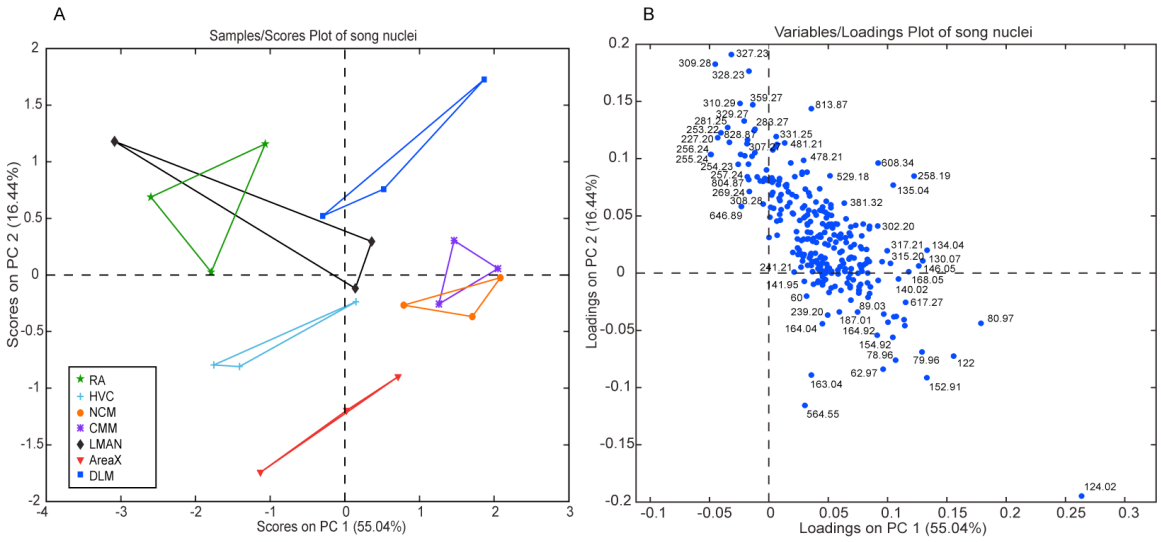

Figure 3.7. Scores plot (A) from principle component analysis using ToF-SIMS data collected from the different song nuclei. Each data point from given song region represents data collected from a different adult brain. A line connects data representing the same song nuclei. Loadings plot (B) shows the masses responsible for the distribution of song nuclei in A.

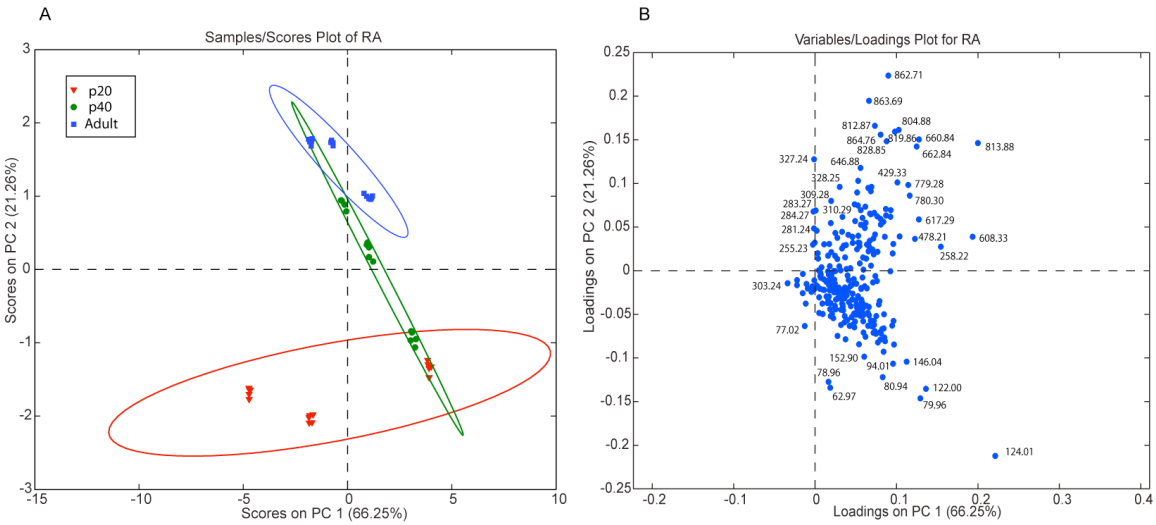

Figure 3.8. Scores plot (A) from principle component analysis using ToF-SIMS data collected from RAs of post-hatch day 20, 40, and adult male zebra finches. Three different males from each age group were used, and with five different spectra were collected from each RA. Ellipses are 95% confidence intervals. Loadings plot (B) shows the masses responsible for the distribution of the different aged RAs in A.

A

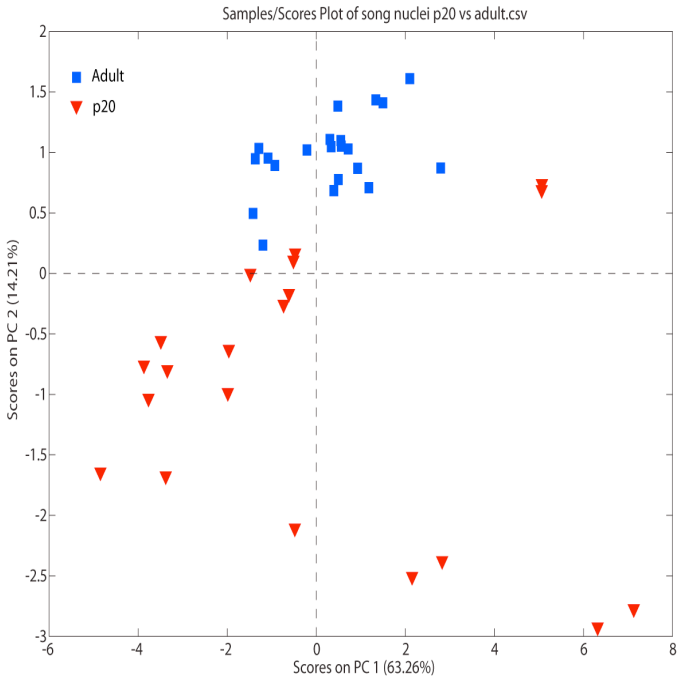

B

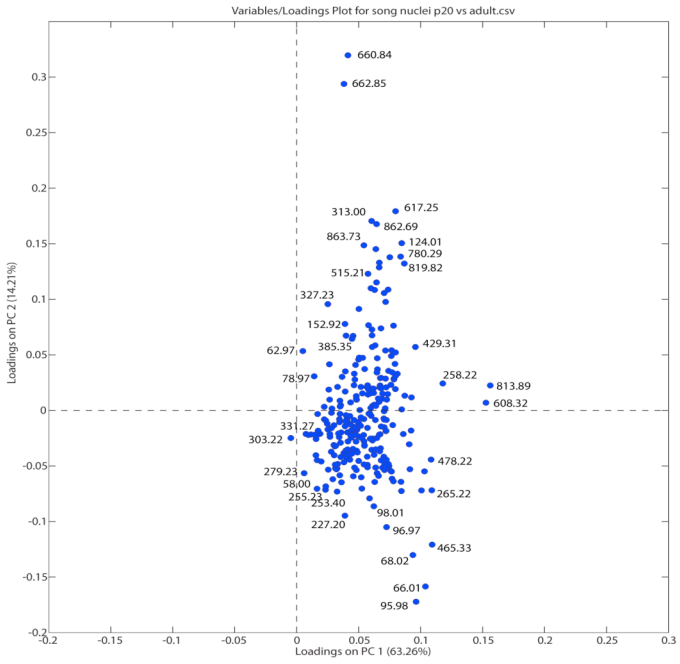

Figure 3.9. Scores plot (A) from principle component analysis using ToF-SIMS data collected from post-hatch day 20 and adult male zebra finches. The song nuclei RA, HVC, NCM, CMM, AreaX, LMAN, and DLM are represented. ToF-SIMS spectra from three distinct birds were collected for each song nuclei. Loadings plot (B) shows the *m/z* peak responsible for the distribution of the different aged song nuclei in A.

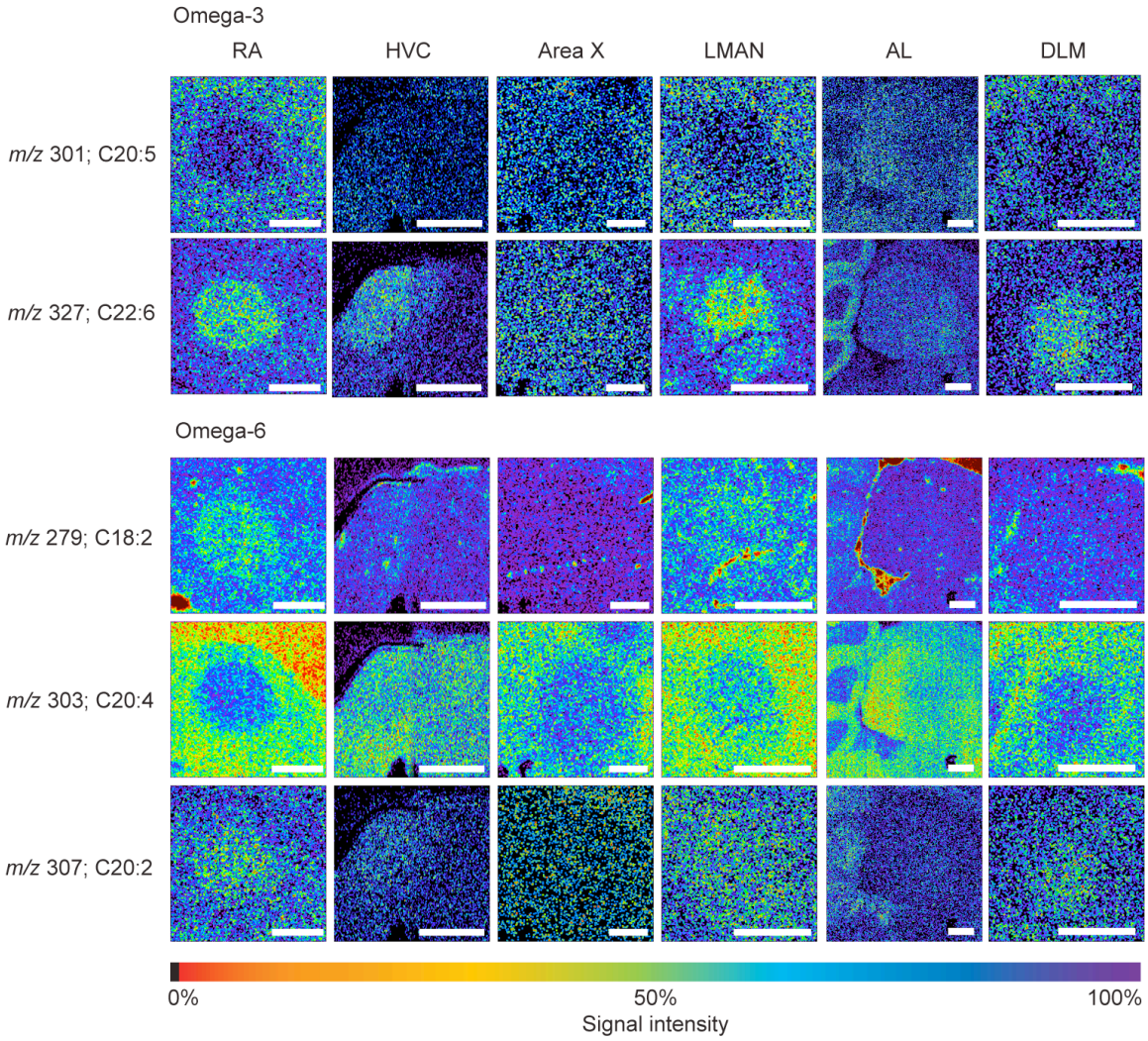

Figure 3.10. ToF-SIMS images show the distribution of essential fatty acids collected across the song nuclei RA, HVC, AreaX, LMAN, AL, and DLM. Omega-3 fatty acids eicosapentaenoic acid (EPA) C20:5 (*m/z* 301), docosahexaenoic acid (DHA) C22:6 (*m/z* 327), and omega-6 fatty acids linoleic acid (LA) C18:2 (*m/z* 279), arachidonic acid (AA) C20:4 (*m/z* 303), and docosadienoic acid C20:2 (*m/z* 307). Scale 500 μm

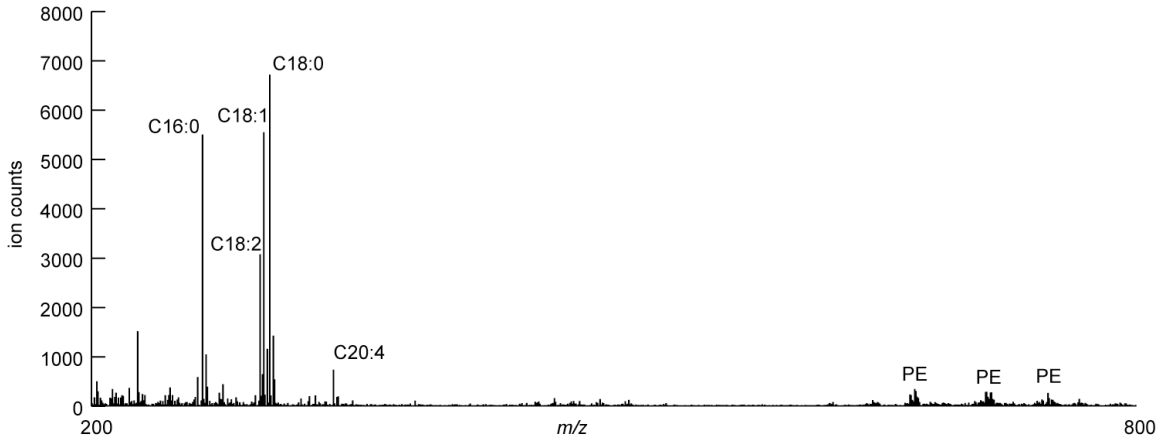

Figure 3.11. ToF-SIMS ion spectra from *m/z* 200 – 800 using a 99% pure sample of phosphatidylethanolamine.

Lipid	RA	LMAN	DLM	HVC	NCM	CMM	AreaX
C14:0*	1.2	1.6	1.2	1.8	1.0	1.3	1.0
C15:0	0.4	0.4	0.3	0.5	0.5	0.5	0.6
C16:1***	2.9	3.4	2.5	3.1	2.4	2.6	2.5
C16:0	38.7	30.9	29.6	32.9	27.2	28.6	32.6
C17:0	1.1	1.0	0.9	1.1	0.9	1.0	1.2
C18:2	2.2	3.0	2.9	2.6	2.1	2.5	2.4
C18:1*	20.2	23.8	19.8	20.7	17.5	17.5	17.3
C18:0**	19.5	17.6	26.9	21.4	23.1	23.5	21.2
C20:5**	0.4	0.5	0.4	0.5	1.5	1.2	0.8
C20:4***	2.4	3.1	2.4	3.0	9.1	6.1	4.9
C20:3*	0.9	1.6	1.1	1.2	1.4	1.5	1.3
C20:2	0.9	1.0	0.9	1.0	0.8	0.9	0.8
C20:1*	1.0	1.2	1.4	1.1	0.7	0.8	0.8
C22:6	1.1	1.6	1.4	0.9	1.1	1.1	1.4
C22:4*	0.6	1.2	0.8	0.8	1.0	0.9	0.9
Cholesterol	6.6	7.9	7.3	7.4	9.9	10.1	10.3

Table 3.2. Average relative concentration of lipids across the different song nuclei.

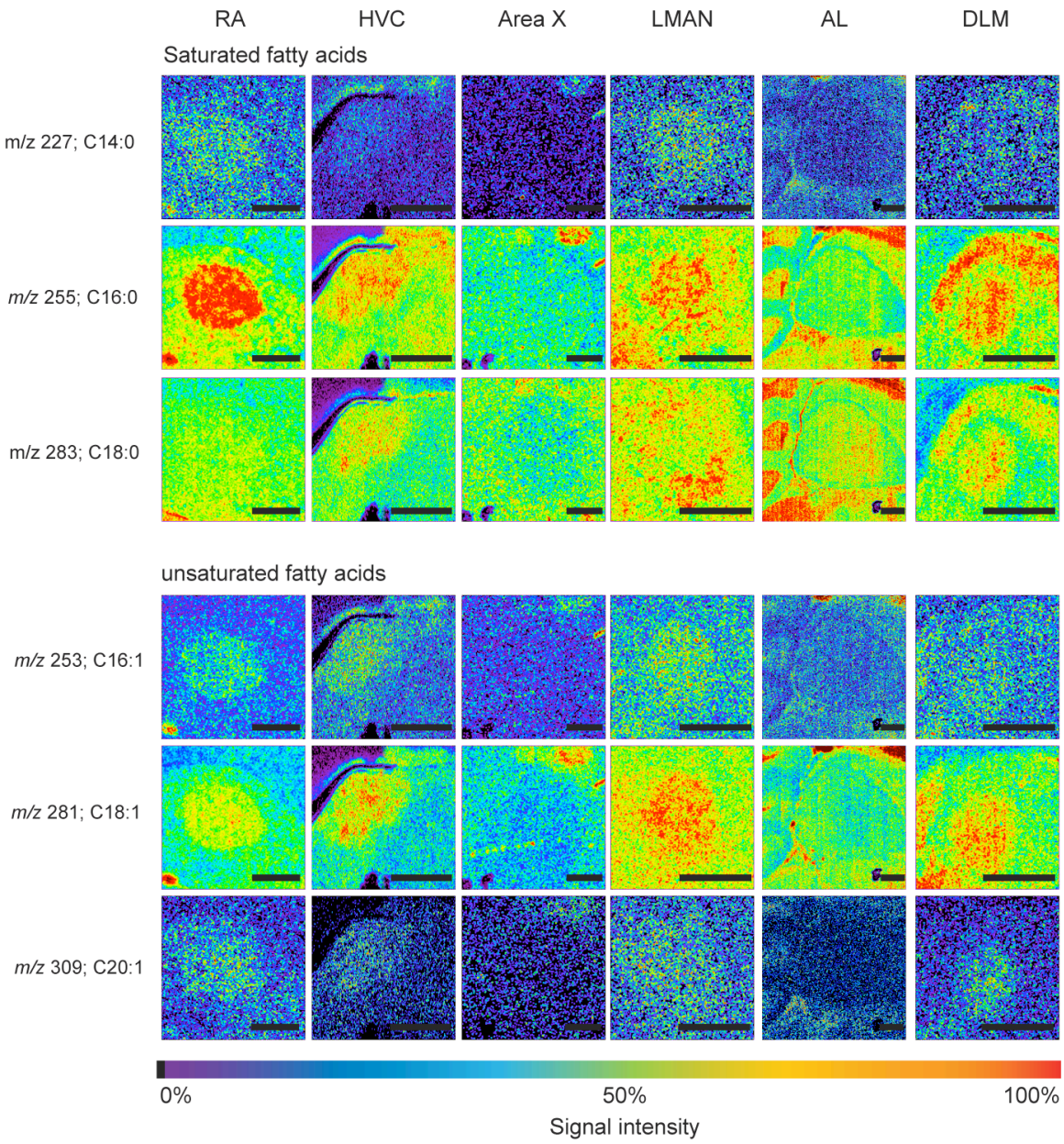

Figure 3.12. ToF-SIMS images show the distribution of non-essential fatty acids collected across the song nuclei RA, HVC, AreaX, LMAN, AL, and DLM. Myristic acid acid C14:0 (*m/z* 227), palmitic acid (*m/z* 255), stearic acid C18:0 (*m/z* 283), palmitoleic acid C16:1 (*m/z* 253), oleic acid C18:1 (*m/z* 281), and eicosenoic acid C20:1 (*m/z* 309). Scale 500 μm

REFERENCES

Altelaar, A. F. M., Klinkert, I., Jalink, K., de Lange, R. P. J., Adan, R. A. H., Heeren, R. M. A. and Piersma, S. R. (2006) Gold-enhanced biomolecular surface imaging of cells and tissue by SIMS and MALDI mass spectrometry. Analytical Chemistry, 78, 734-742.

Amaya, K. R., Monroe, E. B., Sweedler, J. V. and Clayton, D. F. (2007) Lipid imaging in the zebra finch brain with secondary ion mass spectrometry. International Journal of Mass Spectrometry, 260, 121-127.

Bourre, J. M., Dumont, O. S., Piciotti, M. J., Pascal, G. A. and Durand, G. A. (1992) Dietary alpha-linolenic acid deficiency in adult rats for 7 months does not alter brain docosahexaenoic acid content, in contrast to liver, heart and testes. Biochim Biophys Acta, 1124, 119-122.

Brenowitz, E. A., Margoliash, D. and Nordeen, K. W. (1997) An introduction to birdsong and the avian song system. J Neurobiol, 33, 495-500.

Brunelle, A., Touboul, D. and Laprevote, O. (2005) Biological tissue imaging with time-of-flight secondary ion mass spectrometry and cluster ion sources. Journal of Mass Spectrometry, 40, 985-999.

Calderon, F. and Kim, H. Y. (2004) Docosahexaenoic acid promotes neurite growth in hippocampal neurons. J Neurochem, 90, 979-988.

Carrillo, G. D. and Doupe, A. J. (2004) Is the songbird Area X striatal, pallidal, or both? An anatomical study. J Comp Neurol, 473, 415-437.

Clayton, D. F. (1997) Role of gene regulation in song circuit development and song learning. J Neurobiol, 33, 549-571.

Clayton, D. F. and George, J. M. (1999) Synucleins in synaptic plasticity and neurodegenerative disorders. J Neurosci Res, 58, 120-129.

Cocco, S., Diaz, G., Stancampiano, R., Diana, A., Carta, M., Curreli, R., Sarais, L. and Fadda, F. (2002) Vitamin A deficiency produces spatial learning and memory impairment in rats. Neuroscience, 115, 475-482.

Cole-Edwards, K. K. and Bazan, N. G. (2005) Lipid signaling in experimental epilepsy. Neurochem Res, 30, 847-853.

Denisenko-Nehrbass, N. I., Jarvis, E., Scharff, C., Nottebohm, F. and Mello, C. V. (2000a) Site-specific retinoic acid production in the brain of adult songbirds. Neuron, 27, 359-370.

Denisenko-Nehrbass, N. I., Jarvis, E., Scharff, C., Nottebohm, F. and Mello, C. V. (2000b) Site-specific retinoic acid production in the brain of adult songbirds. Neuron, 27, 359-370.

Diau, G. Y., Hsieh, A. T., Sarkadi-Nagy, E. A., Wijendran, V., Nathanielsz, P. W. and Brenna, J. T. (2005) The influence of long chain polyunsaturate supplementation on docosahexaenoic acid and arachidonic acid in baboon neonate central nervous system. BMC Med, 3, 11.

Ellis, C. E., Murphy, E. J., Mitchell, D. C., Golovko, M. Y., Scaglia, F., Barcelo-Coblijn, G. C. and Nussbaum, R. L. (2005) Mitochondrial lipid abnormality and electron transport chain impairment in mice lacking alpha-synuclein. Mol Cell Biol, 25, 10190-10201.

Farries, M. A. and Perkel, D. J. (2002) A telencephalic nucleus essential for song learning contains neurons with physiological characteristics of both striatum and globus pallidus. J Neurosci, 22, 3776-3787.
Fenton, W. S., Hibbeln, J. and Knable, M. (2000) Essential fatty acids, lipid membrane abnormalities, and the diagnosis and treatment of schizophrenia. Biol Psychiatry, 47, 8-21.
Fletcher, J. S., Conlan, X. A., Jones, E. A., Biddulph, G., Lockyer, N. P. and Vickerman, J. C. (2006) TOF-SIMS analysis using C-60- effect of impact energy on yield and damage. Analytical Chemistry, 78, 1827-1831.
George, J. M., Jin, H., Woods, W. S. and Clayton, D. F. (1995) Characterization of a novel protein regulated during the critical period for song learning in the zebra finch. Neuron, 15, 361-372.
Grisham, W. and Arnold, A. P. (1994) Distribution of Gaba-Like Immunoreactivity in the Song System of the Zebra Finch. Brain Research, 651, 115-122.
Gubitosi-Klug, R. A., Mancuso, D. J. and Gross, R. W. (2005) The human Kv1.1 channel is palmitoylated, modulating voltage sensing: Identification of a palmitoylation consensus sequence. Proceedings of the National Academy of Sciences of the United States of America, 102, 5964-5968.
Hartmann, T., Kuchenbecker, J. and Grimm, M. O. (2007) Alzheimer's disease: the lipid connection. J Neurochem, 103 Suppl 1, 159-170.
Holloway, C. C. and Clayton, D. F. (2001) Estrogen synthesis in the male brain triggers development of the avian song control pathway in vitro. Nat Neurosci, 4, 170-175.
Isaac, G., Pernber, Z., Gieselmann, V., Hansson, E., Bergquist, J. and Mansson, J. E. (2006) Sulfatide with short fatty acid dominates in astrocytes and neurons. FEBS J, 273, 1782-1790.
Israeli, E. and Sharon, R. (2009) Beta-synuclein occurs in vivo in lipid-associated oligomers and forms hetero-oligomers with alpha-synuclein. J Neurochem, 108, 465-474.
Jeong, J. K., Velho, T. A. F. and Mello, C. V. (2005) Cloning and expression analysis of retinoic acid receptors in the zebra finch brain. Journal of Comparative Neurology, 489, 23-41.
Johnson, F., Sablan, M. M. and Bottjer, S. W. (1995) Topographic organization of a forebrain pathway involved with vocal learning in zebra finches. J Comp Neurol, 358, 260-278.
Konishi, M. and Akutagawa, E. (1985) Neuronal growth, atrophy and death in a sexually dimorphic song nucleus in the zebra finch brain. Nature, 315, 145-147.
Krezel, W., Ghyselinck, N., Abdel, T., Dupe, V., Kastner, P., Borelli, E. and Chambon, P. (1998) Impaired locomotion and dopamine signaling in retinoid receptor mutant mice. European Journal of Neuroscience, 10, 370-370.
Leekumjorn, S., Cho, H. J., Wu, Y. F., Wright, N. T., Sum, A. K. and Chan, C. (2009) The role of fatty acid unsaturation in minimizing biophysical changes on the structure and local effects of bilayer membranes. Biochimica Et Biophysica Acta-Biomembranes, 1788, 1508-1516.

London, S. E., Monks, D. A., Wade, J. and Schlinger, B. A. (2006) Widespread capacity for steroid synthesis in the avian brain and song system. Endocrinology, 147, 5975-5987.
Lovell, P. V., Clayton, D. F., Replogle, K. L. and Mello, C. V. (2008) Birdsong "Transcriptomics": Neurochemical Specializations of the Oscine Song System. Plos One, 3, -.
Maier, O., Oberle, V. and Hoekstra, D. (2002) Fluorescent lipid probes: some properties and applications (a review). Chem Phys Lipids, 116, 3-18.
Martin, R. E. and Bazan, N. G. (1992) Changing fatty acid content of growth cone lipids prior to synaptogenesis. J Neurochem, 59, 318-325.
McDonnell, L. A., Piersma, S. R., Altelaar, A. F. M., Mize, T. H., Luxembourg, S. L., Verhaert, P. D. E. M., van Minnen, J. and Heeren, R. M. A. (2005) Subcellular imaging mass spectrometry of brain tissue. Journal of Mass Spectrometry, 40, 160-168.
McGee, C. D., Greenwood, C. E. and Cinader, B. (1994) Dietary fat composition and age affect synaptosomal and retinal phospholipid fatty acid composition in C57BL/6 mice. Lipids, 29, 605-610.
Mello, C., Nottebohm, F. and Clayton, D. (1995) Repeated exposure to one song leads to a rapid and persistent decline in an immediate early gene's response to that song in zebra finch telencephalon. J Neurosci, 15, 6919-6925.
Mello, C. V. (2002) Mapping vocal communication pathways in birds with inducible gene expression. Journal of Comparative Physiology a-Neuroethology Sensory Neural and Behavioral Physiology, 188, 943-959.
Monroe, E. B., Jurchen, J. C., Lee, J., Rubakhin, S. S. and Sweedler, J. V. (2005) Vitamin E imaging and localization in the neuronal membrane. J Am Chem Soc, 127, 12152-12153.
Moriguchi, T., Greiner, R. S. and Salem, N., Jr. (2000) Behavioral deficits associated with dietary induction of decreased brain docosahexaenoic acid concentration. J Neurochem, 75, 2563-2573.
Nygren, H., Malmberg, P., Kriegeskotte, C. and Arlinghaus, H. F. (2004) Bioimaging TOF-SIMS: localization of cholesterol in rat kidney sections. FEBS Lett, 566, 291-293.
Ostrowski, S. G., Szakal, C., Kozole, J., Roddy, T. P., Xu, J. Y., Ewing, A. G. and Winograd, N. (2005) Secondary ion MS imaging of lipids in picoliter vials with a buckminsterfullerene ion source. Analytical Chemistry, 77, 6190-6196.
Pernber, Z., Richter, K., Mansson, J. E. and Nygren, H. (2007) Sulfatide with different fatty acids has unique distributions in cerebellum as imaged by time-of-flight secondary ion mass spectrometry (TOF-SIMS). Biochim Biophys Acta, 1771, 202-209.
Pinaud, R. and Mello, C. V. (2007) GABA immunoreactivity in auditory and song control brain areas of zebra finches. Journal of Chemical Neuroanatomy, 34, 1-21.
Reiner, A., Laverghetta, A. V., Meade, C. A., Cuthbertson, S. L. and Bottjer, S. W. (2004) An immunohistochemical and pathway tracing study of the striatopallidal organization of area X in the male zebra finch. J Comp Neurol, 469, 239-261.
Sastry, P. S. (1985) Lipids of nervous tissue: composition and metabolism. Prog Lipid Res, 24, 69-176.

Saum, W. R., McGee, R., Jr. and Love, J. (1981) Alteration of the action potential of tissue cultured neuronal cells by growth in the presence of a polyunsaturated fatty acid. Cell Mol Neurobiol, 1, 319-324.
Schmidt, D., Jiang, Q. X. and MacKinnon, R. (2006) Phospholipids and the origin of cationic gating charges in voltage sensors. Nature, 444, 775-779.
Simopoulos, A. P. (2002) Omega-3 fatty acids in inflammation and autoimmune diseases. J Am Coll Nutr, 21, 495-505.
Sodhi, R. N. S. (2004) Time-of-flight secondary ion mass spectrometry (TOF-SIMS): versatility in chemical and imaging surface analysis. Analyst, 129, 483-487.
Suzuki, T. (2002) Lipid rafts at postsynaptic sites: distribution, function and linkage to postsynaptic density. Neurosci Res, 44, 1-9.
Tahallah, N., Brunelle, A., De La Porte, S. and Laprevote, O. (2008) Lipid mapping in human dystrophic muscle by cluster-time-of-flight secondary ion mass spectrometry imaging. J Lipid Res, 49, 438-454.
Touboul, D., Brunelle, A., Halgand, F., De La Porte, S. and Laprevote, O. (2005) Lipid imaging by gold cluster time-of-flight secondary ion mass spectrometry: application to Duchenne muscular dystrophy. Journal of Lipid Research, 46, 1388-1395.
Wagner, M. S., Graham, D. J., Ratner, B. D. and Castner, D. G. (2004) Maximizing information obtained from secondary ion mass spectra of organic thin films using multivariate analysis. Surface Science, 570, 78-97.
Williams, J. H., Errington, M. L., Lynch, M. A. and Bliss, T. V. (1989) Arachidonic acid induces a long-term activity-dependent enhancement of synaptic transmission in the hippocampus. Nature, 341, 739-742.

CHAPTER 4
METABOLIC PROFILING OF THE ZEBRA FINCH AUDITORY FOREBRAIN AFTER SONG EXPOSURE

ABSTRACT

The auditory lobule (AL) in the zebra finch, a songbird, brain is responsible of interpreting, processing, and forming initial auditory memories and has been the focus of significant study. Previous research in our lab has shown a complex transcriptomic and proteomic response in AL after exposure to a novel conspecific song and habituation compared to a silent control group. Presented here we expand on those results to include a metabolomic analysis of AL using similar conditions. Metabolites constitute a diverse group of small molecules acting as intermediates in biochemical processes such as: energy metabolism (i.e. glucose), amino acid synthesis, and as signaling molecules (i.e. GABA), thus providing an instantaneous physiological picture in a tissue (i.e. AL). Applying Partial Least Squares Discriminant Analysis (PLSDA) successfully identifies differences in the metabolic profiles of ALs from birds exposed to novel song, habituated song, and silence. Significant changes in the metabolites 4-hydroxybutanoic acid (GHB), tryptophan, glutaric acid, and inositol-P are observed between birds exposed to novel song and a silent control group. Analysis of key biochemical pathways suggests glycolysis, serine-glycine synthesis, GHB metabolism, and Uridine-5P synthesis are affected after 15 min of song stimulation. Integrating transcriptional and metabolite data is a first step to visualize and identify molecular interactions in biochemical pathways. These pathways can subsequently be targeted in future studies to observe physiological and behavioral responses during learning and memory.

INTRODUCTION

Songbirds are one of the few animals that rely on learned vocalizations for communications (Doupe & Kuhl 1999, Jarvis 2004). The zebra finch, a songbird, has been widely used as an animal model to study molecular changes in the brain during learning and memory. A region of the auditory forebrain called the “auditory lobule” plays a central role in interpreting and processing of auditory inputs and forming initial

auditory memories. The auditory lobule (AL) is composed of three interconnected subregions, the caudalmedial nidopallium (NCM), cudalmedial mesopallium (CMM) and Field L and is functionally analogous to the mammalian primary and secondary cortical areas (Vates *et al.* 1996, Theunissen & Shaevitz 2006).

Conspecific song playback can trigger robust gene responses in AL, with transient changes having been observed for the immediate early gene *ZENK*, a transcription factor, and caspase-3, a transcript whose enzyme is associated with apoptosis (Mello & Clayton 1995, Huesmann & Clayton 2006), and other genes (Bailey *et al.* 2002). *Zenk* response to song has been well studied and has been shown to be context specific and habituate after repeated exposure (Mello *et al.* 1995, Kruse *et al.* 2004). Songbird neurobiology has traditionally relied on indirect evidence for metabolite changes (Holloway & Clayton 2001, Pinaud & Mello 2007) or focused on a single metabolite (Schmidt *et al.* 2009). Such single molecule studies limit our ability to study global cellular responses during different experiences.

With the sequencing of the zebra finch genome global transcriptional changes have been detected revealing significantly and different responses with novel song, habituated song, and silence (Dong *et al.* 2009). Proteomic studies have also focused on AL to study protein changes under these different song states, however it has yielded few identifiable proteins (Dong et al. 2009). To complement these global analytical methods and study biochemical responses after novel song exposure and habituation the metabolome of AL will be profiled and compared to a silent control group. Utilizing the available transcriptomic data and integrating it with metabolomic data, applying a systems biology approach, will allow us to identify potentially new biochemical pathways to target and study their influence in song learning and memory.

MATERIALS AND METHODS

Song exposure

All animals were housed on a 14/10 day/night cycle, aviaries are in a mixed sex room in single sex flight aviaries. The experiment was carried out over a four-day period using a total of twenty-four adult zebra finches, 12 males and 12 females. On day 1, eight birds, 4 male 4 females were individually isolated in soundproof chambers for 22 hours.

On day 2, at ~11am 4 birds, 2 males and 2 females, were exposed to 15 min, or 90 iterations every 10 seconds, of a novel conspecific song (ZF101) (Fig. 4.1). Habituation experiments involved housing 12 birds, equal number male and female birds 22 hours individually in soundproof chambers half of the birds were exposed to 3 hours of a novel conspecific song (ZF101). After 21 hours, birds that were exposed to song were again exposed to the same conspecific song for 15 min (Fig. 4.1). Immediately after song exposure birds were sacrificed by rapid decapitation, the auditory lobule was removed, frozen in liquid nitrogen, and stored at -80 ^{o}C. Total time from decapitation to freezing was kept to <1 min.

Metabolite and lipid extraction

For metabolite extraction the auditory lobule from one male and one female were combined, 12x wet weight of ice cold 2:1 methanol:choloform was added and 5 μg of DL-Chlorophenyalanine added as an internal standard. Samples were mechanically homogenized (Tissue Master-125, Omni International), 4x wet weight volume of ice cold 100% chloroform, and 6.5x wet weight volume of cold ddH_2O were added. Samples were vortex for 1 min, centrifuge for 2 min at 12,000 rpm. The aqueous layer was removed and dried using a speedvac (Thermo-Savant) at 35 ^{o}C connected to a refrigerated vapor trap (Thermo), and stored at -80 ^{o}C.

Prior to metabolite derivatization, 200 μg of hentriacontanoic acid (C31:0) in pyridine, was added as a standard to control for instrumentation variation and dried using a speedvac set at 35 ^{o}C. For metabolite derivatization 50 μl methoxyamine-hydrochloride in pyridine (20 mg/ml) was added and incubated at 40^{o}C for 90 min, followed by 50μl N-Methyl-N(trimethylsilyl) trifluoroacetamide (MSTFA) at 40^{o}C for 90 min. Samples were then subjected to GC-MS analysis.

Lipid extraction was carried out similar to the Folch method (Folch *et al.* 1957, Kang & Wang 2005). Briefly 20x wt/vol of 2:1 chloroform:methanol with 0.01% BHT was added and 5 μl C23:0 (2 mg/ml) was added as an internal standard. Samples were mechanically homogenized (Tissue Master-125, Omni International), and incubated on dry ice for 30 min, followed by 1:5 wt/vol of 0.9% NaCl, vortex centrifuge 2 min, the organic layer was removed. To the homogenate 100 μl 100% chloroform was added,

vortexed, centrifuged for 2 min and organic layer removed and combined with prior extraction. The organic layer were dried at 35 ^{o}C using a speedvac and stored at -80 ^{o}C. To derivitize the free fatty acids 150 µl of 100% methanol and 150 µl (Trimethylsilyl)diazomethane (2.0M in Hexanes) was added and incubated at room temperature for 1hr. Samples were dried using a speedvac at 35 ^{o}C followed by resuspension in 130 µl of methylene chloride, 95 µl for the FFA and 5 µl of heptacosanoic acid, C27:0 (2 mg/mL) standard were combined prior to GC-MS analysis.

Metabolite and Lipid GC-MS analysis

For metabolite analysis the GC-MS system consisted of an Agilent 7890A (Agilent Inc, Palo Alto, CA, USA) gas chromatograph, an Agilent 5975C mass selective detector and Agilent 7683B autosampler. Gas chromatography was performed on a 60 m HP-5MS column with 0.25 mm inner diameter and 0.25 µm film thickness (Agilent Inc, Palo Alto, CA, USA). Sample volume of 5 µL was injected with a splitless mode with an injection temperature of 250 ^{o}C, the interface set to 250 ^{o}C, and the ion source adjusted to 230 ^{o}C. The helium carrier gas was set at a constant flow rate of 1.5 ml min^{-1}. The temperature program was 5-min isothermal heating at 70 ^{o}C, followed by an oven temperature increase of 5 ^{o}C min^{-1} to 310 ^{o}C and a final 20 min at 310 ^{o}C. Mass spectra were recorded in the m/z 50-800 scanning range.

For fatty acids analysis, GC/MS was carried out on an Agilent 6890N gas chromatograph with an Agilent 5973 mass selective detector and Agilent 7683B autosampler (Agilent Inc, Palo Alto, CA, USA). Gas chromatography was performed on a ZB-WAX (30 m × 0.25 mm I.D., 0.25 µm film thickness) capillary column (Phenomenex, Torrance, CA, USA). The inlet and MSD interface temperatures were 260 ^{o}C with ion source temperature at 230 ^{o}C. An aliquot of 5 µL was injected in splitless mode. The helium carrier gas was kept at a constant flow rate of 1.3 ml min^{-1}. The temperature program was: initial 5-min isothermal heating at 140 ^{o}C, followed by an oven temperature increase of 4 ^{o}C min^{-1} to 185 ^{o}C (15 min isothermal); from 185 ^{o}C to 230 ^{o}C at 4 ^{o}C min^{-1}; from 230 ^{o}C to 260 ^{o}C at 6 ^{o}C (15 min isothermal). Mass spectra were recorded in the m/z 50-800 scanning range.

The spectra of all chromatogram peaks were compared with electron impact mass spectrum libraries NIST08 (NIST, MD, USA), WILEY08 (Palisade Corporation, NY, USA), and the custom library), for fatty acids a FAMEs custom library was generated using a C4-C24 FAME standard (Sigma, St. Louis, MO, USA). To allow comparison between samples all data were normalized to the internal standard in each chromatogram and fresh weight of each sample. The chromatograms and mass spectra were evaluated using the MSD ChemStation (Agilent, Palo Alto, CA, USA) and AMDIS (NIST, Gaithersburg, MD, USA) programs. The retention time and mass spectra were implemented within the AMDIS method formats.

Statistical and pathway analysis

For Partial Least Squares Discriminant Analysis (PLSDA) samples from individual experiments were combined. Data was imported into PLS toolbox (Eigenvector Research Inc.) and 2/3 of the samples from each experiment were used to construct a PLSDA model. Data was preprocessed by autoscaling and Orthoganol Signal Correction (OSC) applied, three latent variables were used and for cross-validation of the model by venetian blinds using three datasplits was applied. The remaining samples (1/3) were used to validate the PLSDA model.

In the metabolic pathway analysis each of the three boxes represents the relative fold change (song/silence) for that metabolite. The top box represents data collected from the experiment conducted in July, followed by Aug and Dec respectively. The numbers on the right of each box is its associated p-values calculated using two-tail t-test assuming unequal variance. Arrows indicates a metabolic reaction and its direction of synthesis, arrows with "=" indicates more than 2 reactions steps are required to synthesize that metabolite. Pathways were constructed using available KEGG pathway information.

Integrating metabolomic and genomic data

Metabolites identified from experiments conducted in July 2009, December 2009 (novel song vs. silence) and February 2010 (habituated vs. silence) were used in the analysis. The August data was excluded due to poor metabolite detection in some samples. Statistically significant metabolites were determined by t-test using a p-value of

<0.05. Each metabolite had its KEGG identification name recorded in order to carry out the analysis. The microarray data used in the analysis was previously generated in our lab (Dong et al. 2009), transcripts with a p-value <0.05 after false discovery rate (fdr) correction was used in the analysis. Metabolite and transcript network was built and analyzed using cytoscape software an open source platform for network analysis and visualization.

RESULTS

Metabolite sex differences

Comparing dissected auditory lobule from males and females isolated o/n resulted in a total of 122 metabolites being detected with eight showing statistically significant differences using a less stringent p-value <0.10 (Table 4.1). One male sample had to be discarded due to a poor GC chromatogram. The eight statistically significant metabolites showed a relative increase in total concentration in males compared to females. The nucleoside adenosine showed the most statistically significant difference, followed by glycerol, which is important in the synthesis of lipids, and 2-diaminoethyl ester phosphoric acid (Table 4.1). Other statistically significant metabolites (p<0.10) were of low relative concentration or not detected in some samples. One of the most significant results is 4-hydroxybutyric acid and 2-hydroxyglutaric acid, which are closely related metabolically and show statistically significant differences between males and females with males having a higher relative level (Table 4.1).

Metabolite differences upon novel song exposure

PLSDA analysis from two independent experiments resulted in the first two latent variables capturing LV1 13% and LV2 8% of the class variation and successfully building a model to predict future samples (Fig 4.2A). Most of the separation based on sample class (song or silence) is along LV1 (x-axis). Samples from birds exposed to song cluster on the positive x-axis while silent birds cluster on the negative x-axis (Fig. 4.2A). Three of four song and silent samples used to validate the PLSDA model were correctly assigned on either the positive or negative x-axis.

The corresponding loadings plot reveals that amino acids tryptophan, tyrosine, lysine, and glutamine show increased relative levels are correlated with song-exposed birds vs. silent control group. In addition to amino acids the neurotransmitters dopamine and noradrenalin, and some sugars among other metabolites are correlated with song exposed birds (Fig. 4.2B). Silent control birds were positively associated and correlating with higher relative levels for some lipid (e.g. DHA and heptanoic acid) and associated metabolites (e.g. ethanolamine and glutaric acid), in addition to intermediate metabolites (e.g. spermidine, glutaric acid, and maleic acid). PLSDA also higher correlation and relative level for the nucleotides uracil and guanine in silent control birds.

Multivariate statistical analysis showed that inositol-phosphate and chiro-inositol are positively associate with higher relative levels in song exposed birds, however scyllo-inositol is associated with silent control birds.

Metabolic pathway analysis

To observe changes in a biochemical pathway context the relative fold change for metabolites involved in glycolysis, citric acid cycle and amino acids and other derived metabolites are shown in figure 4.3. Most metabolites showed an increase fold change for song relative to silent in the July experiment in contradiction to Aug and Dec, where both of these months appear to show similar expression changes. However, fructose, proline, and ornithine are the only metabolites with increased relative levels in song relative silent in all three experiments.

Metabolites within the citric acid cycle, in addition to GABA, urea, and N-acetyl-glutamic acid show little relative change comparing the two treatment groups. However, the sugars fructose, fructose-6P, and α-D-glucose along with 3-phosphoglyceric acid, amino acids cystine and glycine, and ornithine show large changes.

Dopamine and noradrenaline synthesis, and serotonin synthesis do not show a clear metabolic change in song relative to silent birds exposed to novel song for 15min (Fig 4.4A and B). This is in contrast to polyamine (Fig. 4.4C) and GHB synthesis (Fig. 4.4D). In the biosynthesis of polyamines, ornithine shows a robust increase in song relative to silent in all three experiments, in addition to an increase of one of its metabolites 5'-Methylthioadenosine (Fig 4.4C). Similarly in GABA and GHB synthesis,

the metabolite GHB shows an increase in song relative to silent in all three experiments, in addition to its metabolites 3-hydroxybutonic acid.

Changes in metabolites involved in purine metabolism do not show any strong or apparent changes between the two treatment groups (Fig 4.5A). However in pyrimidine metabolism uracil shows a relative decrease across all three experiments while uridine-5P has a increased fold change in song relative to silent with the intermediate metabolite uridine exhibiting a mostly higher level in song (Fig. 4.5B).

Two-way ANOVA comparing song and silence

Applying two-way ANOVA using the novel song and silence experiments conducted in July and December resulted in nine metabolites with a raw p-value <0.05 and 18 metabolites with a raw p-value <0.1 (Table 4.2). After controlling for month-to-month changes only five metabolites have a raw p-value <0.05: glutaric acid, 4-hydroxybutanoic acid (GHB), scyllo-inositol, glycerophosphorylglucerol, and thymine. After false discovery rate "fdr" correction no metabolite had p-value <0.1 (Table 4.2).

Metabolite differences between silent, novel song, and habituated

Combining the data from the three separate experiments, a successful PLSDA model was constructed and used to validate the identity of samples not used in model construction. The first latent variable (LV1) x-axis, capturing ~28% of the variance, successfully separates novel song, habituated, and silent samples, whereas latent variable two (LV2) y-axis, capturing ~9% of the variance, successfully differentiates silent from birds exposed to song, regardless to it being novel or familiar (Fig. 4.6A).

The corresponding loadings plot reveals that the major differentiating metabolites along LV1, comparing novel song and habituated birds, are adenosine-5P, uracil, guanine, and tryptophan which are associated to novel song exposure (Fig. 4.6A). In habituated birds myo-inositol, chiro, inositol, 1-monooctadecanoylglycerol, phosphoric acid, and butylamine are associated metabolites (Fig. 4.6B). Birds exposed to song, regardless of it being novel or familiar, have an increased associating with 4-hydroxybutonic acid (GHB), inositol-P, sucrose, 2-keto-gluconic acid, and chiro-inositol, this is represented by these metabolites distance from the y-axis for LV2. Silent control

birds are associated with increased relative levels for guanine, uracil, heptanoic acid, dedecanol, and ethanolamine (Fig. 4.6B).

Lipidomic analysis comparing silent and novel song exposure

Free fatty acid analysis comparing birds exposed to novel song to silent control group showed no statistical difference using two-tailed t-test, assuming unequal variance (Table 4.3). The average total detected FFA levels are higher in the silent group compared to song, however the differences are not statistically significant.

Metabolomic and transcriptomic analysis

Network analysis by integrating the metabolomics data comparing novel song and silence from the July and December experiments with previously generated microarray data, comparing novel song exposure with silence, reveals a highly integrated network (Fig. 4.7A). Thirteen metabolites show statistical change with a t-test <0.05 and have close interaction with statistically significant transcription changes. Six metabolites: adenine, glycine, mannose-6P, D-glucose, L-tryptophan, and glycolate show significant changes and directly interacts with a least one biochemical reaction whose enzyme encoding transcript also changes under novel song exposure compared to the silent control group (Fig. 4.7B).

The interacting transcriptional and metabolite network comparing habituated and silent control birds shows a less extensive interacting network with only four metabolites showing statistical change between groups (Fig. 4.8A). Of these, two metabolites, the amino acids L-phenylalanine and L-tryptophan show statistically significant changes (p-value <0.05) and directly interact with reactions whose transcripts also show statistically significant changes (Fig. 4.8B).

DISCUSSION

In this study the metabolome of the auditory lobule was profiled from birds exposed to novel song, a habituated song, and silence. Metabolomic differences are observed and we show the predictive ability to identify auditory lobules exposed to either novel song, habituated song, or silence. Integrating previously generated transcriptional

data with metabolomic data, specific metabolic pathways are identified as changing upon song stimulation, one of the most significant changes was 4-hydroxybutanoic acid (GHB) and its related metabolites suggesting an important role in brain signaling upon song exposure.

Transcriptional changes in the auditory lobule in response to song stimulation has not been shown to be sex specific (Mello *et al.* 1992). However, a small pilot study comparing male and female auditory lobules identified a few potential metabolite differences comparing birds kept in silence (Table 4.1). Brain sex differences in mice have not been identified as being significant (Salek *et al.* 2008); however to mitigate potential sex differences auditory lobules from one male and one female were pooled in each sample prior to analysis.

PLSDA using the July and December studies, I was able to construct a successful model that is effective in identifying auditory lobules that were either exposed to novel song or silence. The model shows that neurotransmitters/neuromodulators (e.g. dopamine), amino acids (e.g. tryptophan), and signaling molecules (e.g. inositol-P) are some of the metabolites that show significant variation between song and silence suggesting song induction increases the synthesis or transport of these metabolites in the auditory lobule. In contrast lipid related metabolites are associated with silence samples (e.g. ethanolamine).

Activation of phospholipases to synthesize free fatty acids by hydrolyzing membrane phospholipids is known to be an important cell signaling mechanism (Farooqui & Horrocks 2006, Clements *et al.* 1991). The identification of lipids and related metabolites exhibiting associations with either song or silence samples warranted a targeted study focusing specifically on FFAs. GC-MS analysis comparing novel song vs. silence resulted in no statistically significant changes between samples; however, more sensitive methods such as radiolabeling fatty acids or phospholipases activity assays may be required to detect potentially small cellular FFA changes upon song stimulation (Jones *et al.* 1996).

PLSDA analysis was successful in identifying metabolomic differences between auditory lobules exposed to novel song, a habituated song, or silence. Inositols are important secondary messengers in signal transduction and are important lipid

components (e.g. phosphoinositols) (Deranieh & Greenberg 2009, Fisher *et al.* 2002) and they show significant variation between the three groups, with greater correlation with birds that had been habituated. In contrast RNA and DNA related metabolites (e.g. uracil) and tryptophan are more highly correlated with novel song exposed birds, suggesting RNA or DNA synthesis may be showing greater changes upon novel song vs. habituated. Comparing song, regardless if novel or habituated, and silence shows that neurotransmitters/neuromodulators, and sugars are major differentiating metabolites correlating with song exposure. Fatty acids and RNA and DNA related metabolites in contrast also show significant variation along LV2 but are correlated with auditory lobules under silent conditions.

Applying a multivatiate statistics a successful model was constructed with the ability to identify auditory lobules that were exposed to novel song, habituated, or silence. Specific signaling metabolites, nucleotides, and fatty acids showed the most variation between sample classes and played a key role in metabolite profile differentiating.

To study the metabolomic results in the context of biochemical pathways, the average relative metabolite fold change from three different independent experiments were mapped onto various biochemical pathways with the associated student t-test p-value shown. Focusing on the Citric Acid Cycle (TCA) low and statistically non-significant fold changes of many of the metabolites is observed, suggesting that this pathway is robust and not sensitive to short-term song stimulation.

Focusing on the glycolytic pathway, novel song stimulation compared to silence appears to show a small response in sugar levels in AL. Fructose and sorbitol levels in all three metabolomic experiments show an increase upon novel song stimulation and strong decreases in fructose-6P and glucose-6P. Analysis of metabolomic data in conjunction with the transcriptomic data shows changes in D-glucose and statistically significant changes in two transcripts that metabolize it (Dong *et al.* 2009). In addition D-mannose-6P and the transcript for the D-mannose-6P 1,6-phosphomutase also change, with mannose-6P then being metabolized into fructose-6P. From this data it is uncertain whether active regulation is occurring between the conversion of fructose-6P to fructose-1,6-bisphosphate, however it appears to be a point of significant change in response to

novel song. In other avian animal models changes in visual or auditory contexts and auditory imprinting have been shown to stimulate sugar uptake in the avian brain (Maier & Scheich 1983, Muller & Scheich 1986). Changes in sugar metabolism (e.g. glycolysis) are observed in birds that are stimulated with novel song and habituated compared to silence. Correcting for monthly effects glucose showed a statistically significant change between novel song and silence (p-value <0.1), fructose however had strong month-to-month effect (Table 4.2). Change in sugar metabolism and glycolysis suggest an increased sugar requirement in AL upon song stimulation, indicating an increased ATP demand, which is agreement with previous evidence (Dong *et al.* 2009).

Amino acids are important metabolites in protein and neurotransmitter synthesis (e.g. dopamine). The amino acids serine and glycine both synthesized from 3-phosphoglycerate (3-PGA), a glycolytic metabolite, show statistically significant increases in one of the metabolomic experiments, although a two-way ANOVA did not show statistical significance. Network analysis did reveal significant changes in glycine as well as the transcript for the synthetic enzyme necessary in conversion of glycine to serine. Glycine is an inhibitory neurotransmitter (Lopez-Corcuera *et al.* 2001) that modulates the potentiating action of gluamate at N-methyl-D-aspartate (NMDA) receptors (Lester *et al.* 1993) and shows a non-significant decrease in ALs from birds exposed to novel song vs. silence. In addition, neither glutamate nor GABA, metabolized from glutamate and an inhibitory neurotransmitter, show any significant change upon novel song stimulation. A role for glycine neuromodulating has been suggested through microarray studies focusing on HVC, another song nuclei, by identifying higher expression levels of the glycine receptor subunit alpha-2 (GLRA2) in the HVC shelf (Lovell *et al.* 2008), a component of the auditory system (Jarvis *et al.* 2005). These results suggest that the inhibitory neurotransmitters glycine and GABA are not induced after 15 min of novel song exposure.

The metabolite 4-hydroxybutanoic acid (GHB), a metabolite of GABA, is also suggested to have neurotransmitter/neuromodular properties (Gobaille *et al.* 1999). PLSDA and two-way ANOVA analysis shows a statistically significant increase in novel song samples as does its metabolite 3-hydroxybutanoic acid. Interestingly glutaric acid a metabolite derived from 3-hydroxybutanoic acid and necessary for fatty acid synthesis,

shows a statistically significant decrease in novel song vs. silence. A decrease in glutaric acid could be a cellular response to an increased need for GHB and 3-hydroxybutanoic acid, resulting in increased β-oxidation (Maitre 1997, Crunelli *et al.* 2006, Walkenstein *et al.* 1964). An active role for GHB upon song stimulation is also evidenced by an increase in inositol-P which is controlled in a Ca^{2+} manner by GHB (Maitre 1997). 4-hydroxybutanoic acid can also regulate GABA, cGMP, and it is suggested to potentially regulate glycine levels (Gobaille *et al.* 1999). These results suggest that GHB plays a neuromodulatory role in the auditory lobule upon song stimulation.

Other known neurotransmitters such as dopamine, noradrenaline, and serotonin do not show statistically significant changes, although tryptophan a precursor for serotonin synthesis does show a statistical increase in song vs. silence. Network analysis with our labs genomic data suggests tryptophan levels may be responding to increase tRNA synthesis during both novel and habituated song conditions. In addition to tryptophan, the habituated song condition also shows significant expression changes in phenylalanine and phenylalanine:tRNA ligase. Up-regulation of tRNA would not be unexpected since genomic studies have identified significant transcriptional changes in the auditory lobule upon song stimulation (Dong *et al.* 2009); therefore an increased demand for protein synthesis and tRNAs is likely needed.

Uracil is an RNA specific nucleotide necessary for transcription and translation. Across all three metabolomic experiments uracil resulted in a relative decrease upon novel song exposure. Uridine, metabolize from uracil exhibited an overall fold increase in song, and uridine-5P, metabolized from uridine, resulted in a >0.75 fold increase in two out of three novel song vs. to silence experiments. Using a p-value <0.1 as a cut off uridine-5P showed a statistically significant increase by two-way ANOVA. Uridine-5P is subsequently phosphorylated to UDP and UTP then incorporated into RNA during transcription. The complementary purine derivative nucleotide, adenine, has a fairly significant statistical change in addition transcripts encoding enzymes that metabolize adenine show significant changes under novel song conditions. Based on genomic and metabolomic data the evidence suggests significant transcriptional and translational changes in AL upon novel song stimulation.

The results presented demonstrate the ability to identify unique metabolic profiles between auditory lobules that have been exposed to a novel conspecific song, habituated song, and silence. Visualizing the metabolomic data within biochemical pathway framework led to identifying potential changes in sugar metabolism in glycolysis and RNA and tRNA synthesis upon song stimulation. In contrast metabolites in the TCA cycle appear to show little to no change after 15 min of song stimulation. One of the most interesting results is the increase in GHB, and relative concentration of its derived metabolites and metabolites known to be influenced by GHB. Future studies targeting GHB may yield an important functional role for this metabolite in song learning and memory.

ACKNOWLEDGEMENTS

I would like to thank Alexander Ulanov for his assistance with the GC-MS and Jenny Drnevich for carrying out the two-way ANOVA. I would especially like to thank Dr. Nathan Price, Younhee Ko, and Caroline Milne for carrying out the network analysis. This investigation was support by the National Institutes of Health under Ruth L. Kirschstein National Research Service Award F31 NS060179-01A1.

FIGURES AND TABLES

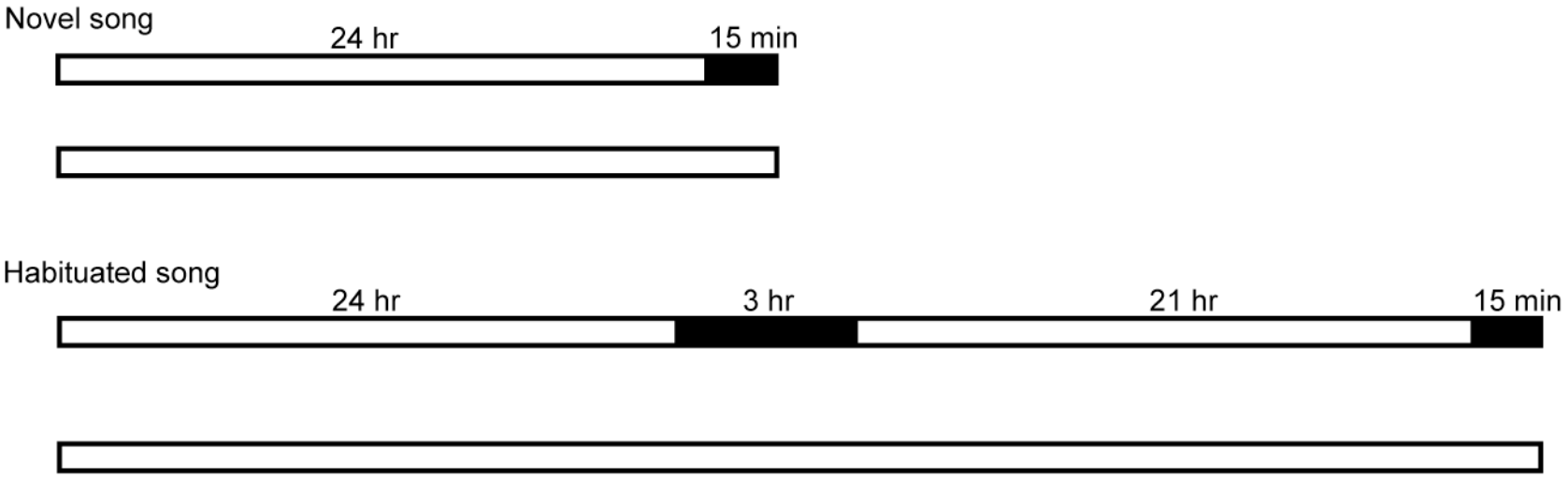

Figure 4.1. Experimental treatment groups. Each bird was individually isolated in a soundproof chamber in silence for the period of time represented by the white-boxed area. One half of the birds were subsequently exposed song for the indicated time represented by the shaded black area.

	F1	F2	F3	F4	AVG "F"	SD "F"	M2	M3	M4	AVG "M"	SD "M"	t-test, P<0.05
Adenosine	188.3	352.0	278.4	243.3	265.5	68.5	441.6	366.2	470.4	426.1	53.8	0.018
3,4-Dihydroxyphenylethylamine	ND	3.1	2.1	2.1	2.4	0.6	5.3	4.7	6.8	5.6	1.1	0.021
Glycerol	172.4	197.1	146.4	155.0	167.7	22.4	393.1	425.8	555.3	458.1	85.8	0.023
Phosphoric acid, 2-diaminoethyl ester	779.0	1478.2	752.0	810.9	955.0	349.6	1780.9	1435.2	2114.9	1777.0	339.8	0.030
4-hydroxybutanoic acid	ND	0.5	0.6	ND	0.6	0.1	ND	2.0	2.3	2.1	0.2	0.044
2-Hydroxyglutaric acid	9.1	6.0	9.4	8.9	8.3	1.6	14.1	12.5	18.7	15.1	3.2	0.051
Ribitol	ND	9.9	8.6	8.9	9.1	0.6	42.9	24.9	27.9	31.9	9.7	0.054
Ethyleneglycol	0.2	2.4	2.7	2.5	1.9	1.1	3.7	3.3	3.5	3.5	0.2	0.069
B-Hydroxybutyric acid	9.8	17.2	10.6	5.0	10.6	5.0	20.9	14.1	24.2	19.7	5.1	0.074

Table 4.1. Relative metabolite concentration between female “F” and male “M” auditory lobules. Statistical analysis using student t-test two-tail and unequal variance (p-value <0.10).

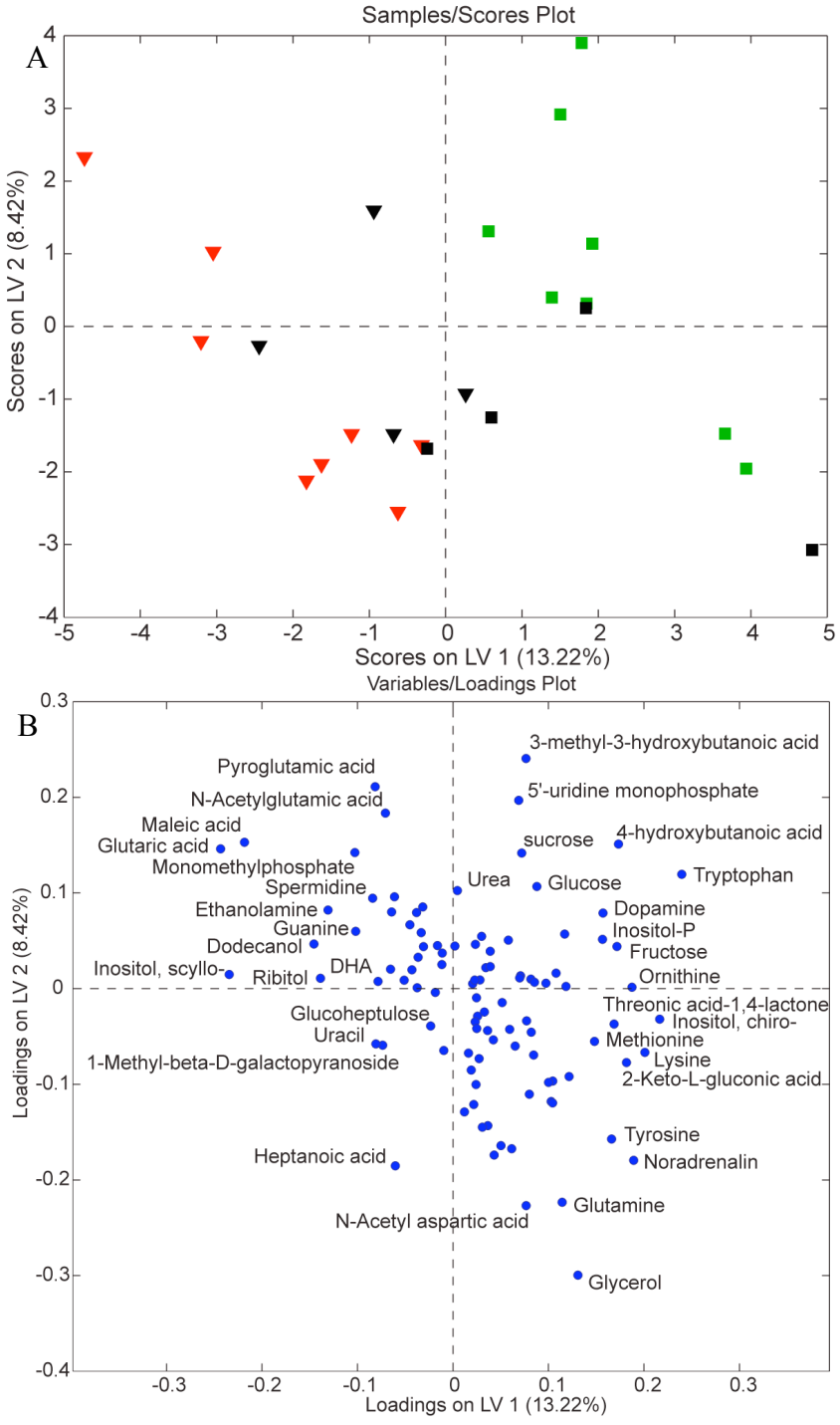

Figure 4.2. (A) PLSDA scores plot showing the distribution of samples exposed to song □ and silence ▽. Samples used to construct the PLSDA model are in red and those used to validate it are in black. (B) PLSDA loadings plot showing the metabolites with most variation and relation to sample groups shown in (A).

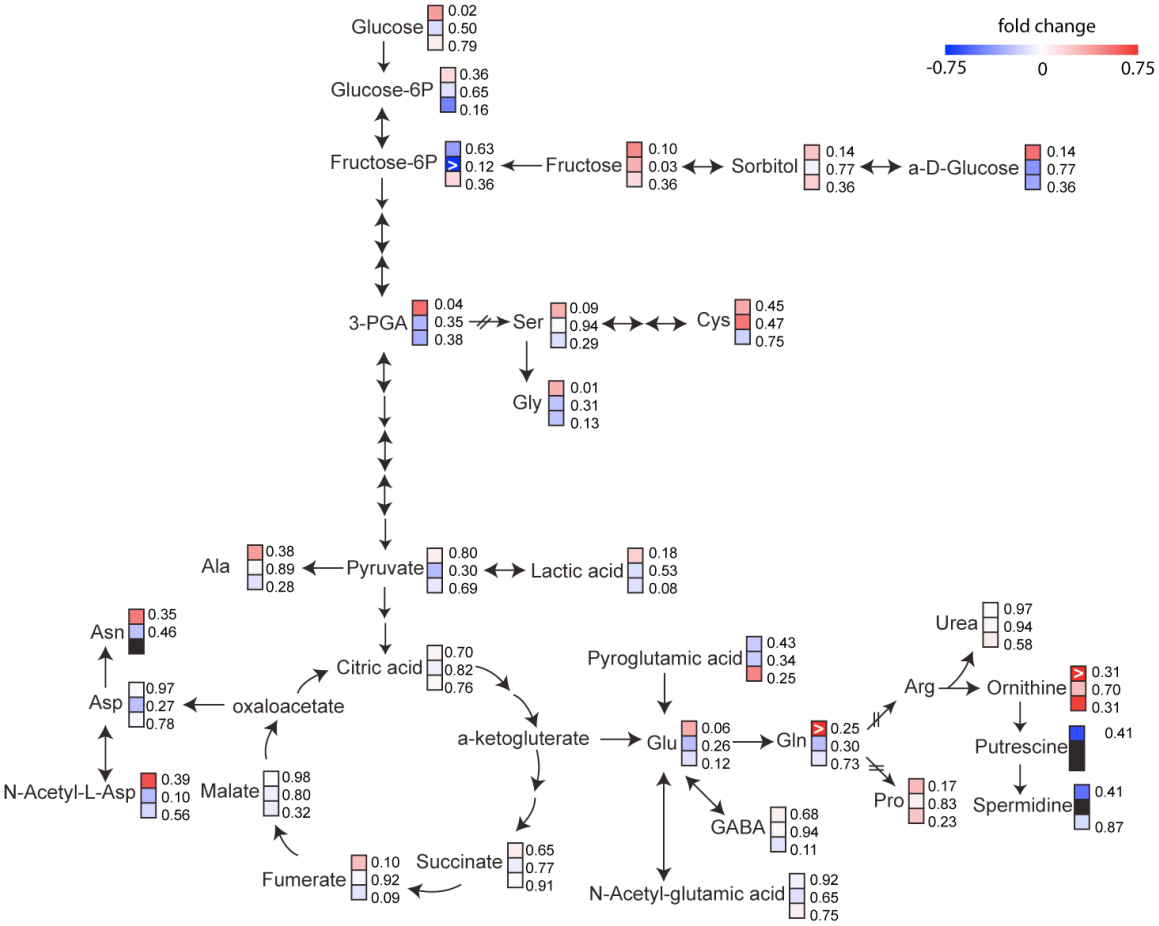

Figure 4.3. Relative fold change of metabolites comparing song/silent in the glycolytic and TCA cycle and associated metabolites. Squares represent, from top to bottom, results from July, Aug, and Dec experiments (respectively), ">" represents a greater than 0.75 fold +/- change in that metabolite, arrow with "=" indicates more than two reactions are required in the synthesis of that metabolite. Numbers are the p-values using two-tail t-test with unequal variance corresponding to the associated experiment. Black boxes represent no metabolite detected in that experiment.

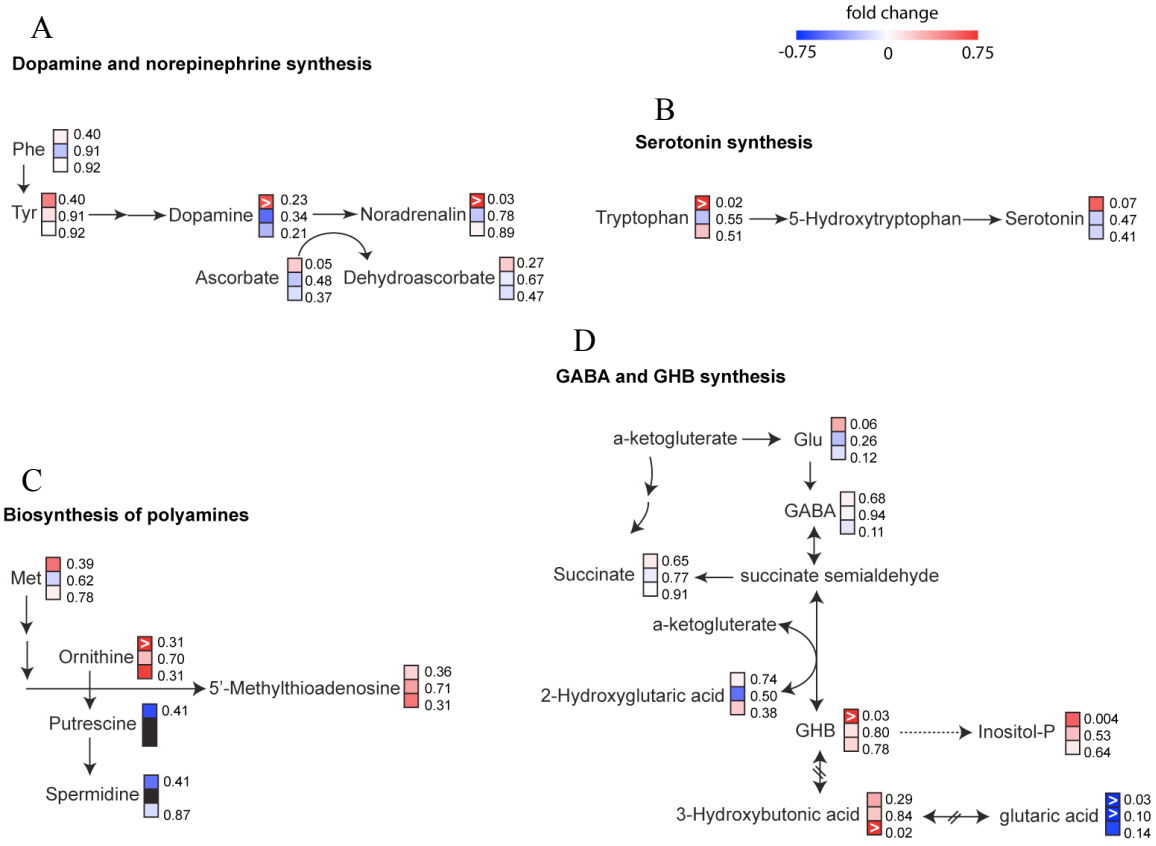

Figure 4.4. Relative fold change of metabolites comparing song/silent across metabolic pathways in the synthesis of neurotransmitters and polyamines. Squares represent, from top to bottom, results from July, Aug, and Dec experiments (respectively), ">" represents a greater than 0.75 fold change in that metabolite, arrow with"=" represents a greater than 2 step reaction in the synthesis of that metabolite, dashed arrow indicates metabolite regulation. Numbers are the p-values using two-tail t-test with unequal variance corresponding to the associated experiment. Black boxes represent no metabolite detected in that experiment.

A

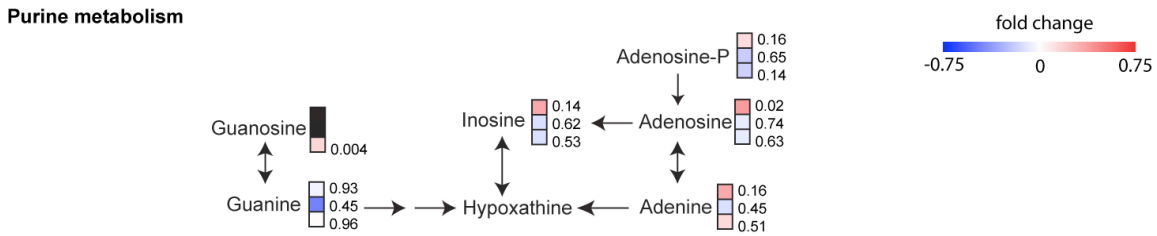

B

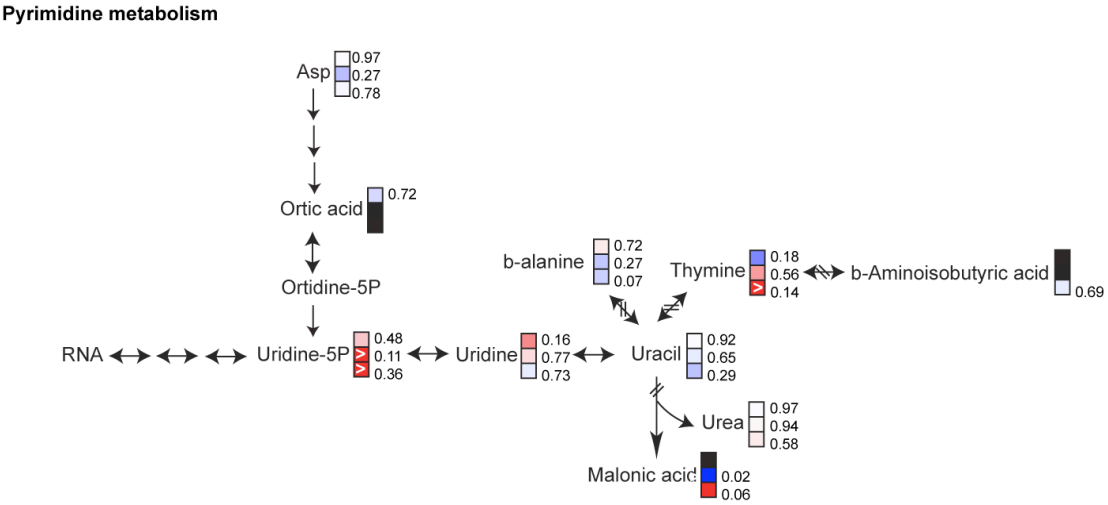

Figure 4.5. Relative fold change of metabolites comparing song/silent in purine and pyrimidine synthesis. Squares represent, from top to bottom, results from July, Aug, and Dec experiments (respectively), ">" represents a greater than 0.75 fold change in that metabolite, "=" represents a greater than 2 step reaction in the synthesis of that metabolite. Numbers are the p-values using two-tail t-test with unequal variance corresponding to the associated experiment. Black boxes represent no metabolite detected in that experiment.

p.value.Trt1	p.value.Month1	p.value.Trt1:Month1	p.value.adj.Trt1	p.value.adj.Month1	p.value.adj.Trt1:Month1	ID
0.00335	0.2281	0.08607	0.172209	0.29083	0.739622	Glutaric acid
0.00338	0.00001	0.10175	0.172209	0.000052	0.739622	3-hydroxybutanoic acid
0.0119	0.57862	0.02118	0.404453	0.663139	0.607673	4-hydroxybutanoic acid
0.02219	0	0.95891	0.456113	0	0.983427	Lysine
0.02779	0.28614	0.40118	0.456113	0.351969	0.870642	Inositol-P
0.03014	0.68844	0.21901	0.456113	0.755065	0.739622	Tryptophan
0.03575	0.5258	0.39536	0.456113	0.617675	0.870642	ethanolamine
0.03577	0	0.13319	0.456113	0	0.739622	Glycolic acid
0.04537	0.05164	0.04528	0.514226	0.086351	0.659832	Inositol, scyllo-
0.05419	0.03432	0.01986	0.527606	0.05834	0.607673	Glycerophosphorylglycerol
0.06229	0.00035	0.94921	0.527606	0.000972	0.983427	fructose
0.07178	0	0.44488	0.527606	0	0.887956	Proline
0.08011	0.03211	0.77943	0.527606	0.055507	0.983427	heptanoic acid
0.08213	0.1217	0.97379	0.527606	0.177333	0.983427	Adenine
0.08789	0.00003	0.00802	0.527606	0.000119	0.607673	Thymine
0.08808	0.00424	0.27529	0.527606	0.0092	0.751882	Hypoxanthine
0.09019	0.86015	0.86867	0.527606	0.860148	0.983427	glucose
0.09311	0.35496	0.11361	0.527606	0.425957	0.739622	5'-uridine monophosphate

Table 4.2. Two-Way ANOVA comparing metabolites changes between novel song vs. silence from experiments conducted in July and Dec. List includes metabolites with a p-value <0.1 using raw p-value looking at the effect of treatment alone.

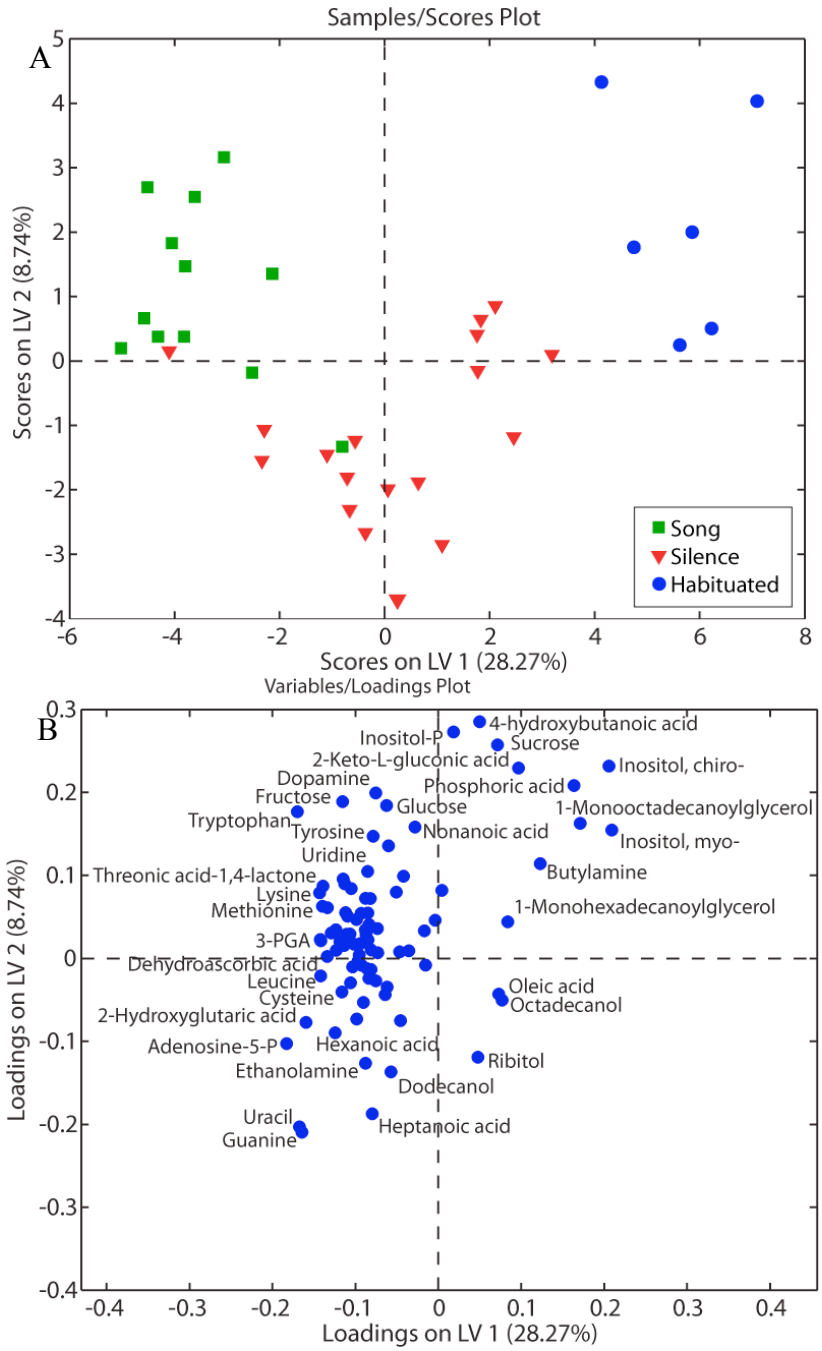

Figure 4.6. (A) PLSDA scores plot showing the distribution of samples exposed to song □, silence ▽, and habituated ○. To construct model 2/3 of the samples from each experiment and condition were used, to validate the remaining 1/3 were used. (B) PLSDA loadings plot showing the metabolites with most variation and relation to sample groups shown in (A).

Fatty acid	Average (Silent)	STDev	Average (Song)	STDev	p-value
Tetradecanoic acid	0.00241	0.00091	0.00250	0.00116	0.88087
Hexadecanoic acid	0.31179	0.09321	0.33459	0.11619	0.71599
9-Hexadecenoic acid	0.00819	0.00262	0.00854	0.00345	0.84612
Heptadecanoic acid	0.00063	0.00023	0.00055	0.00013	0.50375
Octadecanoic acid	0.24898	0.06641	0.25109	0.07830	0.96093
9-Octadecenoic acid	0.09482	0.02896	0.10093	0.03142	0.73336
cis-9,12-Octadecadienoic acid	0.01607	0.00562	0.01579	0.00393	0.92298
Eicosanoic acid	0.00038	0.00023	0.00054	0.00029	0.33001
11-Eicosenoic acid	0.00116	0.00050	0.00127	0.00046	0.68232
cis-8,11,14-Eicosatrienoic acid	0.00841	0.00238	0.00795	0.00285	0.76840
5,8,11,14-Eicosatetraenoic acid	0.12119	0.03695	0.12675	0.05724	0.84618
4,7,10,13,16,19-Docosahexaenoic acid	0.23160	0.06924	0.24827	0.08353	0.71473
Total	**1.04562**	**0.30007**	**1.09877**	**0.35797**	**0.78629**

Table 4.3. Average relative fatty acid concentration normalized to wet tissue weight and C23:0, standard deviation and student t-test using two-tail unequal variance.

A

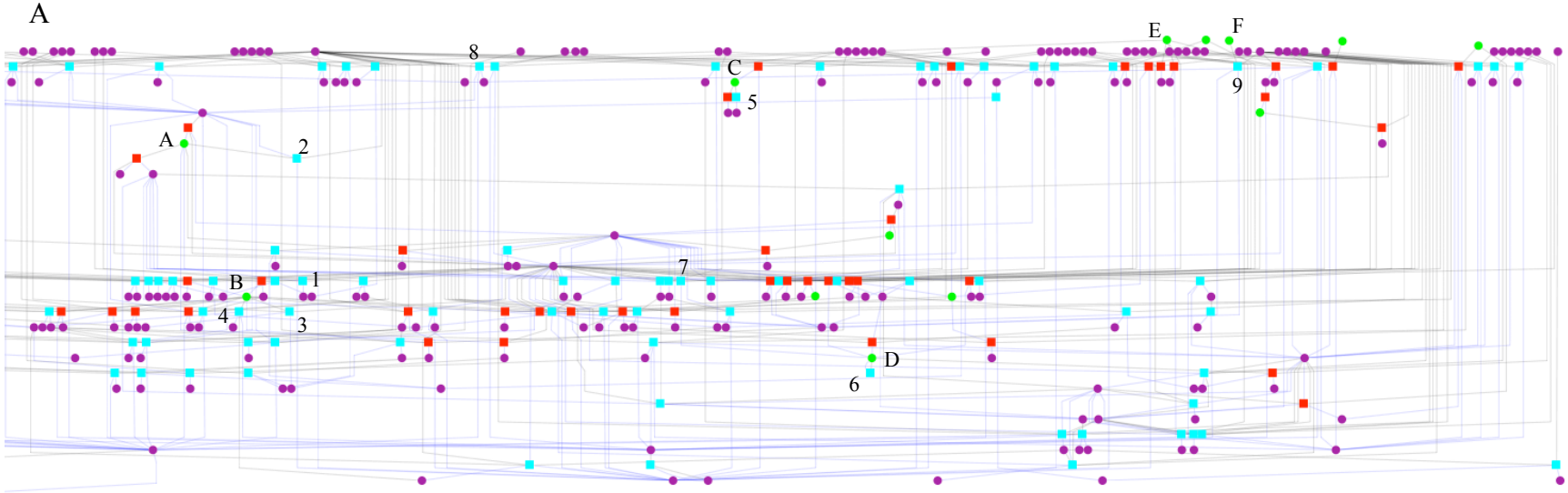

B

Metabolite	Kegg Reaction	Network legend	Reaction	Enzyme	Pathway
adenine	R04936	A1	Se-Adenosylselenohomocysteine + H2O <=> Adenosine + Selenohomocysteine	Se-Adenosylselenohomocysteine hydrolase	Selenoamino acid metabolism
	R00185	A2	ATP + Adenosine <=> ADP + AMP	ATP:adenosine 5-phosphotransferase	Purine metabolism
Glycine	R00945	B3	5,10-Methylenetetrahydrofolate + Glycine + H2O <=> Tetrahydrofolate + L-Serine	5,10-Methylenetetrahydrofolate:glycine hydroxymethyltransferase	Glycine, serine and threonine metabolism
	R00830	B4	Succinyl-CoA + Glycine <=> 5-Aminolevulinate + CoA + CO2	Succinyl-CoA:glycine C-succinyl-transferase(decarboxylating)	Glycine, serine and threonine metabolism
Mannose-6P	R01818	C5	D-Mannose 6-phosphate <=> D-Mannose 1-phosphate	D-Mannose 6-phosphate 1,6-phosphomutase	Amino sugar and nucleotide sugar metabolism
D-Glucose	R01602	D6	alpha-D-Glucose <=> beta-D-Glucose	alpha-D-Glucose 1-epimerase	Glycolysis / Gluconeogenesis
	R01788	D7	alpha-D-Glucose 6-phosphate + H2O <=> alpha-D-Glucose + Orthophosphate	alpha-D-Glucose 6-phosphate phosphohydrolase	Galactose metabolism
L-Tryptophan	R03664	E8	ATP + L-Tryptophan + tRNA(Trp) <=> AMP + Diphosphate + L-Tryptophanyl-tRNA(Trp)	L-Tryptophan -tRNA(Trp) ligase (AMP-forming)	Tryptophan metabolism
Glycolate	R00475	F9	Glycolate + Oxygen <=> Glyoxylate + H2O2	(S)-2-Hydroxy-acid:oxygen 2-oxidoreductase	Glyoxylate and dicarboxylate metabolism

Figure 4.7. (A) Network analysis comparing birds exposed to novel song and silence. ○ represent metabolites, green are metabolites that are differentially expressed comparing novel song to silence using a t-test and a p-value <0.05, purple are connecting metabolites. □ represent reactions based on microarray data, blue represent statistically significant changes in transcripts that are involved in those reactions, red are connecting reactions. (B) Metabolites that show a statistical difference comparing novel song vs. silence (p-value <0.05), and have a direct interaction with reactions whose enzyme transcripts also show a statistic change under similar conditions.

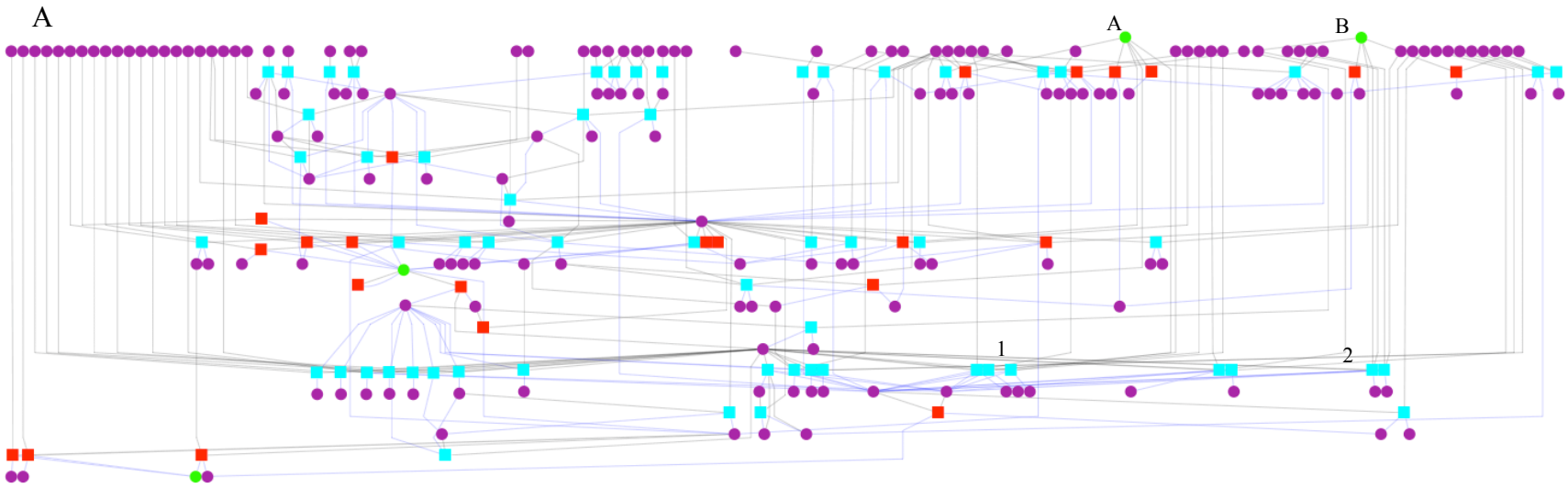

B

Metabolite	Kegg Reaction		Reaction	Enzyme	Pathway
L-Phenylalanine	R03660	A1	ATP + L-Phenylalanine + tRNA(Phe) <=> AMP + Diphosphate + L-Phenylalanyl-tRNA(Phe)	L-Phenylalanine:tRNA(Ala) ligase (AMP-forming)	Aminoacyl-tRNA biosynthesis
L-Tryptophan	R03664	B2	ATP + L-Tryptophan + tRNA(Trp) <=> AMP + Diphosphate + L-Tryptophanyl-tRNA(Trp)	L-Tryptophan -tRNA(Trp) ligase (AMP-forming)	Tryptophan metabolism

Figure 4.8. (A) Network analysis comparing birds that are habituated and silence. ○ represent metabolites, green are metabolites that are differentially expressed comparing novel song to silence using a t-test and a p-value <0.05, purple are connecting metabolites. □ represent reactions based on microarray data, blue represent statistically significant changes in transcripts that are involved in those reactions, red are connecting reaction. (B) Metabolites that show a statistical difference comparing novel song vs. silence (p-value <0.05), and have a direct interaction with reactions whose enzyme transcripts also show a statistic change under similar conditions.

REFERENCES

Bailey, D. J., Rosebush, J. C. and Wade, J. (2002) The hippocampus and caudomedial neostriatum show selective responsiveness to conspecific song in the female zebra finch. Journal of Neurobiology, 52, 43-51.

Clements, M. P., Bliss, T. V. and Lynch, M. A. (1991) Increase in arachidonic acid concentration in a postsynaptic membrane fraction following the induction of long-term potentiation in the dentate gyrus. Neuroscience, 45, 379-389.

Crunelli, V., Ernri, Z. and Leresche, N. (2006) Unravelling the brain targets of gamma-hydroxybutyric acid. Curr Opin Pharmacol, 6, 44-52.

Deranieh, R. M. and Greenberg, M. L. (2009) Cellular consequences of inositol depletion. Biochem Soc T, 37, 1099-1103.

Dong, S., Replogle, K. L., Hasadsri, L., Imai, B. S., Yau, P. M., Rodriguez-Zas, S., Southey, B. R., Sweedler, J. V. and Clayton, D. F. (2009) Discrete molecular states in the brain accompany changing responses to a vocal signal. Proc Natl Acad Sci U S A, 106, 11364-11369.

Doupe, A. J. and Kuhl, P. K. (1999) Birdsong and human speech: common themes and mechanisms. Annu Rev Neurosci, 22, 567-631.

Farooqui, A. A. and Horrocks, L. A. (2006) Phospholipase A(2)-generated lipid mediators in the brain: The good, the bad, and the ugly. Neuroscientist, 12, 245-260.

Fisher, S. K., Novak, J. E. and Agranoff, B. W. (2002) Inositol and higher inositol phosphates in neural tissues: homeostasis, metabolism and functional significance. J Neurochem, 82, 736-754.

Folch, J., Lees, M. and Sloane Stanley, G. H. (1957) A simple method for the isolation and purification of total lipides from animal tissues. J Biol Chem, 226, 497-509.

Gobaille, S., Hechler, V., Andriamampandry, C., Kemmel, V. and Maitre, M. (1999) gamma-Hydroxybutyrate modulates synthesis and extracellular concentration of gamma-aminobutyric acid in discrete rat brain regions in vivo. J Pharmacol Exp Ther, 290, 303-309.

Holloway, C. C. and Clayton, D. F. (2001) Estrogen synthesis in the male brain triggers development of the avian song control pathway in vitro. Nat Neurosci, 4, 170-175.

Huesmann, G. R. and Clayton, D. F. (2006) Dynamic role of postsynaptic caspase-3 and BIRC4 in zebra finch song-response habituation. Neuron, 52, 1061-1072.

Jarvis, E., Gunturkun, O., Bruce, L. et al. (2005) Avian brains and a new understanding of vertebrate brain evolution. Nat Rev Neurosci, 6, 151-159.

Jarvis, E. D. (2004) Learned birdsong and the neurobiology of human language. Ann N Y Acad Sci, 1016, 749-777.

Jones, C. R., Arai, T., Bell, J. M. and Rapoport, S. I. (1996) Preferential in vivo incorporation of [3H]arachidonic acid from blood in rat brain synaptosomal fractions before and after cholinergic stimulation. J Neurochem, 67, 822-829.

Kang, J. X. and Wang, J. (2005) A simplified method for analysis of polyunsaturated fatty acids. BMC Biochem, 6, 5.

Kruse, A. A., Stripling, R. and Clayton, D. F. (2004) Context-specific habituation of the zenk gene response to song in adult zebra finches. Neurobiol Learn Mem, 82, 99-108.
Lester, R. A. J., Tong, G. and Jahr, C. E. (1993) Interactions between the Glycine and Glutamate Binding-Sites of the Nmda Receptor. J Neurosci, 13, 1088-1096.
Lopez-Corcuera, B., Geerlings, A. and Aragon, C. (2001) Glycine neurotransmitter transporters: an update. Mol Membr Biol, 18, 13-20.
Lovell, P. V., Clayton, D. F., Replogle, K. L. and Mello, C. V. (2008) Birdsong "transcriptomics": neurochemical specializations of the oscine song system. Plos One, 3, e3440.
Maier, V. and Scheich, H. (1983) Acoustic Imprinting Leads to Differential 2-Deoxy-D-Glucose Uptake in the Chick Forebrain. P Natl Acad Sci-Biol, 80, 3860-3864.
Maitre, M. (1997) The gamma-hydroxybutyrate signalling system in brain: Organization and functional implications. Prog Neurobiol, 51, 337-361.
Mello, C., Nottebohm, F. and Clayton, D. (1995) Repeated exposure to one song leads to a rapid and persistent decline in an immediate early gene's response to that song in zebra finch telencephalon. J Neurosci, 15, 6919-6925.
Mello, C. V. and Clayton, D. F. (1995) Differential induction of the ZENK gene in the avian forebrain and song control circuit after metrazole-induced depolarization. J Neurobiol, 26, 145-161.
Mello, C. V., Vicario, D. S. and Clayton, D. F. (1992) Song presentation induces gene expression in the songbird forebrain. Proc Natl Acad Sci U S A, 89, 6818-6822.
Muller, S. C. and Scheich, H. (1986) Social Stress Increases [C-14] 2-Deoxyglucose Incorporation in 3 Rostral Forebrain Areas of the Young Chick. Behav Brain Res, 19, 93-98.
Pinaud, R. and Mello, C. V. (2007) GABA immunoreactivity in auditory and song control brain areas of zebra finches. J Chem Neuroanat, 34, 1-21.
Salek, R. M., Colebrooke, R. E., Macintosh, R., Lynch, P. J., Sweatman, B. C., Emson, P. C. and Griffin, J. L. (2008) A metabolomic study of brain tissues from aged mice with low expression of the vesicular monoamine transporter 2 (VMAT2) gene. Neurochem Res, 33, 292-300.
Schmidt, K. L., Chin, E. H., Shah, A. H. and Soma, K. K. (2009) Cortisol and corticosterone in immune organs and brain of European starlings: developmental changes, effects of restraint stress, comparison with zebra finches. Am J Physiol-Reg I, 297, R42-R51.
Theunissen, F. E. and Shaevitz, S. S. (2006) Auditory processing of vocal sounds in birds. Curr Opin Neurobiol, 16, 400-407.
Vates, G. E., Broome, B. M., Mello, C. V. and Nottebohm, F. (1996) Auditory pathways of caudal telencephalon and their relation to the song system of adult male zebra finches. J Comp Neurol, 366, 613-642.
Walkenstein, S. S., Wiser, R., Kimmel, H. and Gudmunds.C (1964) Metabolism of Gamma-Hydroxybutyric Acid. Biochim Biophys Acta, 86, 640-642.

CHAPTER 5

DISCUSSION

In this dissertation I applied advances in analytical tools and methods to map the distribution of small molecules (e.g. fatty acids) across functionally important brain regions in the zebra finch brain. In addition I showed that the auditory lobule exhibits a unique metabolic profile when presented with a novel conspecific song, a habituated song, or silence. The results show potential responses in uridine-5P and GHB metabolism in addition to glycolysis and serine/glycine metabolism. The first steps have been taken to integrate, applying systems biology, our labs previously generated genomic data and my metabolomic data with this biochemical pathways in sugar metabolism, tRNA and adenine metabolism show changes after novel song stimulation.

Chapter 2 applied advances in ToF-SIMS to image the subcellular distribution (2.3μm) of small molecules across a zebra finch brain section. Resulting in, to the best of my knowledge, the highest resolution mass spec image of a biological tissue, consisting of 11.5 megapixles. Moreover I identified neuroanatomical structures (e.g. cell free laminar striations, white and gray matter areas, and the song nuclei RA and HVC) revealing a relative increase of palmitic acid, oleic acid, stearic acid, among other lipids, in areas corresponding to the song nuclei RA and HVC compared to surrounding tissue. In contrast phosphate and arachidonic acid show a relative decrease in these same song nuclei compared to surrounding tissue. This chapter served as bases to explore the use of ToF-SIMS to detect and map molecular heterogeneities focusing on two song nuclei that are critical in song-motor control in the zebra finch brain.

In chapter 3, I explored further small molecule heterogeneities across the song system using ToF-SIMS. I expanded the number of brain regions to include all of the major song nuclei: RA, HVC, LMAN, AreaX, DLM, and the auditory lobule. Applying principle component analysis, an unsupervised multivariate statistical method, to the ToF-SIMS data resulting in the separation of the song nuclei based on their functional role in the song system as well as their location in the brain structure. I also showed that the song nuclei exhibit unique chemical profiles at different stages in brain development and some fatty acids show distribution differences corresponding to cellular composition

in the song nuclei. These experiments reveal for the first time heterogeneous lipid distributions in the zebra finch brain and across areas involved in learning and memory.

In chapter 4, I was interested in answering the question of whether metabolites, which are small molecules, change in the auditory lobule upon song stimulation. The aim of this investigation was to identify specific metabolites and biochemical pathways to focus on in the future and study their potential role in song learning and memory. Auditory lobules exposed to either a novel conspecific song, a habituated song, or silence, exhibited a distinct metabolic profile. Analysis of the metabolic results in the context of a biochemical network I identified key reactions as potentially changing upon song stimulation these included: sugar metabolism and serine to glycine metabolism. However, the most significant changes appear to be 4-hydroxybutanoic acid (GHB) and its associated metabolites, in addition to metabolites associated with RNA metabolism. An initial systems biology approach has also identified various biochemical reactions, such as tryptophan and phenylalanine tRNA synthesis, suggesting a significant change in tRNA synthesis upon song stimulation.

The experiments carried out in this dissertation serve as bases for future experiments investigating the role small molecules play in songbird neurobiology. Some future areas worth exploring include the use of ToF-SIMS to study possible perturbation of membrane lipids as cause or consequence of neurological disease states; for example, the lipid biding protein α-synuclein is central in the development of Parkinson's Disease (PD). In addition, ToF-SIMS would be a valuable tool to investigate the impact of excluding specific fatty acids from the zebra finch diet to study its impact on learning and memory. The system biology approach employed in this thesis is an important fist step in studying learning and memory using a global analytical approach. Future studies would greatly benefit from improved proteomic results and data collection from multiple time points after song stimulation.

Overall this thesis is a significant first step in studying small molecules in the zebra finch song system and opens many new avenues in songbird and neurobiology research. Future research would benefit from identification of unknown molecules from ToF-SIMS analysis. In addition to increased metabolomic, proteomic, and genomic studies and experiments targeting specific metabolic pathways (i.e. GHB).

CURRICULUM VITAE

Kensey R. Amaya

kamaya@illinois.edu

Work: 1206 W. Gregory Dr. #2500	Urbana, IL 61801	(217) 244-1207
Home: 510 N. Hickory Apt B	Champaign, IL 61820	(217) 417-0344

EDUCATION

Ph.D. Cell Biology University of Illinois at Urbana-Champaign 4/6/2010

Thesis: Imaging small molecules and metabolomic profiling of the zebra finch song system**;**

Advisor: Dr. David Clayton

M.S. Animal Sciences University of Illinois at Urbana-Champaign 5/2004

Thesis: Genomic approach to the elucidation of ammonia assimilation and the characterization of a glutamine synthetase type III from *Ruminococcus albus 8*;

Advisor: Dr. Isaac Cann

B.S. Biology University of Michigan – Ann Arbor 4/2002

AWARDS and RECOGNITION

- National Institutes of Health (NIH) Training Fellowship, 2008-2010
- National Institutes of Health (NIH) Research Festival, 2009
- Thomas E. Buetow Memorial Fund, Travel Grant, 2006
- Cell and Molecular Biology & Molecular Biophysics - poster award, 2006
- USDA Training Fellowship, 2004-06
- American Society for Microbiology News (ASM) – Journal Highlight, July 2004

RESEARCH EXPERIENCE

- **Research Assistant,** University of Illinois Urbana-Champaign, 2004-present

Project 1: Chemical profiling and imaging small molecules by ToF-SIMS of the zebra finch song system.

Project 2: Metabolomic and free fatty acid analysis comparing birds exposed to novel song, habituated song, and silence.

Methodologies: Mass Spectrometry (e.g. ToF-SIMS), GC-MS, Immunohistochemistry, Metabolite extraction, Lipid extraction, Chemometrics (e.g. PCA, PLSDA), Fluorescent Microscopy, Animal Surgery, Cryosectioning

- **Research Assistant**, University of Illinois Urbana-Champaign, 2002-2004

Project 1: Biochemical characterization of a new glutamine synthetase, a protein involved in nitrogen assimilation, from the anaerobic bacterium *Ruminococcus albus 8*.

Methodologies: Anaerobic media preparation, Genomic DNA isolation, Bacterial Cloning, mRNA Isolation, Northern blot, HPLC, Column Chromatography, Site-directed Mutagenesis, ATPase Activity Assay, Sequence Alignment, Enzyme Kinetics

- **Undergraduate Researcher**, University of Michigan – Ann Arbor, 2000-2002

Project 1: Bioinformatics/genomics approach to identify essential and non-essential genes in the *Haemophilus influenzae* genome.

Methodologies: Bioinformatics, Bacterial Cloning, PCR

- **Summer Internship**, New England Biolabs, Ipswich, MA, 1996-2001

Project 1: Develop intein-based vector constructs and test their efficacy in purification of target proteins.

Methodologies: Bacterial Cloning, Site-directed Mutagenesis, PCR, Column Chromatography, Western blot

PUBLICATIONS

Southworth, M. W., **Amaya, K.**, Evans, T. C., Xu, M. Q., and Perler, F. B. (1999) Purification of proteins fused to either the amino or carboxy terminus of the *Mycobacterium xenopi* gyrase A intein. Biotechniques, Jul; 27(1):110-4, 116, 118-20.

Akerley, B. J., Rubin, E. J., Novick, V. L., **Amaya, K.**, Judson, N., and Mekalanos, J. J. (2002) A genome-scale analysis for identification of genes required for growth or survival of *Haemophilus influenzae*. Proc. Natl. Acad. Sci. USA, Jan 22; 99(2):966-71.

Cann, I. K. O., **Amaya, K.**, Southworth, M. W., Perler, F. B. (2004) A bacteriophage-based genetic system for selection of non-splicing inteins. Appl. Environ. Microbiol. May 70(5):3158-3162.

Amaya, K. R., Kocherginskaya, S. A., Mackie, R. I., Cann, I. K. O. (2005) Biochemical and mutational analysis of glutamine synthetase type III from the rumen anaerobe *Ruminococcus albus 8*. J. Bacteriol. Nov; 187(21):7481-7491.

Amaya, K. R., Monroe, E. B., Sweedler, J. V., Clayton, D. F. (2007) Lipid imaging in the zebra finch brain with secondary ion mass spectrometry. Int. J. of Mass Spectrum.; 260:121-127.

MANUSCRIPTS

Amaya, K. R., Sweedler, J. V., Clayton, D. F (20xx) Imaging and chemical analysis using Time of Flight – Secondary Ion Mass Spectrometry of the zebra finch song system – in preparation.

Amaya, K. R., Younhee, K., Milne, C., Price, N., Clayton, D. F. (20xx) Metabolomic profiling of the zebra finch auditory forebrain after song exposure – in preparation.

BOOK CHAPTERS

Southworth, M. W., **Amaya, K.**, Evans, T. C., Xu, M. Q., and Perler, F. B. (2001) Purification of proteins fused to either the amino or carboxy terminus of the *Mycobacterium xenopi* gyrase A intein. In Cloning and Expression Vectors for Gene Analysis, Q. Lu and M. Weiner, eds. (Westborough: Eaton Publishing), pp. 55-59.

PRESENTATIONS

Amaya, K. R. and Clayton, D. F.; Metabolomic response and network analysis after song exposure in the zebra finch (2010) Gordon research conference on Genes and Behavior; Ventura, CA; March 14 – 19.

Amaya, K. R. and Clayton, D. F.; Metabolomic response and network analysis after song exposure in the zebra finch (2010) Gordon research student conference on Genes and Behavior; Ventura, CA; March 13 – 14.

Amaya, K. R. and Clayton, D.F.; Lipid imaging and metabolic profiling of the adult zebra finch auditory lobule (2009) Society for Neuroscience (SFN), Chicago, IL.

Amaya, K. R., Sweedler, J. V., Clayton, D. F.; Small molecule profile analysis of the adult and juvenile zebra finch song nuclei by Time of Flight – Secondary Ion Mass Spectrometry (2007) Society for Neuroscience (SFN), San Diego, CA.

Amaya, K. R., Monroe E. B., Spila, T. P., Sweedler, J. V., Clayton, D. F. Imaging song nuclei in the juvenile and adult male zebra finch brain by Time of Flight-Secondary Ion Mass Spectrometry (2006) Cell and Molecular Biology & Molecular Biophysics -19th annual symposium.

Amaya, K. R., Monroe E. B., Spila, T. P., Sweedler, J. V., Clayton, D. F. Imaging song nuclei in

the juvenile and adult male zebra finch brain by Time of Flight-Secondary Ion Mass Spectrometry (2006) Society for Neuroscience (SFN), Atlanta, GA.

Amaya, K. R., Mackie, R. I., Cann, I. K. O. Biochemical and mutational analysis of glutamine synthetase type III from the rumen anaerobe *Ruminococcus albus 8*. (2004) American Society for Microbiology (ASM), 104th annual general meeting, New Orleans, LA

Amaya, K. R., Cann, I. K. O., and Mackie, R. I, Genome mining to elucidate the mechanism of nitrogen regulation in the rumen anaerobe *Ruminococcus albus* 8. 2003 Conference on Gastrointestinal Function, Chicago, IL USA, March 10-13

OTHER PROFESSIONAL EXPERIENCES

Teaching Assistant, Department of Molecular and Cellular Biology, University of Illinois

- Directed two biology laboratory sections for ~40 undergraduates, 2007

Forum Organizer, USDA fellowship, University of Illinois

- Assisted in the organization of a public policy forum, 2004

MEMBERSHIPS

Society for Neuroscience (SFN)